Cell Journal (Yakhteh)

Guide for Authors

Aims and Scope: The "Cell Journal (Yakhteh)" is a peer review and monthly English publication of Royan Institute of Iran. The aim of the journal is to disseminate information through publishing the most recent scientific research studies on exclusively Cellular, Molecular and other related topics. **Cell J**, has been certified by the Ministry of Culture and Islamic Guidance since 1999 and also accredited as a scientific and research journal by HBI (Health and Biomedical Information) Journal Accreditation Commission since 2000 which is an open access journal. **This journal holds the membership of the Committee on Publication Ethics (COPE).**

1. Types of articles

The articles in the field of Cellular and Molecular can be considered for publications in **Cell J.** These articles are as below:

A. Original articles

Original articles are scientific reports of the original research studies. The article consists of English Abstract (structured), Introduction, Materials and Methods, Results, Discussion, Conclusion, Acknowledgements, Author's Contributions, and References **(Up to 40).**

B. Review articles

Review articles are the articles written by well experienced authors and those who have excellence in the related fields. The corresponding author of the review article must be one of the authors of at least three published articles appearing in the references. The review article consists of English Abstract (unstructured), Introduction, Conclusion, Author's Contributions, and References **(Up to 70).**

C. Systematic Reviews

Systematic reviews are a type of literature review that collect and critically analyzes multiple research studies or papers. The Systematic reviews consist of English Abstract (unstructured), Introduction, Materials and Methods, Results, Discussion, Conclusion, Acknowledgements, Author's Contributions, and References **(Up to 70).**

D. Short communications

Short communications are articles containing new findings. Submissions should be brief reports of ongoing researches. The short communication consists of English Abstract (unstructured), the body of the manuscript (should not hold heading or subheading), Acknowledgements, Author's Contributions, and References **(Up to 30).**

E. Case reports

Case reports are short discussions of a case or case series with unique features not previously described which make an important teaching point or scientific observation. They may describe novel techniques or use equipment, or new information on diseases of importance. It consists of English Abstracts (Unstructured), Introduction, Case Report, Discussion, Acknowledgements, Author's Contributions, and References **(Up to 30).**

F. Editorial

Editorials are articles should be written in relevant and new data of journals' filed by either the editor in chief or the editorial board.

G. Imaging in biology

Images in biology should focus on a single case with an interesting illustration such as a photograph, histological specimen or investigation. Color images are welcomed. The text should be brief and informative.

H. Letter to the editors

Letter to the editors are in response to previously published **Cell J** articles, and may also include interesting cases that do not meet the requirement of being truly exceptional, as well as other brief technical or clinical notes of general interest.

I. Debate

Debates are articles which show a discussion of the positive and negative view of the author concerning all aspect of the issue relevant to scientific research.

2. Submission process

It is recommended to see the guidelines for reporting different kinds of manuscripts. This guide explains how to prepare the

manuscript for submission. Before submitting, we suggest authors to familiarize themselves with **Cell J** format and content by reading the journal via the website (www.celljournal.com). The corresponding author ensures that all authors are included in the author list and agree with its order, and they must be aware of the manuscript submission.

A. Author contributions statements

It is essential for authors to include a statement of responsibility in the manuscript that specifies the contribution of every one of them. This participation must include conception and design of the manuscript, data acquisition or data analysis and interpretation, drafting of the manuscript and/or revising it for critically important intellectual content, revision and final approval of the manuscript and statistical analysis, obtaining funding, administrative, technical, or material support, or supervision. Authors who do not meet the above criteria should be acknowledged in the **Acknowledgments section.**

B. Cover letter and copyright

Each manuscript should be accompanied by a cover letter, signed by all authors specifying the following statement: "The manuscript has been seen and approved by all authors and is not under active consideration for publication. It has neither been accepted for publication nor published in another journal fully or partially (except in abstract form). **Also, no manuscript would be accepted in case it has been pre-printed or submitted to other websites.** I hereby assign the copyright of the enclosed manuscript to **Cell J.**" Corresponding author must confirm the proof of the manuscript before online publishing. Also, it is needed to suggest three peer reviewers in the field of their manuscript.

C. Manuscript preparation

Authors whose first language is not English encouraged to consult a native English speaker in order to confirm his manuscripts to American or British (not a mixture) English usage and grammar. It is necessary to mention that we will check the plagiarism of your manuscript by iThenticate Software. The manuscript should be prepared in accordance with the "International Committee of Medical Journal Editors (ICMJE)". Please send your manuscript in two formats word and PDF (including: title, name of all the authors with their degree, abstract, full text, references, tables and figures) and also send tables and figures separately in the site. The abstract and text pages should have consecutive line numbers in the left margin beginning with the title page and continuing through the last page of the written text. Each abbreviation must be defined in the abstract and text when they are mentioned for the first time. Avoid using abbreviation in the title. Please use the international and standard abbreviations and symbols

It should be added that an essential step toward the integration and linking of scientific information reported in published literature is using standardized nomenclature in all fields of science and medicine. Species names must be italicized (*e.g., Homo sapiens*) and also the full genus and species written out in full, both in the title of the manuscript and at the first mention of an organism in a paper.

It is necessary to mention that genes, mutations, genotypes, and alleles must be indicated in italics. Please use the recommended name by consulting the appropriate genetic nomenclature database, e.g., HUGO for human genes. In another words; if it is a human gene, you must write all the letters in capital and italic (*e.g., OCT4, c-MYC*). If not, only write the first letter in capital and italic (*e.g., Oct4, c-Myc*). **In addition, protein designations are the same as the gene symbol but are not italicized.**

Of note, Cell J will only consider publishing genetic association study papers that are novel and statistically robust. Authors are advised to adhere to the recommendations outlined in the STREGA statement (http://www.strega-statement.org). The following criteria must be met for all submissions:

1. Hardy-Weinberg Equilibrium (HWE) calculations must be carried out and reported along with the P-values if applicable [see Namipashaki et al. 2015 (Cell J, Vol 17, N 2, Pages: 187-192) for a discussion].

2. Linkage disequilibrium (LD) structure between SNPs (if multiple SNPs are reported) must be presented.

3. Appropriate multiple testing correction (if multiple independent SNPs are reported) must be included.

Submissions that fail to meet the above criteria will be rejected before being sent out for review.

Each of the following manuscript components should begin in the following sequence:

Authors' names and order of them must be carefully considered (full name(s), highest awarded academic degree(s), email(s), and institutional affiliation(s) of all the authors in English. Also, you must send mobile number and full postal address of the corresponding author).

Changes to Authorship such as addition, deletion or rearrangement of author names must be made only before the manuscript has been accepted in the case of approving by the journal editor. In this case, the corresponding author must explain the reason of changing and confirm them (which has been signed by all authors of the manuscript). If the manuscript has already been published in an online issue, an erratum is needed.

Title is providing the full title of the research (do not use abbreviations in title).

Running title is providing a maximum of 7 words (no more than 50 characters).

Abstract must include Objective, Materials and Methods, Results, and Conclusion (no more than 300 words).

Keywords, three to five, must be supplied by the authors at the foot of the abstract chosen from the Medical Subject Heading (MeSH). Therefore; they must be specific and relevant to the paper.

The following components should be identified after the abstract:

Introduction: The Introduction should provide a brief background to the subject of the paper, explain the importance of the study, and state a precise study question or purpose.

Materials and Methods: It includes the exact methods or observations of experiments. If an apparatus is used, its manufacturer's name and address should be stipulated in parenthesis. If the method is established, give reference but if the method is new, give enough information so that another author can perform it. If a drug is used, its generic name, dose, and route of administration must be given. Standard units of measurements and chemical symbols of elements do not need to be defined.

Statistical analysis: Type of study and statistical methods should be mentioned and specified by any general computer program used.

Ethical considerations*:* Please state that informed consent was obtained from all human adult participants and from the parents or legal guardians of minors and include the name of the appropriate institutional review board that approved the project. It is necessary to indicate in the text that the maintenance and care of experimental animals complies with National Institutes of Health guidelines for the humane use of laboratory animals, or those of your Institute or agency.

Clinical trial registration: All of the Clinical Trials performing in Iran must be registered in Iranian Registry of Clinical Trials (www.irct.ir). The clinical trials performed abroad, could be considered for publication if they register in a registration site approved by WHO or www.clinicaltrials.gov. If you are reporting phase II or phase III randomized controlled trials, you must refer to the CONSORT Statement for recommendations to facilitate the complete and transparent reporting of trial findings. Reports that do not conform to the CONSORT guidelines may need to be revised before peer-reviewing.

Results: They must be presented in the form of text, tables, and figures. Take care that the text does not repeat data that are presented in tables and/or figures. Only emphasize and summarize the essential features of the main results. Tables and figures must be numbered consecutively as appeared in the text and should be organized in separate pages at the end of the manuscript while their location should be mentioned in the main text.

Tables and figures: If the result of your manuscript is too short, it is better to use the text instead of tables & figures. Tables should have a short descriptive heading above them and also any footnotes. Figure's caption should contain a brief title for the whole figure and continue with a short explanation of each part and also the symbols used (no more than 100 words). All figures must be prepared based on cell journal's guideline in color (no more than 6 Figures and Tables) and also in TIF format with 300 DPI resolution.

Of Note: Please put the tables & figures of the result in the results section not any other section of the manuscript.

Supplementary materials would be published on the online version of the journal. This material is important to the understanding and interpretation of the report and should not repeat material within the print article. The amount of supplementary material should be limited. Supplementary material should be original and not previously published and will undergo editorial and peer review with the main manuscript. Also, they must be cited in the manuscript text in parentheses, in a similar way as when citing a figure or a table. Provide a caption for each supplementary material submitted.

Discussion: It should emphasize the present findings and the variations or similarities with other researches done by other researchers. The detailed results should not be repeated in the discussion again. It must emphasize the new and important aspects of the study.

Conclusion: It emphasizes the new and important aspects of the study. All conclusions are justified by the results of the study.

Acknowledgements: This part includes a statement thanking those who contributed substantially with work relevant to the study but does not have authorship criteria. It includes those who provided technical help, writing assistance and name of departments that provided only general support. You must mention financial support in the study. Otherwise; write this sentence "There is no financial support in this study".

Conflict of interest: Any conflict of interest (financial or otherwise) and sources of financial support must be listed in the Acknowledgements. It includes providers of supplies and services from a commercial organization. Any commercial affiliation must be disclosed, regardless of providing the funding or not.

Of Note: If you have already any patent related to the subject of your manuscript, or you are going to apply for such a patent, it must be mentioned in this part.

References: The references must be written based on the Vancouver style. Thus the references are cited numerically in the text and listed in the bibliography by the order of their appearance. The titles of journals must be abbreviated according to the style used in the list of Journals Indexed in PubMed. Write surname and initials of all authors when there are six or less. In the case of seven or more authors, the names of the first six authors followed by "et al." must be listed. You can download Endnote file for Journal references style: endnote file

The reference of information must be based on the following order:

Article:

Surname(s) and first letter of name &middle name(s) of author(s) .Manuscript title. Journal title (abbr).publication date (year); Volume & Issue: Page number.

Example: Manicardi GC, Bianchi PG, Pantano S, Azzoni P, Bizzaro D, Bianchi U, et al. Presence of endogenous nicks in DNA of ejaculated human spermatozoa and its relationship to chromomycin A3 accessibility. Biol Reprod. 1995; 52(4): 864-867.

Book:

Surname(s) and first letter of name & middle name(s) of author(s).Book title. Edition. Publication place: publisher name; publication date (year); Page number.

Example: Edelman CL, Mandle CL. Health promotion throughout the lifespan. 2nd ed. ST Louis: Mosby; 1998; 145-163.

Chapter of book:

Surname(s) and first letter of name & middle name(s) of author(s).Chapter title. In: Surname(s) and first letter of name & middle name(s) of editor(s), editors. Book title. Edition. Publication place: publisher name; publication date (year); Page number.

Example: Phillips SJ, Whisnant JP. Hypertension and stroke. In: Laragh JH, Brenner BM, editors. Hypertension: pathophysiology, diagnosis, and management. 2nd ed. New York: Raven Press; 1995; 465-478.

Abstract book:

Example: Amini rad O.The antioxidant effect of pomegranate juice on sperm parameters and fertility potential in mice. Cell J. 2008;10 Suppl 1:38.

Thesis:

Name of author. Thesis title. Degree. City name. University. Publication date (year).

Example: Eftekhari Yazdi P. Comparison of fragment removal and co-culture with Vero cell monolayers on development of human fragmented embryos. Presented for the Ph.D., Tehran. Tarbiyat Modarres University. 2004.

Internet references

Article:

Example: Jahanshahi A, Mirnajafi-Zadeh J, Javan M, Mohammad-Zadeh M, Rohani M. Effect of low-frequency stimulation on adenosineA1 and A2A receptors gene expression in dentate gyrus of perforant path kindled rats. Cell J. 2008; 10 (2): 87-92. Available from: http://www.celljournal.org. (20 Oct 2008).

Book:

Example: Anderson SC, Poulsen KB. Anderson's electronic atlas of hematology.[CD-ROM]. Philadelphia: Lippincott Williams & Wilkins; 2002.

D. Proofs are sent by email as PDF files and should be checked and returned within 72 hours of receipt. It is the authors' responsibility to check that all the text and data as contained in the page proofs are correct and suitable for publication. **We are requested to pay particular attention to author's names and affiliations as it is essential that these details be accurate when the article is published.**

E. Pay for publication: Publishing an article in **Cell J** requires Article Processing Charges (APC) that will be billed to the submitting author following the acceptance of an article for publication. For more information please see www.celljournal.org.

F. Ethics of scientific publication: Manuscripts that have been published elsewhere with the same intellectual material will refer to duplicate publication. If authors have used their own previously published work or work that is currently under review, as the basis for a submitted manuscript, they are required to cite the previous work and indicate how their submitted manuscript offers novel contributions beyond those of the previous work. Research and publication misconduct is considered a serious breach of ethics.

The Journal systematically employs iThenticate, plagiarism detection and prevention software designed to ensure the originality of written work before publication. Plagiarism of text from a previously published manuscript by the same or another author is a serious publication offence. Some parts of text may be used, only where the source of the quoted material is clearly acknowledged.

3. General information

A. You can send your manuscript via online submission system which is available on our website. If the manuscript is not prepared according to the format of **Cell J**, it will be returned to authors.

B. The order of article appearance in the Journal is not demonstrating the scientific characters of the authors.

C. Cell J has authority to accept or reject the manuscript.

D. The received manuscript will be evaluated by associate editor. **Cell J** uses a single-blind peer review system and if the manuscript suits the journal criteria, we select the reviewers. If three reviewers pass their judgments on the manuscript, it will be presented to the editorial board of **Cell J.** If the editorial board has a positive judgment about the manuscript, reviewers' comments will be presented to the corresponding author (the identification of the reviewers will not be revealed). The executive member of journal will contact the corresponding author directly within 3-4 weeks by email. If authors do not receive any reply from journal office after the specified time, they can contact journal office. Finally, executive manager will respond promptly to authors' request.

The Final Checklist

The authors must ensure that before submitting the manuscript for publication, they have to consider the following parts:

1. The first page of manuscript should contain title, name of the author/coauthors, their academic qualifications, designation & institutions they are affiliated with, mailing address for future correspondence, email address, phone, and fax number.

2. Text of manuscript and References prepared as stated in the "guide for authors" section.

3. Tables should be on a separate page. Figures must be sent in color and also in JPEG (Jpg) format.

4. Cover Letter should be uploaded with the signature of all authors.

5. An ethical committee letter should be inserted at the end of the cover letter.

The Editor-in-Chief: Ahmad Hosseini, Ph.D.

Cell Journal *(Yakhteh)*

P.O. Box: 16635-148, Iran

Tel/Fax: + 98-21-22510895

Emails: Celljournal@royaninstitute.org

info@celljournal.org

IN THE NAME OF GOD

Dr. Saeed Kazemi Ashtiani

Gone But not Forgotten

In the memory of the late Director of Royan Institute, Founder of Stem Cells Research in Iran and Chairman of ***Cell Journal*** *(Yakhteh)*. May he rest in peace.

PUBLISHED & SPONSORED BY:
Publication of Royan Institute (ACECR)

Indexed in:
1. Thomson Reuters (ISI)
2. PubMed
3. PubMed Central (PMC)
4. National Library Medicine (NLM)
5. Biosis Preview
6. Index Medicus for the Eastern Mediterranean Region (IMEMR)
7. Regional Information Center for Sciences and Technology (RICeST)
8. Index Copernicus International
9. Cambridge Scientific Abstract (CSA)
10. EMBASE
11. Scopus
12. Cinahl Database
13. Google Scholar
14. Chemical Abstract Service (CAS)
15. Proquest
16. Directory of Open Access Journals (DOAJ)
17. Open Academic Journals Index (OAJI)
18. Directory of Research Journals Indexing (DRJI)
19. Scientific Information Database (SID)
20. Iranmedex
21. Islamic World Science Citation Center (ISC)
22. Magiran
23. Science Library Index
24. Biological Abstracts
25. Essential Science Indicators
26. EuroPub

ACECR

Editorial Office Address (Dr. Ahmad Hosseini):
Royan Institute, P.O.Box: 16635-148,
Tehran, Iran
Tel & Fax: (+9821)22510895
Website: www.celljournal.org
Emails: info@celljournal.org
celljournal@royaninstitute.org

Printing Company:
Naghshe e Johar Co.
No. 103, Fajr alley, Tehranpars Street,
Tehran, Iran.

Cell Journal(Yakhteh), Vol 24, No 6, June 2022, Serial Number: 101, Pages: 285-352

CONTENTS

Original Articles

Original Article

Long Non-Coding RNA ZEB2-AS1 Promotes Hepatocellular Carcinoma Progression by Regulating The *miR-582-5p/FOXC1* Axis

Shimin Wu, Ph.D.*, Juan Chen, B.D., Ying Liang, M.D., Qian Luo, B.D., Yaoyao Tong, M.D., Ling Xie, B.D.

Center for Clinical Laboratory, General Hospital of The Yangtze River Shipping, Wuhan Brain Hospital, Wuhan, Hubei, China

Corresponding Address: Center for Clinical Laboratory, General Hospital of The Yangtze River Shipping, Wuhan Brain Hospital, Wuhan, Hubei, China
Email: youfuyou805@163.com

Received: 04/February/2021, Accepted: 26/June/2021

Abstract

Objectives: Long non-coding RNAs (lncRNAs) feature prominently in tumors. Reportedly, lncRNA zinc finger E-box-binding homeobox 2 antisense RNA 1 (ZEB2-AS1) is aberrantly expressed in a variety of tumors. The present study was aimed to explore ZEB2-AS1 functions and determine mechanism in hepatocellular carcinoma (HCC) progression.

Materials and Methods: In this experimental study, expressions of *ZEB2-AS1*, microRNA *(miR)-582-5p* and forkhead box C1 (*FOXC1*) mRNA in HCC tissues and cell lines were detected via quantitative reveres transcription polymerase chain reaction (qRT-PCR). After establishing gain- and loss-of-functions models, cell counting kit-8, 5-bromo-2'-deoxyuridine (BrdU), Transwell assays and flow cytometry analysis were conducted to examine HCC cell multiplication, migration, invasion and apoptosis, respectively. The targeted relationship between *miR-582-5p* and *ZEB2-AS1* was verified via dual-luciferase reporter gene assay. Western blot was utilized for detecting FOXC1 expression in HCC cells after selectively regulating *ZEB2-AS1* and *miR-582-5p*.

Results: In HCC tissues and cells, *ZEB2-AS1* expression was increased. High *ZEB2-AS1* expression was related to relatively large tumor volume, increased tumor-node-metastasis (TNM) stage and positive lymph node metastasis of the patients. *ZEB2-AS1* overexpression facilitated HCC cell multiplication, migration, invasion and suppressed apoptosis, while *ZEB2-AS1* knock-down caused the opposite effects. It was also confirmed that *ZEB2-AS1* could competitively bind with *miR-582-5p* to repress its expression, and indirectly up-regulate *FOXC1* expression level in HCC cells.

Conclusion: The current study revealed that *ZEB2-AS1* was over-expressed in HCC tissues and cells. It also up-regulated *FOXC1*, through sponging *miR-582-5p*, to promote HCC progression. This provides new perspectives for elucidating the pathogenesis of HCC.

Keywords: Forkhead Box C1, Hepatocellular Carcinoma, Long Non-Coding RNA, *miR-582-5p*

Cell Journal(Yakhteh), Vol 24, No 6, June 2022, Pages: 285-293

Citation: **Wu SM, Chen J, Liang Y, Luo Q, Tong YY, Xie L. Long non-coding RNA ZEB2-AS1 promotes hepatocellular carcinoma progression by regulating the miR-582-5p/FOXC1 axis. Cell J. 2022; 24(6): 285-293. doi: 10.22074/cellj.2022.7963.**

Introduction

Globally, known to rank third among the causes of cancer-related deaths, hepatocellular carcinoma (HCC) makes up about 90% of primary liver cancer cases (1, 2), and half of deaths occurred in China (3). Hepatitis C or B virus (HCV or HBV) infection is one of the primary risk factors for HCC tumorigenesis (4). Despite the recent improvements in treatments, such as liver transplantation, hepatectomy, radiotherapy, chemotherapy and targeted therapy, five-year overall survival rate of HCC patients is still very low as a result of metastasis and recurrence (5, 6).

Recognized as a kind of non-coding RNA, long non-coding RNAs (lncRNAs) are with limited or without protein coding ability. They consist of over 200 nucleotides in length (7). lncRNAs regulate diverse biological processes, for instance, cell differentiation, proliferation, embryonic development and tumorigenesis (8, 9). A great deal of research has shown that lncRNAs feature prominently in cancer biology, regulating tumor cell proliferation, drug resistance and epithelial-mesenchymal transition (EMT) (10-12). Previous studies proved that lncRNA zinc finger E-box-binding homeobox 2 antisense RNA 1 (*ZEB2-AS1*) was aberrantly expressed in several tumors and was strongly associated with tumorigenesis and cancer progression. For example, *ZEB2-AS1* facilitated colorectal carcinoma cell multiplication and repressed apoptosis by enhancing β-catenin protein expression (13). Down-regulated *ZEB2-AS1* expression suppressed HCC cell multiplication and metastasis via modulating *ZEB2* expression (14). However, the mechanism of *ZEB2-AS1* underlying HCC progression needs in-depth investigation.

Known as a type of single-stranded small non-coding RNAs, microRNAs (miRNAs or miRs) bind to mRNA 3′-untranslated region (3′-UTR) to negatively modulate gene expression, inducing the degradation of targeted messenger RNAs (mRNAs) (15). Reportedly, *miR-582-5p* functions as a tumor suppressor in different cancers.

For example, in bladder cancer, *miR-582-5p* represses cell multiplication via reducing human monopolar spindle 1 (HMPS1/TTK) expression (16). *miR-582-5p* was lowly expressed in HCC and it repressed cell multiplication by targeting *CDK1* and *AKT3* (17). Nevertheless, *miR-582-5p* molecular mechanism in HCC needs to be further investigated.

The forkhead box (FOX) transcriptional factor family shared a winged helix-turn-helix DNA binding domain and this domain is crucial in regulating cell differentiation, metabolism, proliferation, migration, invasion and apoptosis (18-20). Reportedly, overexpression of forkhead box C1 (*FOXC1*) induced transactivation of *CXCR1* and *CCL2* and facilitated HCC cell migration and invasion (21).

In the current research, we reported that *ZEB2-AS1* was up-regulated in HCC cell lines and tissues.

Materials and Methods

Tissue samples

Endorsed by the Research Ethics Committee of Wuhan Brain Hospital (Wuhan, China, Approval No. 2019-0517), this study was performed. All patients' informed consent was obtained and the present study enrolled 50 HCC patients who admitted to the hospital. The clinicopathological data of all patients were obtained and none of them underwent chemotherapy or radiotherapy before the surgery. The cancerous and the corresponding adjacent tissues were surgically removed and collected. Additionally, the cancer tissues of 20 breast cancer patients were obtained from our hospital, and then all the tissues were preserved at -196˚C in liquid nitrogen.

Cell culture and transfection

In this experimental study, HCC cell lines (BEL7402, HCCLM3, SMMC-7721 and Huh7) and normal liver cell line (MIHA) were obtained from China Center for Type Culture Collection (Wuhan, China). From the American Type Culture Collection (Manassas, USA), we bought human breast cancer cell line MCF-7. These cells were cultured in Dulbecco's modified Eagle's medium (DMEM, Invitrogen, USA) containing 10% fetal bovine serum (FBS), 100 μg/ml streptomycin and 100 U/ml penicillin (ThermoFisher Scientific, USA) at 37˚C in 5% CO_2.

Small interfering RNA (siRNA) against *ZEB2-AS1* (si-*ZEB2-AS1*-1, si-*ZEB2-AS1*-2 and si-*ZEB2-AS1*-3), siRNA control (si-NC), *miR-582-5p* inhibitors (*miR-582-5p*-in), inhibitors control (miR-in), *miR-582-5p* mimics (*miR-582-5p*), mimics control (miR-NC), *ZEB2-AS1* overexpression vector (*ZEB2-AS1*) and empty vector (Vector) were synthesized by RiboBio (Guangzhou, China). The oligonucleotides and plasmids were transfected into HCC cells using Lipofectamine 3000 (Invitrogen).

Quantitative reverse transciption polymerase chain reaction

TRIzol reagent (Vazyme, China) was utilized for total RNA isolation. PrimeScript RT reagent kit (TaKaRa, China) was applied for complementary DNA (cDNA) synthesis. For miRNAs, the PrimeScript miRNA cDNA Synthesis Kit (TaKaRa) was adopted to carry out reverse transcription. SYBR Premix Ex Taq I was employed to conduct qRT-PCR. *GAPDH* and *U6* acted as internal references for mRNA and miRNA, respectively. The $2^{-\Delta\Delta Ct}$ method was applied for calculation of the relative expression level. The primers used were as follows:

ZEB2-AS1-

F: 5′-GGCTGGATAGCAAAGGAC-3′
R: 5′-ACACTCTTGGCGAGGT-3′

miR-582-5p-

F: 5′-GCACACATTGAAGAGGACAGAC-3′
R: 5′-TATTGAAGGGGGTTCTGGTG-3′

FOXC1-

F: 5′-CAGAACAGCATCCGCCACA-3′
R: 5′-TGTTGTAGGAGTCCGGGTC-3′

U6-

F: 5′-GCTTCGGCAGCACATATACTAAAAT-3′
R: 5′-CGCTTCACGAATTTGCGTGTCAT-3′

GAPDH-

F: 5′-CACCCACTCCTCCACCTTTG-3′
R: 5′-CCACCACCCTGTTGCTGTAG-3′

Cell counting kit-8 (CCK-8) assay

CCK-8 assay was conducted to evaluate cell proliferation. HCC cells were inoculated at 1×10^3 cells/well in 96-well plates, and they were cultured at 37˚C in 5% CO_2 for 24 hours. After culturing cells for 0, 1, 2, 3 and 4 days, 10 μl of CCK-8 reagent (Beyotime Biotechnology, China) was added to each well, followed by cell culture at 37˚C in 5% CO_2 for another 2 hours. The absorbance at 450 nm was measured using a microplate reader (Bio-Rad, USA). Four days later, cell proliferation curve was drawn.

5-Bromo-2-deoxyUridine (BrdU) assay

The BrdU method was used to determine DNA synthesis in proliferating cells. BrdU assay was conducted 48 hours after transfection. Briefly, the cells were inoculated in 96-well plates (2×10^3 cells/well) and cultured for 48 hours. Subsequently, the cells were incubated with a final concentration of 10 μM BrdU solution (Wuhan AmyJet Scientific Inc., China) for 4 hours at room temperature, followed by medium removal after the incubation period. The cells were fixed for 30 minutes with paraformaldehyde and then incubated with anti-BrdU antibody (Sigma-Aldrich, China) for 1 hour at room temperature in dark. After that, they were washed with PBS three times and

subsequently incubated with DAPI staining solution at room temperature for 30 minutes in dark. Eventually, the cells were observed under a fluorescence microscope.

Transwell assay

For migration assay, the upper Transwell compartment (BD Biosciences, USA) was loaded with 1×10^5 cells (in 200 µl of serum-free DMEM). Then, the lower one was loaded with 700 µl of 10% FBS-containing DMEM. 24 hours later, cells on the membrane underside were stained and then they were counted in three randomly selected high-power fields, under the microscope. For invasion assay, the chambers were precoated with a layer of Matrigel and the same procedures were conducted as described above.

Flow cytometry assay

Annexin V-fluorescein isothiocyanate (FITC)/propidium iodide (PI) apoptosis detection kit (Vazyme, China) was adopted to evaluate the apoptosis of HCCLM3 and BEL7402 cells. The cells were harvested 48 hours after transfection and the cell concentration was adjusted to 1×10^6 cells/ml with binding buffer. Subsequently, the cells were incubated overnight with pre-cooled 70% ethanol at 4˚C. After being centrifuged, the cells was re-suspended in binding buffer (200 µl). The re-suspended cells were then stained with PI staining solution (5 µl) and Annexin V-FITC staining solution (10 µl) in dark for 15 minutes at room temperature. Afterwards, a MoFlo XDP flow cytometer (Beckman Coulter, USA) was utilized to analyze apoptotic cells. Data were processed by BD FACSDiva™ software (BD Bioscience, USA).

Xenograft model in nude mice

Animal Care and Use Committee of Wuhan Brain Hospital approved all animal experiments. Male BALB/c nude mice were bought from Experimental Animal Center of Wuhan University (Wuhan, China). Twenty nude mice (age: 5 weeks) were randomly divided into two groups, with 10 mice in each group. In the lung metastasis experiment, HCCML3 cells (2×10^6 cells per mouse), overexpressing ZEB2-AS1, or the control cells were injected into the tail vein of nude mice. The mice were euthanized after 3 weeks and the lungs tissues were collected for pathological examination. Lung metastasis was evaluated by hematoxylin-eosin (HE) staining. In brief, after fixation at room temperature for 4 hours, using 4% paraformaldehyde, the lung tissues were dehydrated with ethanol and embedded in paraffin blocks. Then, the tissues were sliced and lung tissue sections with a thickness of 5 µm were dewaxed in xylene, rehydrated in ethanol of decreasing concentrations and washed with PBS. Then, HE staining solution (Beyotime, China) was employed to stain the sections for 5 minutes at room temperature. Next, the sections were dehydrated, sealed and observed under a light microscope.

Western blotting

To obtain protein samples, RIPA lysis buffer was employed for lysing the cells and the supernatant was collected after centrifugation. A bicinchoninic acid kit (Abcam, USA) was utilized for determining the concentration of each protein sample. Next, equivalent amounts of proteins were dissolved by sodium dodecyl sulfate-polyacrylamide gel electrophoresis (SDS-PAGE) and then transferred to the polyvinylidene fluoride membrane (Millipore, USA), which were subsequently blocked with 5% skimmed milk. Then, the membranes were incubated with anti-*FOXC1* antibody (1:1000; Abcam, USA) and anti-*GAPDH* antibody (1:1000; Abcam, USA) for 12 hours at 4˚C. Then, the membranes, after washing, were incubated with horseradish peroxidase-conjugated goat anti-rabbit IgG (1:2000; Abcam, USA) for 2 hours in room temperature. Subsequently, the enhanced chemiluminescence reagent (Beyotime, China) was employed for developing the protein bands and a ChemiDoc MP system (Bio-Rad, USA) was utilized for the visualization.

Dual-luciferase reporter gene assay

To generate the wild-type (WT) luciferase reporter vector (*ZEB2-AS1*-WT and *FOXC1*-WT), the sequences of *ZEB2-AS1* or *FOXC1* 3′-UTR containing the binding site for *miR-582-5p* were integrated into the pmirGLO luciferase reporter vector (Promega, USA). Meanwhile, the binding sites were mutated to produce the corresponding mutant (MUT) luciferase reporter vectors (*ZEB2-AS1*-MUT and *FOXC1*-MUT). The constructed vectors and *miR-582-5p* or miR-NC were co-transfected into HCCLM3 and BEL7402 cells. Ultimately, 48 hours after transfection, the luciferase reporter detection system (Promega) was utilized to analyze the luciferase activity of the cells.

Statistical treatment

All experiments were conducted in triplicate. All data in the experiments were analyzed by GraphPad Prism 8.0 software (GraphPad Software Inc., USA) and SPSS 22.0 (SPSS Inc., USA). A Chi-square test (χ^2 test) was employed for analyzing the relationship between clinicopathological features and *ZEB2-AS1* expression in HCC samples. The measurement data were expressed as mean ± standard deviation (mean ± SD). Comparison of data among the multiple groups was performed by one-way analysis of variance, and a t test was performed for the comparison between two groups. $P<0.05$ denoted that a difference was of statistical significance.

Results

ZEB2-AS1 was highly expressed in HCC and it was related to the patient's poor prognosis

To assess *ZEB2-AS1* expression, qRT-PCR was conducted in normal tissues (n=50), HCC tissues (n=50) and breast cancer tissues (n=20). It was indicated that *ZEB2-AS1* expression was markedly up-regulated in the HCC tissues against the normal tissues and breast cancer

tissues (Fig.1A). Besides, qRT-PCR was conducted to detect *ZEB2-AS1* expression in the normal liver cell line (MIHA cells), HCC cell lines (SMMC-7721, BEL7402, HCCLM3 and Huh7 cells) and breast cancer cell line, MCF-7. It was unveiled that, in contrast to the MIHA and MCF-7 cells, *ZEB2-AS1* expression in the four types of HCC cell was up-regulated (Fig.1B). Subsequently, the GEPIA database was employed for analyzing the relationship between HCC patients overall survival time and *ZEB2-AS1* expression, and it was discovered that in comparison with HCC patients with low *ZEB2-AS1* expression, those with the high expression had a lower overall survival rate (Fig.1C). Moreover, the correlation between HCC patient clinicopathological indicators and *ZEB2-AS1* expression was analyzed by chi-square test, and the results suggested that high *ZEB2-AS1* expression was linked to relatively large tumor volume, increased tumor-node-metastasis (TNM) stage and positive lymph node metastasis (Table 1). The aforementioned evidences implied that *ZEB2-AS1* played a cancer-promoting role in HCC.

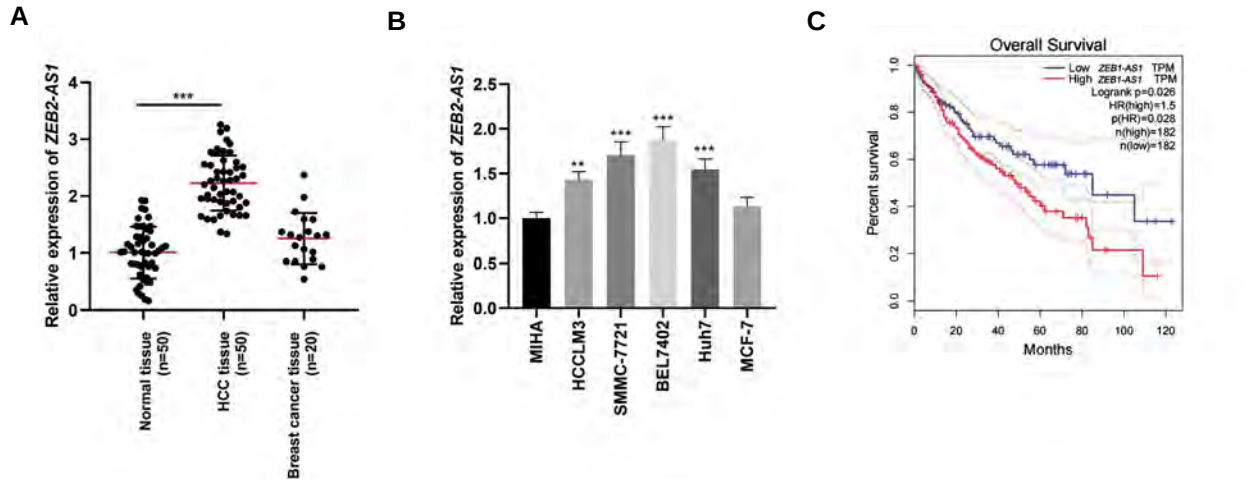

Fig.1: *ZEB2-AS1* is over-expressed in HCC tissues and cells. **A.** Detection by qRT-PCR of *ZEB2-AS1* expression in HCC tissues (n=50), adjacent normal tissues (n=50) and breast cancer tissues (n=20). **B.** Detection by qRT-PCR of *ZEB2-AS1* expression in normal human liver cell line (MIHA cells), HCC cell lines (BEL7402, SMMC-7721, HCCLM3, and Huh7 cells) and human breast cancer cells MCF-7. **C.** GEPIA database was employed for analyzing the relationship between *ZEB2-AS1* expression and HCC patient prognosis. All experiments were repeated 3 times, each in triplicate. **; P<0.01, ***; P<0.001, HCC; Hepatocellular carcinoma, qRT-PCR; Quantitative reverse transciption polymerase chain reaction, and GEPIA; Gene expression profiling interactive analysis.

Table 1: Correlation of *ZEB2-AS1* expression with multiple clinicopathological characteristics in hepatocellular carcinoma (HCC) patients (n=50)

Characteristics	Number	*ZEB2-AS1* expression		χ^2	P value
		High	Low		
Age (Y)					
≥ 60	28	17	11		
< 60	32	9	13	1.9361	0.1641
Gender					
Male	38	21	17		
Female	12	5	7	0.6755	0.4112
Tumor size (cm)					
≥ 5	32	21	11		
< 5	18	5	13	6.6111	0.0101
Hepatitis					
Negative	30	14	16		
Positive	20	12	8	0.8547	0.3552
TNM stage					
Ⅰ - Ⅱ	17	4	13		
Ⅲ-Ⅳ	33	22	11	8.3648	0.0038
Lymph node metastasis					
Negative	21	6	15		
Positive	29	20	9	7.9623	0.0048

ZEB2-AS1 facilitated HCC cell proliferation, migration, invasion and inhibited cell apoptosis

To probe into *ZEB2-AS1* role in HCC progression, we selected HCCLM3 cells with the lowest *ZEB2-AS1* expression and BEL7402 cells with the highest expression to construct *ZEB2-AS1* overexpression or knock-down models, respectively (Fig.2A). Then, CCK-8 and BrdU assays were conducted to detect HCC cell multiplication. Against the control group, overexpression of *ZEB2-AS1* remarkably promoted HCCLM3 cell proliferation, while *ZEB2-AS1* knock-down notably repressed BEL7402 cell proliferation (Fig.2B-D). Additionally, Transwell assays showed that *ZEB2-AS1* overexpression significantly facilitated HCCLM3 cell migration and invasion, while knocking-down *ZEB2-AS1* inhibited BEL7402 cell migration and invasion (Fig.2E-H). Flow cytometry analysis revealed that overexpression of *ZEB2-AS1* suppressed HCCLM3 cell apoptosis and *ZEB2-AS1* knock-down increased BEL7402 cell apoptosis (Fig.2I, J). The results of HE staining revealed that as opposed to the Vector/HCCML3 group, there were significantly more metastasis nodules in the mouse lung tissues of the *ZEB2-AS1*/HCCML3 group (Fig.S1, See Supplementary Online Information www.celljournal.org). The above results indicated that *ZEB2-AS1* facilitated HCC growth and metastasis.

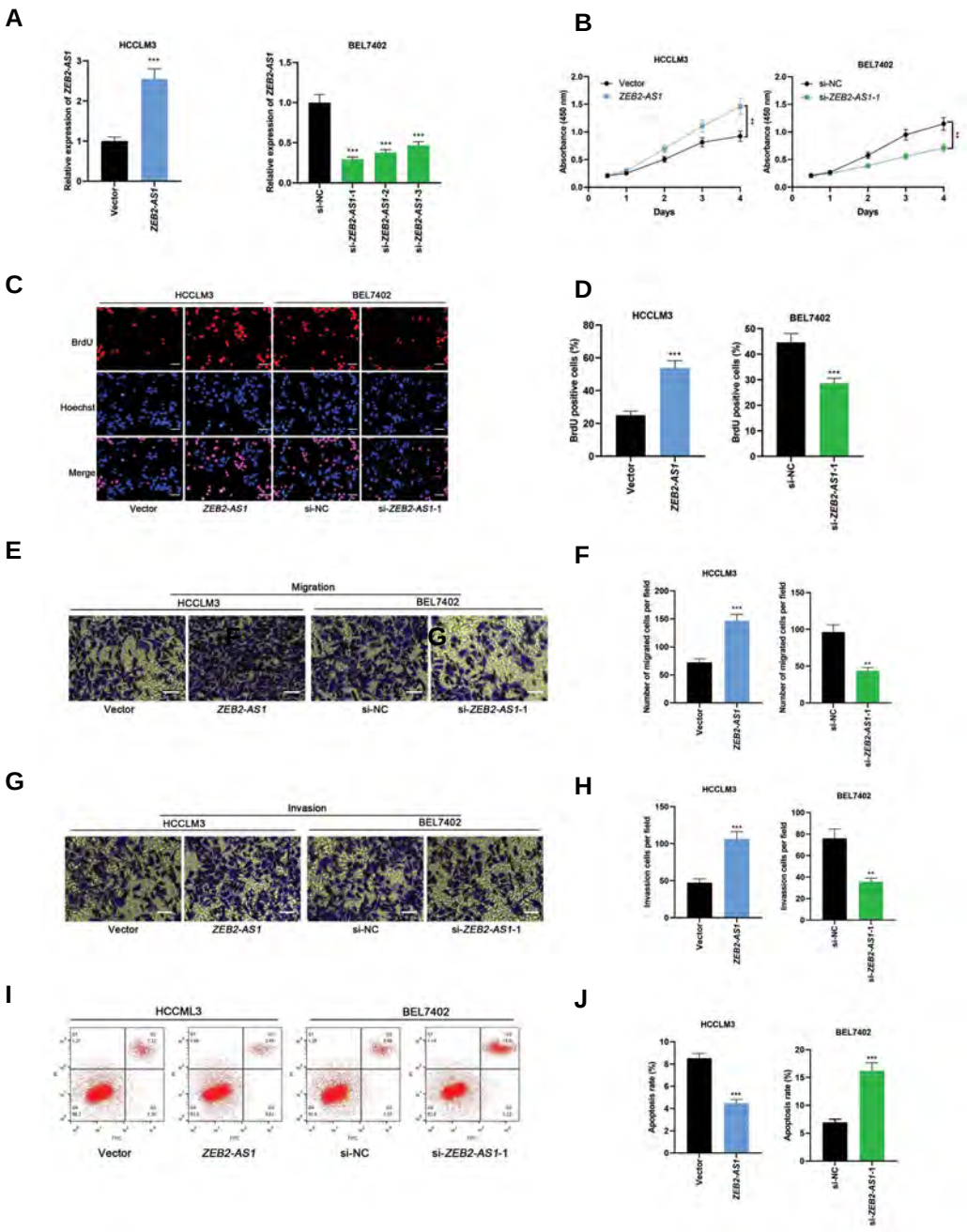

Fig.2: Effects of *ZEB2-AS1* on HCC cell proliferation, migration, invasion and apoptosis. **A.** Detection by qRT-PCR of *ZEB2-AS1* expression in HCCLM3 cells transfected with *ZEB2-AS1* overexpression plasmids and BEL7402 cells transfected with *ZEB2-AS1* siRNAs. **B-D.** CCK-8 and BrdU assays (scale bars: 75 μm) were conducted for detecting HCC cell proliferation after *ZEB2-AS1* overexpression or knock-down. **E-H.** Transwell assay was used to detect HCC cell migration and invasion (scale bars: 250 μm). **I, J.** Flow cytometry was conducted to evaluate apoptosis rate of HCCLM3 and BEL7402 cells after overexpression or knock-down of ZEB2-AS1. All experiments were repeated 3 times, each in triplicate. **; P<0.01, ***; P<0.001, HCC; Hepatocellular carcinoma, qRT-PCR; Quantitative reverse transciption PCR, siRNA; Small interfering RNA, CCK-8; Cell counting kit-8, and BrdU; 5-Bromo-2-deoxyUridine.

ZEB2-AS1 directly targeted *miR-582-5p*

To decipher mechanism of *ZEB2-AS1* in HCC progression, bioinformatics was adopted for predicting miRNAs pairing with *ZEB2-AS1* and it was uncovered that there existed potential binding sites between *ZEB2-AS1* and *miR-582-5p* (Fig.3A). Dual-luciferase reporter gene assay validated that *miR-582-5p* mimics could markedly reduce *ZEB2-AS1*-WT luciferase activity, but exerted no remarkable impact on *ZEB2-AS1*-MUT luciferase activity (Fig.3B). Subsequently, qRT-PCR displayed that *ZEB2-AS1* overexpression significantly inhibited *miR-582-5p* expression, while *ZEB2-AS1* knockdown markedly up-regulated *miR-582-5p* expression (Fig.3C). Additionally, qRT-PCR was conducted for evaluating *miR-582-5p* expression in 50 cases of HCC and para-cancerous tissues, and it was discovered that *miR-582-5p* expression was dramatically down-regulated in HCC tissues in comparison with adjacent normal tissues (Fig.3D). At the same time, we observed that *miR-582-5p* and *ZEB2-AS1* expressions in HCC tissues were inversely related (Fig.3E). The aforementioned evidences suggested that *ZEB2-AS1* directly targets *miR-582-5p* and negatively regulates its expression in HCC.

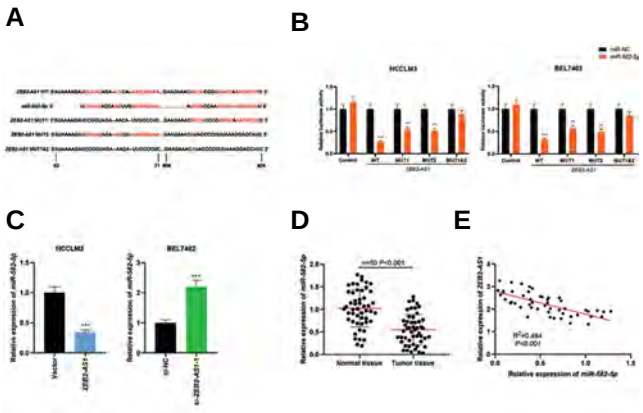

Fig.3: *miR-582-5p* is the target of *ZEB2-AS1* in HCC cells. **A.** Bioinformatics was adopted for predicting binding site between *ZEB2-AS1* and miR-582-5p. **B.** Binding relationship between *miR-582-5p* and *ZEB2-AS1* in HCC cells was detected by dual-luciferase reporter gene assay. **C.** Detection via qRT-PCR of *miR-582-5p* expression in HCC cells with overexpression or knock-down of *ZEB2-AS1*. **D.** Detection via qRT-PCR of *miR-582-5p* expression in 50 cases of HCC tissues and adjacent normal tissues. **E.** Detection of the correlation between *ZEB2-AS1* and *miR-582-5p* expressions in HCC tissues via qRT-PCR. All experiments were repeated 3 times, each in triplicate. **; P<0.01, ***; P<0.001, HCC; Hepatocellular carcinoma, and qRT-PCR; Quantitative reverse transciption polymerase chain reaction.

miR-582-5p reversed the impact of *ZEB2-AS1* on HCC cell multiplication, migration, invasion and apoptosis

To dig deeper into the role of the *ZEB2-AS1/miR-582-5p* axis in HCC, we transfected *ZEB2-AS1* overexpression plasmid, *miR-582-5p* mimic, *ZEB2-AS1* overexpression plasmid+*miR-582-5p* into HCCLM3 cells, respectively and transfected si-*ZEB2-AS1*-1, *miR-582-5p* inhibitors, si-*ZEB2-AS1*-1+*miR-582-5p* inhibitor into BEL7402 cells, respectively. Furthermore, HCC cell multiplication, migration and invasion were detected through CCK-8, BrdU, Transwell assays and flow cytometry analysis. The results manifested that, as opposed to the control group, *ZEB2-AS1* overexpression markedly facilitated HCC cell proliferation, migration, invasion and inhibited cell apoptosis, while *miR-582-5p* mimics suppressed HCC cell proliferation, migration, invasion and increased cell apoptosis, in addition to weakening the effects of *ZEB2-AS1* overexpression on HCC cells; additionally, knocking-down *ZEB2-AS1* dramatically restrained HCC cell proliferation, migration, invasion and promoted cell apoptosis, while *miR-582-5p* inhibitors facilitated HCC cell proliferation, migration and invasion. It also suppressed cell apoptosis and partially counteracted the inhibiting effects of si-*ZEB2-AS1*-1 on the malignant phenotypes of HCC cells (Fig.4A-E).

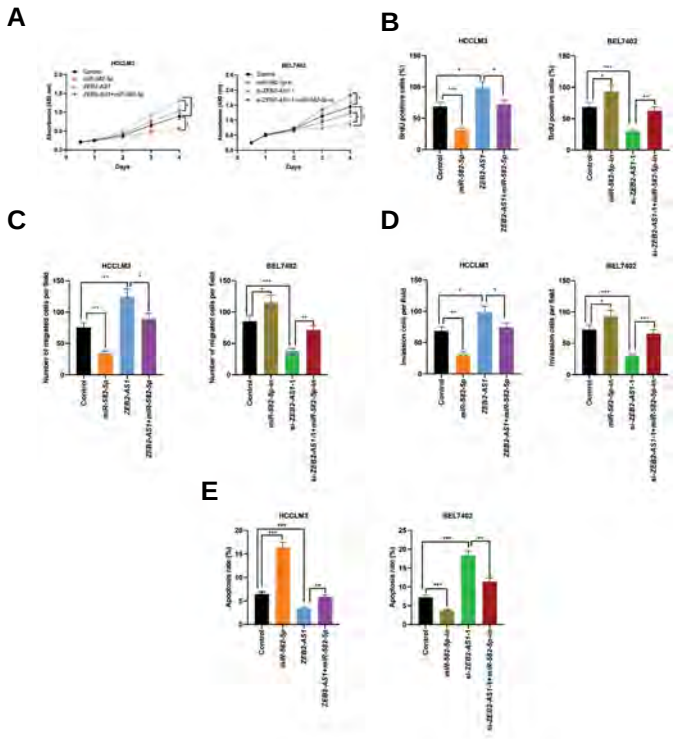

Fig.4: *miR-582-5p* reverses effects of *ZEB2-AS1* on HCC cell proliferation, migration, invasion and apoptosis. *ZEB2-AS1* overexpression plasmid, *miR-582-5p* mimic, *ZEB2-AS1* overexpression plasmid+*miR-582-5p* were transfected into HCCLM3 cells, respectively, and si-*ZEB2-AS1*-1, *miR-582-5p* inhibitors, si-*ZEB2-AS1*-1+*miR-582-5p* inhibitor were transfected into BEL7402 cells, respectively. **A, B.** CCK-8 and BrdU assays were utilized for examining HCCLM3 and BEL7402 cell proliferation. **C, D.** HCCLM3 and BEL7402 cell migration and invasion were detected through Transwell assays. **E.** Flow cytometry analysis was utilized to detect HCCLM3 and BEL7402 cell apoptosis. All experiments were repeated 3 times, each in triplicate. *; P<0.05, **; P<0.01, ***; P<0.001, HCC; Hepatocellular carcinoma, qRT-PCR; Quantitative reverse transciption polymerase chain reaction, CCK-8; Cell counting kit-8, and BrdU; 5-Bromo-2-deoxyUridine.

ZEB2-AS1 elevated *FOXC1* expression by adsorbing *miR-582-5p*

A previous study has shown that *miR-582-5p* targeted and regulated *FOXC1* (22). Consistently, the TargetScan database exhibited that there existed a

binding site between *miR-582-5p* and *FOXC1* (Fig.5A). Subsequently, results of the dual-luciferase reporter gene assay manifested that *miR-582-5p* mimics could significantly inhibit *FOXC1*-WT luciferase activity, but failed to change the luciferase activity of *FOXC1*-MUT (Fig.5B, C). qRT-PCR displayed that *FOXC1* expression was increased in HCC tissues and cells (Fig.5D, E). Additionally, *ZEB2-AS1* overexpression enhanced *FOXC1* expression in HCCLM3 cells, while *miR-582-5p* mimics could down-regulate *FOXC1* expression and weaken the promoting effect of *ZEB2-AS1* overexpression on *FOXC1* expression (Fig.5F, G). On the other hand, knock-down of *ZEB2-AS1* could inhibit *FOXC1* expression, while *miR-582-5p* inhibitors could promote *FOXC1* expression and partially reverse the effect of si-*ZEB2-AS1*-1 on *FOXC1* expression (Fig.5H, I). Moreover, in HCC tissues, *miR-582-5p* and *FOXC1* mRNA expressions were inversely related, while *ZEB2-AS1* and *FOXC1* mRNA expressions were positively correlated (Fig.5J, K). The above-mentioned results suggested that *ZEB2-AS1* played a role in HCC by regulating the *miR-582-5p/FOXC1* axis.

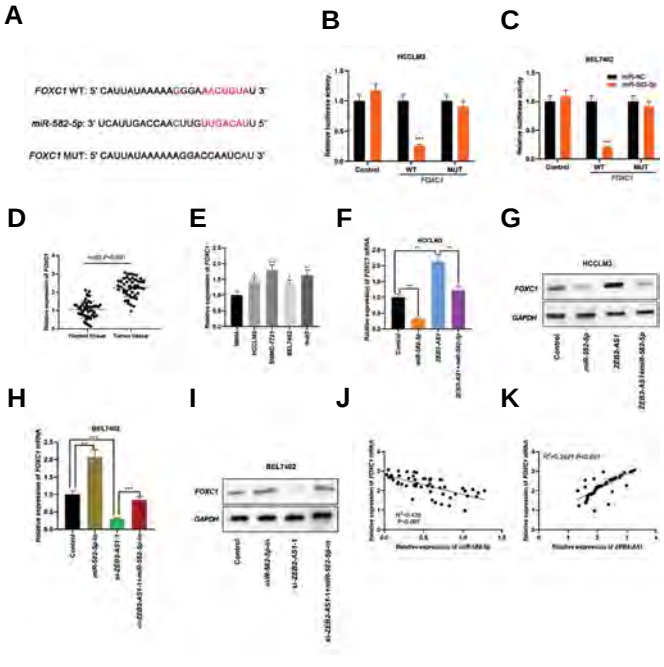

Fig.5: Regulation of *FOXC1* expression by the *ZEB2-AS1/miR-582-5p* axis. **A.** Bioinformatics was used for predicting binding site between *miR-582-5p* and *FOXC1*. **B, C.** Binding relationship between *miR-582-5p* and *FOXC1* in HCC cells was detected via dual-luciferase reporter gene assay. **D, E.** Detection of *FOXC1* expression by qRT-PCR in 50 cases of the HCC tissues and adjacent normal tissues, as well as normal human liver cell line (MIHA cells) and HCC cell lines (BEL7402, SMMC-7721, HCCLM3, and Huh7 cells). **F-I.** qRT-PCR and Western blot were used to detect regulatory effect of *miR-582-5p* or *ZEB2-AS1* on *FOXC1* protein expression. Original blots are shown in Supplementary material. **J, K.** qRT-PCR was employed for analyzing the correlation between *FOXC1* mRNA and *miR-582-5p* as well as *ZEB2-AS1* expression in HCC tissues. All experiments were repeated 3 times, each in triplicate. *; P<0.05, **; P<0.01, ***; P<0.001, HCC; Hepatocellular carcinoma, and qRT-PCR; Quantitative reverse transcription polymerase chain reaction.

Discussion

In recent years, growing evidences showed lncRNAs are strongly associated with the tumorigenesis and progression of a variety of malignancies. Thus, it can be used as specific markers for certain tumors, and feature prominently in regulating cancer cell proliferation and metastasis. For example, lncRNA LOC284454 promoted HCC cell invasion and migration by suppressing *E-cadherin* expression (23). Reportedly, *ZEB2-AS1* expression was increased in lung cancer tissues. It is suggested that *ZEB2-AS1* can facilitate lung cancer cell multiplication and inhibit apoptosis (24). Depletion of *ZEB2-AS1* expression suppressed HCC cell growth and metastasis. In the current study, cancer-promoting role of *ZEB2-AS1* in HCC was also confirmed, which is in line with the previous study (14). It was manifested that *ZEB2-AS1* expression was increased in HCC tissues and cells. High *ZEB2-AS1* expression was related to unfavorable clinicopathologic characteristics. What is more, *ZEB2-AS1* overexpression remarkably boosted HCC cell multiplication, migration, invasion and suppressed cell apoptosis, while *ZEB2-AS1* knock-down had the opposite effects. The aforementioned evidences demonstrated that *ZEB2-AS1* could act as a potential HCC prognostic biomarker and therapeutic target.

miRNAs participate in regulating carcinogenesis and cancer progression (25). It was reported that *miR-582-5p* was aberrantly expressed in various cancers and it could play a cancer-suppressing role. For example, *miR-582-5p* inhibited bone metastasis of prostate cancer cells by inhibiting TGF-β signal transduction (26). The up-regulation of *miR-582-5p* repressed endometrial cancer cell multiplication and promoted apoptosis by targeting *AKT3* (27). This study unveiled that *miR-582-5p* expression was underexpressed in HCC tissues. Moreover, *miR-582-5p* overexpression notably repressed cell multiplication, migration, invasion and promoted cell apoptosis, while *miR-582-5p* inhibition had the opposite effects. These suggested that *miR-582-5p* inhibited HCC progression as a tumor suppressor.

lncRNAs can directly interact with miRNAs and act as competing endogenous RNAs (ceRNAs) to modulate mRNA expression. For example, *ZEB2-AS1* up-regulated *HMGB1* expression via sponging *miR-204* to promote the growth and invasion of pancreatic cancer cells (28). *ZEB2-AS1* boosted laryngeal squamous cell cancer development via modulating *miR-6840-3p/PLXNB1* axis (29). In this study, we found, through bioinformatics analysis, that there existed binding sites between *miR-582-5p* and *ZEB2-AS1*. Dual-luciferase reporter gene assay validated that *ZEB2-AS1* could sponge *miR-582-5p*. Additionally, *miR-582-5p* could weaken the effect of *ZEB2-AS1* on HCC cell multiplication, migration, invasion and apoptosis. Therefore, we concluded that *ZEB2-AS1* participated in facilitating HCC cell multiplication, migration, invasion and suppressing apoptosis via targeting *miR-582-5p*.

FOXC1 gene is located on chromosome 6p25, and it functions as a transcription factor (30). The FOX family partakes in various biological processes, for instance, embryonic development, cell cycle regulation, metabolic control, stem cell niche maintenance and signal transduction (31). *FOXC1* takes part in the progression of various tumors, and highly expressed *FOXC1* is strongly associated with the cancer patient poor prognosis (32). *FOXC1* expression was increased in lung cancer and *FOXC1* facilitated lung cancer cell proliferation and invasion, and its high expression was related to the low survival rate of lung cancer patients (33). In colorectal cancer, *FOXC1* contributed to chemoresistance and it facilitated tumor growth by regulating the *miR-31-5p/LATS2* pathway (34). A previous study showed that dysregulation of *miR-582-5p/FOXC1* axis could inhibit migration and invasion of salivary adenoid cystic cancer cells (22). In this study, with the TargetScan database, it was revealed that there existed a binding site between *miR-585-5p* and *FOXC1* 3′UTR. It was further validated by dual-luciferase reporter gene assay that *miR-582-5p* could bind to *FOXC1* 3′-UTR. Furthermore, overexpression of *ZEB2-AS1* or knock-down of *miR-582-5p* was able to remarkably up-regulate *FOXC1* expression. Therefore, we concluded that *ZEB2-AS1* was able to participate in regulating HCC progression via targeting *miR-582-5p/FOXC1* axis. Our work also partly explained the mechanism of *FOXC1* dysregulation in HCC.

Conclusion

Collectively, *ZEB2-AS1* promoted HCC cell proliferation, migration and invasion via modulating the *miR-582-5p/FOXC1* axis. Our study helps elucidate the mechanism underlying HCC development, in addition to presenting potential treatment targets and biomarkers for HCC.

Acknowledgments

This work is supported by Wuhan Science and Technology Bureau, No. 2017060201010154. The data used to support the findings of this study are available from the corresponding author upon request. The authors declare that they have no competing interests.

Authors' Contributions

SM.W., J.C.; Conceived and designed the experiments. Y.L., YY.T.; Performed the experiments. Q.L.; Supervised the experiments. L.X.; Analysed the data. J.C.; Wrote the manuscript, which was revised by SM.W. All authors have read and approved the final manuscript.

References

1. Wang D, Bai T, Chen G, Liu J, Chen M, Zhao Y, et al. Upregulation of long non-coding RNA FOXP4-AS1 and its regulatory network in hepatocellular carcinoma. Onco Targets Ther. 2019; 12: 7025-7038.
2. Liu J, Li W, Zhang J, Ma Z, Wu X, Tang L. Identification of key genes and long non-coding RNA associated ceRNA networks in hepatocellular carcinoma. PeerJ. 2019; 7: e8021.
3. Hartke J, Johnson M, Ghabril M. The diagnosis and treatment of hepatocellular carcinoma. Semin Diagn Pathol. 2017; 34(2): 153-159.
4. Tang X, Feng D, Li M, Zhou J, Li X, Zhao D, et al. Transcriptomic analysis of mRNA-lncRNA-miRNA interactions in hepatocellular carcinoma. Sci Rep. 2019; 9: 16096.
5. Tong MJ, Rosinski AA, Huynh CT, Raman SS, Lu DS. Long-term survival after surveillance and treatment in patients with chronic viral hepatitis and hepatocellular carcinoma. Hepatol Commun. 2017; 1(7): 595-608.
6. Su Y, Lv X, Yin W, Zhou L, Hu Y, Zhou A, et al. CircRNA Cdr1as functions as a competitive endogenous RNA to promote hepatocellular carcinoma progression. Aging (Albany NY). 2019; 11(9): 8182-8203.
7. Tiansheng G, Junming H, Xiaoyun W, Peixi C, Shaoshan D, Qianping C. LncRNA metastasis-associated lung adenocarcinoma transcript 1 promotes proliferation and invasion of non-Small cell lung cancer cells via down-regulating miR-202 expression. Cell J. 2020; 22(3): 375-385.
8. Quinn JJ, Chang HY. Unique features of long non-coding RNA biogenesis and function. Nat Rev Genet. 2016; 17(1): 47-62.
9. Peng WX, Koirala P, Mo YY. LncRNA-mediated regulation of cell signaling in cancer. Oncogene. 2017; 36(41): 5661-5667.
10. Liu F, Yuan JH, Huang JF, Yang F, Wang TT, Ma JZ, et al. Long noncoding RNA FTX inhibits hepatocellular carcinoma proliferation and metastasis by binding MCM2 and miR-374a. Oncogene. 2016; 35(41): 5422-5434.
11. Tang X, Zhang W, Ye Y, Li H, Cheng L, Zhang M, et al. LncRNA HOTAIR contributes to sorafenib resistance through suppressing miR-217 in hepatic carcinoma. Biomed Res Int. 2020; 2020: 9515071.
12. Kou JT, Ma J, Zhu JQ, Xu WL, Liu Z, Zhang XX, et al. LncRNA NEAT1 regulates proliferation, apoptosis and invasion of liver cancer. Eur Rev Med Pharmacol Sci. 2020; 24(8): 4152-4160.
13. Guo X, Jing YM, Lou HZ, Lou QA. Effect and mechanism of long non-coding RNA ZEB2-AS1 in the occurrence and development of colon cancer. Math Biosci Eng. 2019; 16(6): 8109–8120.
14. Lan T, Chang L, Wu L, Yuan Y. Downregulation of ZEB2-AS1 decreased tumor growth and metastasis in hepatocellular carcinoma. Mol Med Rep. 2016; 14(5): 4606-4612.
15. Stavast CJ, Erkeland SJ. The non-canonical aspects of microRNAs: many roads to gene regulation. Cells. 2019; 8(11): 1465.
16. Tian Y, Guan Y, Su Y, Luo W, Yang G, Zhang Y. MiR-582-5p inhibits bladder cancer-genesis by suppressing TTK expression. Cancer Manag Res. 2020; 12: 11933-11944.
17. Zhang Y, Huang W, Ran Y, Xiong Y, Zhong Z, Fan X, et al. miR-582-5p inhibits proliferation of hepatocellular carcinoma by targeting CDK1 and AKT3. Tumour Biol. 2015; 36(11): 8309-8316.
18. Dai W, Meng X, Mo S, Xiang W, Xu Y, Zhang L, et al. FOXE1 represses cell proliferation and Warburg effect by inhibiting HK2 in colorectal cancer. Cell Commun Signal. 2020; 18(1): 7.
19. Lee YH, Lee HT, Chen CL, Chang CH, Hsu CY, Shyu WC. Role of FOXC1 in regulating APSCs self-renewal via STI-1/PrPC signaling. Theranostics. 2019; 9(22): 6443-6465.
20. Lin YJ, Shyu WC, Chang CW, Wang CC, Wu CP, Lee HT, et al. Tumor hypoxia regulates forkhead box C1 to promote lung cancer progression. Theranostics. 2017; 7(5): 1177-1191.
21. Huang W, Chen Z, Zhang L, Tian D, Wang D, Fan D, et al. Interleukin-8 induces expression of FOXC1 to promote transactivation of CXCR1 and CCL2 in hepatocellular carcinoma cell lines and formation of metastases in mice. Gastroenterology. 2015; 149(4):1053-1067.
22. Wang WW, Chen B, Lei CB, Liu GX, Wang YG, Yi C, et al. miR-582-5p inhibits invasion and migration of salivary adenoid cystic carcinoma cells by targeting FOXC1. Jpn J Clin Oncol. 2017; 47(8): 690-698.
23. Wang YL, Liu JY, Yang JE, Yu XM, Chen ZL, Chen YJ, et al. LncUCID promotes G1/S transition and hepatoma growth by preventing DHX9-mediated CDK6 down-regulation. Hepatology. 2019; 70(1): 259-275.
24. Guo Y, Hu Y, Hu M, He J, Li B. Long non-coding RNA ZEB2-AS1 promotes proliferation and inhibits apoptosis in human lung cancer cells. Oncol Lett. 2018; 15(4): 5220-5226.
25. Qian Y, Wu X, Wang H, Hou G, Han X, Song W. MicroRNA-4290 suppresses PDK1-mediated glycolysis to enhance the sensitivity of gastric cancer cell to cisplatin. Braz J Med Biol Res. 2020; 53(5): e9330.
26. Huang S, Zou C, Tang Y, Wa Q, Peng X, Chen X, et al. miR-582-

3p and miR-582-5p suppress prostate cancer metastasis to bone by repressing TGF-β signaling. Mol Ther Nucleic Acids. 2019; 16: 91-104.
27. Li L, Ma L. Upregulation of miR-582-5p regulates cell proliferation and apoptosis by targeting AKT3 in human endometrial carcinoma. Saudi J Biol Sci. 2018; 25(5): 965-970.
28. Gao H, Gong N, Ma Z, Miao X, Chen J, Cao Y, et al. LncRNA ZEB2-AS1 promotes pancreatic cancer cell growth and invasion through regulating the miR-204/HMGB1 axis. Int J Biol Macromol. 2018; 116: 545-551.
29. Xu Q, Liu H, Yu B, Chen W, Zhai L, Li X, et al. Long noncoding RNA ZEB2-AS1 facilitates laryngeal squamous cell carcinoma progression by miR-6840-3p/PLXNB1 axis. Onco Targets Ther. 2019; 12: 7337-7345.
30. Elian FA, Yan E, Walter MA. FOXC1, the new player in the cancer sandbox. Oncotarget. 2017; 9(8): 8165-8178.
31. Quintero-Ronderos P, Laissue P. The multisystemic functions of FOXD1 in development and disease. J Mol Med (Berl). 2018; 96(8): 725-739.
32. Yang Z, Jiang S, Cheng Y, Li T, Hu W, Ma Z, et al. FOXC1 in cancer development and therapy: deciphering its emerging and divergent roles. Ther Adv Med Oncol. 2017; 9(12): 797-816.
33. Bai X, Shao J, Zhou S, Zhao Z, Li F, Xiang R, et al. Inhibition of lung cancer growth and metastasis by DHA and its metabolite, RvD1, through miR-138-5p/FOXC1 pathway. J Exp Clin Cancer Res. 2019; 38(1): 479.
34. Hsu HH, Kuo WW, Shih HN, Cheng SF, Yang CK, Chen MC, et al. FOXC1 regulation of miR-31-5p confers oxaliplatin resistance by targeting LATS2 in colorectal cancer. Cancers (Basel). 2019; 11(10): 1576.

Original Article

LINC00265 Promotes Metastasis and Progression of Hepatocellular Carcinoma by Interacting with E2F1 at The Promoter of *CDK2*

Beihai Ge, Ph.D.[1], Xian Zhang, M.Sc.[1], Wei Zhou, B.S.[2], Yun Mo, B.S.[1], Zhou Su, B.S.[1], Guolong Xu, B.S.[1], Qiang Chen, M.Sc.[3*]

1. Department of Neurology, Guangxi Zhuang Autonomous Region Brain Hospital, Liuzhou, Guangxi, China
2. Department of Neurosurgery, Guangxi Zhuang Autonomous Region Brain Hospital, Liuzhou, Guangxi, China
3. Department of Psychiatry, Guangxi Zhuang Autonomous Region Brain Hospital, Liuzhou, Guangxi, China

**Corresponding Address: Department of Psychiatry, Guangxi Zhuang Autonomous Region Brain Hospital, Liuzhou, Guangxi, China*
Email: cq3846@126.com

Received: 07/April /2021, Accepted: 18/July/2021

Abstract

Objectives: This study aimed to explore biological function of long intergenic non-protein coding RNA 265 (LINC00265) in hepatocellular carcinoma (HCC) cells, and evaluate its potential function as a biomarker.

Materials and Methods: In this experimental study, GEPIA database and Kaplan-Meier Plotter database were employed to analyze LINC00265 expression in HCC tissue samples and its predicting value for prognosis. LINC00265 expression in HCC tissues and cells was detected by quantitative real-time polymerase chain reaction (qRT-PCR). After overexpressing and knocking-down of LINC00265 in HCC cells, cell counting kit-8 (CCK-8) and 5-Ethynyl-2'-deoxyuridine (EdU) assays were adopted to detect proliferation of HCC cells. Transwell assay was used to detect migration and invasion of HCC cells. Interaction of LINC00265 with E2F transcription factor 1 (E2F1) was verified by the catRAPID online analysis tool, RNA pull-down experiment and RNA binding protein immunoprecipitation (RIP) assay. Binding of E2F1 to the promoter region of cyclin-dependent kinases 2 (*CDK2*) was detected by dual-luciferase reporter assay and chromatin immunoprecipitation. Regulatory effects of LINC00265 and E2F1 on *CDK2* expression were probed by Western blot.

Results: LINC00265 expression was increased in HCC tissues and cells. LINC00265 overexpression promoted proliferation, migration and invasion of HCC cells, and knocking-down LINC00265 worked oppositely. LINC00265 could bind to E2F1 and it could enhance combination of E2F1 and *CDK2* promoter regions, thus promoting *CDK2* transcription. LINC00265 overexpression promoted expression of *CDK2* in HCC cells.

Conclusion: Our data suggested that LINC00265 can promote malignant behaviors of HCC cells by recruiting E2F1 to the promoter region of *CDK2*.

Keywords: Cyclin-Dependent Kinases 2, E2F Transcription Factor 1, Hepatocellular Carcinoma, LINC00265, Proliferation

Cell Journal(Yakhteh), Vol 24, No 6, June 2022, Pages: 294-301

Citation: Ge B, Zhang X, Zhou W, Mo Y, Su Zh, Xu G, Chen Q. LINC00265 promotes metastasis and progression of hepatocellular carcinoma by interacting with E2F1 at the promoter of CDK2. Cell J. 2022; 24(6): 294-301. doi: 10.22074/cellj.2022.8035.

Introduction

Liver cancer is identified as the sixth most prevailing tumor in the globe and the fourth-largest cause of cancer-related death, among which hepatocellular carcinoma (HCC) accounts for about 90% cases (1). At present, the main treatment methods for HCC include surgical resection, liver transplantation and radiofrequency ablation (2). Although treatment for HCC has progressed in recent years, the overall 5-years survival rate of HCC patients is only about 7% (3). Therefore, it is particularly important to explore pathogenesis of HCC as well as providing new ideas and targets for clinical diagnosis and treatment of HCC.

Long non-coding RNAs (lncRNAs), recognized as eukaryotic transcripts with over 200 nucleotides in length, are devoid of protein-coding ability. lncRNA regulates gene expression at the transcriptional and post-transcriptional levels, thus participating in regulating some biological processes related to diseases (4, 5). The scientific consensus is that a variety of lncRNAs are abnormally expressed in various tumors and lncRNAs can serve as tumor promoters or suppressors to participate in the progression of tumors (6-8). The cancer genome atlas (TCGA) database shows that long intergenic non-protein coding RNA 265 (LINC00265), an important member of lncRNA family, is overexpressed in colorectal cancer (CRC) tissues, which is associated with the poor prognosis of CRC patients; knocking-down of LINC00265 inhibited viability and invasion of CRC cells, induced cell cycle arrest and promoted apoptosis (9). Another study reported that LINC00265 overexpression promoted glycolysis and lactic acid production of CRC cells by up-regulating TRIM44 expression, thus accelerating growth of the tumor cells (10). Instead, biological function and molecular mechanism of LINC00265 in HCC warrant further investigation.

E2F transcription factor 1 (E2F1) is involved in regulating various biological processes, including cell proliferation, differentiation and apoptosis. E2F1 can potentiate the malignant biological behaviors of HCC

cells (11). Cyclin-dependent kinases 2 (*CDK2*) is vital in cell cycle regulation and partakes in a series of biological processes, including DNA damage repair, intracellular transport, protein degradation, signal transduction, DNA and RNA anabolism and translation (12). Previous studies showed that knocking-down of *CDK2* can effectively inhibit the progression of lung cancer, breast cancer and HCC (13-15).

The present study aimed to investigate the role and mechanism of LINC00265/E2F1/CDK2 axis in HCC.

Materials and Methods

Tissue samples

In this experimental study, with the approval of the Ethics Committee of Guangxi Zhuang Autonomous Region Brain Hospital (Guangxi, China; Approval No. 20160105) and the informed consent of all patients, we selected 46 HCC patients who were treated in Guangxi Zhuang Autonomous Region Brain Hospital and collected the resected cancer tissues and their corresponding adjacent tissues, respectively. The tissues were stored at -80˚C after surgical resection. All patients had complete clinical and clinicopathological data. They did not receive any neoadjuvant treatment, such as radiotherapy or chemotherapy, before the surgery.

Cell culture and transfection

Human normal hepatocytes (THLE-3) and HCC cell lines (BEL-7402, Hep3B, and Huh7) were purchased from the Cell Center of the Chinese Academy of Sciences (Shanghai, China). HCC cell line HCCLM3 was obtained from the China Center for Type Culture Collection, (CCTCC, Wuhan, China). The cells were inoculated into Roswell Park Memorial Institute (RPMI)-1640 medium (Thermo-Fisher Scientific, USA) with 10% fetal bovine serum (FBS, Thermo-Fisher Scientific, USA), and cultured at 37˚C in 5% CO_2. The cells were sub-cultured every 2-3 days and the cells in logarithmic growth phase were harvested for the subsequent experiment. E2F1 overexpression plasmid (oe-E2F1), *CDK2* overexpression plasmid (oe-*CDK2*), LINC00265 overexpression plasmid (oe-LINC00265), negative control of overexpression plasmids (oe-NC), siRNAs targeting *CDK2* (si-*CDK2*), siRNAs targeting E2F1 (si-E2F1) and negative control of siRNA (si-NC) were constructed by GenePharma (Shanghai, China). For transfection, BEL-7402 and Hep3B cells were transferred into a 6-well cell plate at a density of 3×10^5 cells/well. They were cultured at 37˚C in 5% CO_2 for 24 hours. Subsequently, the cells were transfected by Lipofectamine® 3000 (Invitrogen, USA). Transfection efficiency was verified by quantitative real-time polymerase chain reaction (qRT-PCR) and Western blot after 48 hours.

Quantitative real-time polymerase chain reaction

Total RNA of tissues and cells was extracted by TRIzol reagent (Invitrogen), followed by detection of purity and reverse transcription into cDNA. Then, qRT-PCR was performed with SYBR®Premix-Ex-Taq™ (Takara, Japan) on the ABI7300 system (Thermo-Fisher Scientific, USA). Relative expression of LINC00265 was calculated by $2^{-\Delta\Delta Ct}$ method using GAPDH as the internal reference. The utilized primer sequences are as following:

LINC00265-

F: 5′-GGAAGAGAGACTGACTGGGC-3′
R: 5′-GTTTCGCTGTCACCCCTCTG-3′

GADPH-

F: 5′-GTCAACGGATTTGGTCTGTATT-3′
R: 5′-AGTCTTCTGGGTGGCAGTGAT-3′

Cell counting kit-8 (CCK-8) assay

BEL-7402 and Hep3B cells, in the logarithmic growth phase, were trypsinized by trypsin, with the cell density adjusted to 2×10^4 cells/ml. The cells were then inoculated into 96-well plates with 100 µl of cell suspension per well, followed by culturing for 24, 48, 72 and 96 hours, respectively. After that, the cells were incubated with 10 µl CCK-8 solution (Dojindo Molecular Technologies, Japan). After 1 hour, value of optical density at 450 nm ($OD_{450\ nm}$) was measured by a microplate reader.

5-Ethynyl-2’-deoxyuridine (EdU) experiment

BEL-7402 and Hep3B cells in the experimental and the control groups were transferred into the 24-well plate, incubated with 200 µl of 5 µmol/L EdU medium (Beyotime Biotechnology, China) for 2 hours and then immersed in phosphate buffered saline (PBS). Next, the cells were fixed with paraformaldehyde for 10 minutes at ambient temperature and incubated with 200 µl of 2 mg/ml glycine for 5 minutes. They were subsequently immersed in PBS on the shaking table for 5 minutes. After that, 100 µl PBS with 0.5% Triton X-100 was dripped into each well, followed by incubation of them for 10 minutes on a shaking table and rinsing with PBS twice for 5 minutes each time. Subsequently, the above cells were stained with Apollo at room temperature for 30 minutes and then incubated with 1×Hoechst 33342 DNA staining solution for 20 minutes. After washing with PBS, the cells were observed and number of the cells was counted under a fluorescent microscope.

Transwell experiment

BEL-7402 and Hep3B cells, trypsinized with 0.25% trypsin, were centrifuged, resuspended and then dispersed. Matrigel (Corning, China) was adopted for invasion experiments, but not for migration experiments. The transfected cells (5×10^4 cells/well) were transferred into the upper compartment of the Transwell chamber and then 500 µl of complete medium containing 10% serum was added to the lower compartment, with which the cells were cultured at 37˚C for 24 hours. Then, the cells which failed to migrate or invade were removed from the upper surface of the membrane. The cells which passed through membrane were fixed with 4% paraformaldehyde for 10

minute, and stained with 0.5% crystal violet. After rinsing with tap water, the membrane was observed under an inverted microscope and number of the cells was counted.

Subcellular fractionation

The NE-PER™ Nuclear and Cytoplasmic Extraction Reagent (Thermo-Fisher Scientific, USA) was used to isolate and collect cytoplasmic and nuclear fractions of Hep3B and BEL-7402 cells. Then, RNA expression levels of LINC00265, U6 (nuclear control transcript) and GAPDH (cytoplasmic control transcript) were analyzed by qRT-PCR.

RNA pull-down assay

To detect interaction of LINC00265 with E2F1, RNA pull-down assay was performed using a Magnetic RNA-Protein Pull-Down Kit (Thermo Fisher Scientific, USA). The protein extracts of HCC cells mixed with biotinylated LINC00265 were incubated with magnetic beads. Ultimately, the eluted proteins from magnetic beads were harvested, and Western blot was performed to detect the protein enrichment.

RNA binding protein immunoprecipitation (RIP) experiment

RIP assay was performed with a Magna RIP™ RIP kit (Millipore, USA). Briefly, BEL-7402 and Hep3B cells in the logarithmic growth phase were suspended with RIP buffer to prepare the cell lysate. Then the lysate was incubated with magnetic beads coupled with anti-E2F1 antibody and negative control IgG. Next, RNA in the lysate was immunoprecipitated and purified and cDNA was obtained by reverse transcription. LINC00265 immunoprecipitation enrichment was detected by qRT-PCR.

Chromatin immunoprecipitation (ChIP) assay

Briefly, BEL-7402 and Hep3B cells were fixed with formaldehyde for 10 minutes. The ultrasonic breaker was set to 10 seconds per ultrasonic cycle with 10-second intervals with 15 cycles to break the chromatin. The product was centrifuged at 12000 g at 4˚C for 10 minutes. The supernatant was collected and divided into two test tubes, which were incubated with mouse IgG (1:100, Abcam, China) or anti-E2F1 antibody (2 μg/ml of cell lysate, Abcam, China) at 4˚C for overnight. Then, DNA-protein complex was precipitated by Protein Agarose/Sepharose. Subsequently, the cross-linking was reversed overnight at 65˚C and DNA fragments were extracted by phenol/chloroform method. Next, qRT-PCR was conducted to amplify *CDK2* sequence with the *CDK2*-specific primers and determine E2F1 binding to the *CDK2* promoter region.

Dual-luciferase reporter assay

Briefly, wild-type *CDK2* and mutant *CDK2* target fragments were constructed and integrated into the pGL3 vector (Promega, USA) to construct pGL3-*CDK2*-wild type (*CDK2*-WT) and pGL3-*CDK2*-mutant (*CDK2*-MUT) reporter vector. BEL-7402 and Hep3B cells were co-transfected with *CDK2*-WT (or *CDK2*-MUT) and oe-NC (or oe-E2F1). After 48 hours, luciferase activity was determined. The firefly luciferase activity was normalized to Renilla luciferase activity.

Western blot

Total protein of the cells was extracted with RIPA lysis buffer (Beyotime, China), with the protein concentration determined by the BCA method. After denaturation, the protein samples were loaded into each well (20 μg per lane), separated by SDS-PAGE and electrically transferred to the polyvinylidene fluoride (PVDF) membrane. After that, the membrane was blocked with tris buffered saline with tween 20 (TBST) solution containing 5% skimmed milk at ambient temperature for 1 hour. The PVDF membrane was then incubated with the primary antibodies including anti-*CDK2* antibody (1:1000), anti-E2F1 antibody (1:1000) and anti-GAPDH antibody (1:1000, all from Abcam, China) overnight at 4˚C, followed by washing in TBST for 4 times, each time for 8 minutes. Next, the PVDF membrane was incubated with the corresponding secondary goat anti-rabbit antibody (1:2000, Abcam, China) for 1.5 hours at room temperature, followed by rinsing with TBST 4 times, each time for 8 minutes. Ultimately, X-ray imaging was performed with ECL Western blot Substrate kit (Thermo-Fisher Scientific, USA) to show the protein bands.

Statistical analysis

All experiments were conducted in triplicate. All data were analyzed by SPSS 20.0 statistical analysis software (SPSS Inc., Chicago, IL, USA). Data were expressed by mean ± standard deviation ($x \pm SD$). To compare two groups, one-sample Kolmogorov-Smirnov test was used to test for normality distribution. For the data which were normally distributed, an independent sample t test was used. For the data with skewed distribution, Mann-Whitney test was used. To make the comparison among three or more groups, a One-way ANOVA test was used, and if there was a significant difference, Turkey's post-hoc test was performed to make the comparison between the two groups. For enumeration data, they were expressed in a contingency table, and subsequently chi-square test and Fisher's exact test were adopted for the comparison of the two groups. Statistically, $P<0.05$ was considered significant.

Results

LINC00265 was highly expressed in HCC

By searching GEPIA database (http://gepia.cancer-pku.cn/), we observed that LINC00265 expression was observably raised in the HCC tissue samples, compared to the normal liver tissues (Fig.1A). Consistently, qRT-PCR showed that LINC00265 expression in the HCC tissues was significantly elevated against the adjacent tissues (Fig.1B). Receiver operating characteristic (ROC) curve analysis was used to evaluate diagnostic accuracy of LINC00265. The results suggested that LINC00265 could be considered as a discriminative biomarker for HCC with 97.83% sensitivity and 91.30% specificity in the optimal cutoff value of 1.49

(AUC=0.98, P<0.001, Fig.1C). Additionally, GEPIA database and Kaplan-Meier Plotter database (http://kmplot.com/) showed that high expression of LINC00265 was associated with shorter disease-free survival time of HCC patients (Fig. S1A, B, See Supplementary Online Information at www.celljournal.org). Furthermore, LINC00265 expression in four HCC cell lines, compared to that in THLE-3 cells, was markedly up-regulated (Fig.1D). Chi-square test highlighted that LINC00265 expression was associated with increased tumor node metastasis (TNM) stage of the patients (Table 1), which indicated that LINC00265 might be pivotal in facilitating cancer progression in HCC.

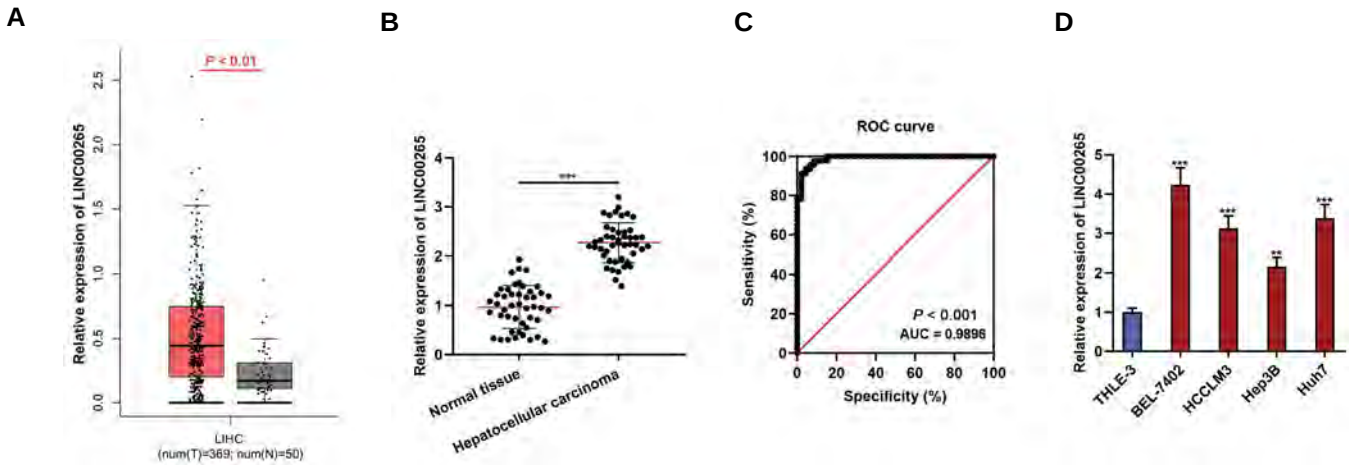

Fig.1: Expression characteristics of LINC00265 in HCC tissues and cells. **A.** Expression of LINC00265 in HCC tissues (red column, n=369) and normal tissues (grey column, n=50) was analyzed by the GEPIA database. **B.** Expression of LINC00265 in HCC tissues (n=46) and normal tissues (n=46) was detected by qRT-PCR. **C.** ROC analysis of the value of LINC00265 expression for distinguishing HCC tissues from normal tissues. **D.** Expression of LINC00265 in human normal liver cells THLE-3 and four human HCC cell lines (BEL-7402, HCCLM3, Hep3B and Huh7) was detected by qRT-PCR. All experiments were repeated three times with three replicates for each repeat. LIHC; Liver hepatocellular carcinoma, T; Tumor, N; Normal, HCC; Hepatocellular carcinoma, qRT-PCR; Quantitative real-time polymerase chain reaction, ROC; Receiver operating characteristic, **; P<0.01, and ***; P<0.001.

Table 1: Association of clinicopathological features with expression of LINC00265 in HCC tissues

Pathological parameters	Number	LINC00265 expression		$\chi 2$	P value
	(n=46)	High (n=23)	Low (n=23)		
Gender				0. 5111	0. 4746
Male	36	19	17		
Female	10	4	6		
Age (Y)				2. 6807	0. 1015
<50	13	4	9		
≥50	33	19	14		
Cirrhosis				1. 0952	0. 2953
Absent	42	22	20		
Present	4	1	3		
Tumor size (cm)				2. 4731	0. 1158
<5	15	5	10		
>5	31	18	13		
TNM stage				7. 2632	0. 0070*
I+II	19	5	14		
III+IV	27	18	9		
Tumor multiplicity				0. 3538	0. 5519
Single	20	9	11		
Multiple	26	14	12		
Degree of differentiation				1. 4603	0. 2269
Low, medium	28	16	12		
High	18	7	11		

HCC; Hepatocellular carcinoma, TNM; Tumor node metastasis, and *; P<0.05.

Effects of LINC00265 on the malignant biological behaviors of HCC cells

To pinpoint biological function of LINC00265 in HCC cells, Hep3B and BEL-7402 cells were used for subsequent experiments. We transfected LINC00265 overexpression plasmid into Hep3B cells. We also transfected si-LINC00265#1 and si-LINC00265#2 into BEL-7402 cells. Transfection efficiency verified by qRT-PCR (Fig.2A). CCK-8, EdU and Transwell assays indicated that as against the control group, LINC00265 overexpression demonstrably promoted proliferation, migration and invasion of Hep3B cells, while knocking-down LINC00265 worked oppositely in BEL-7402 cells (Fig.2B-F).

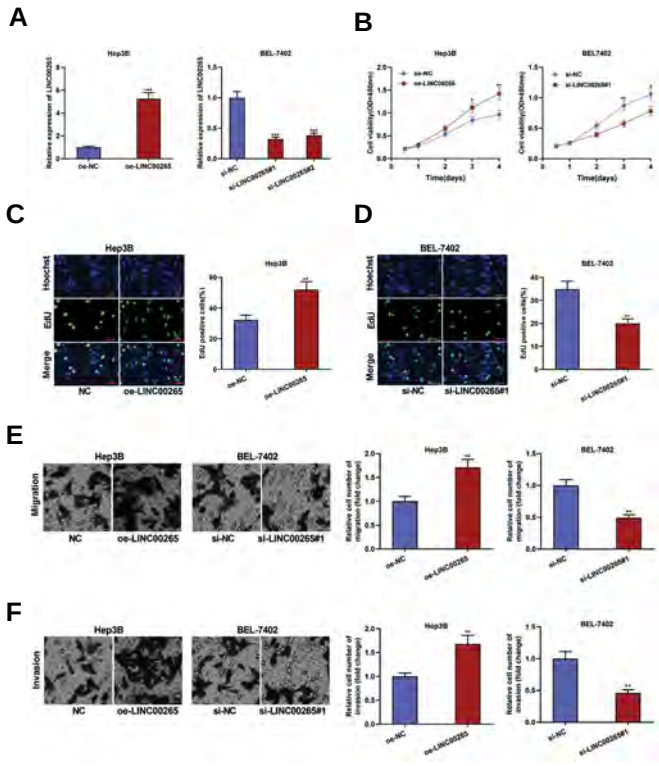

Fig.2: Effects of LINC00265 on proliferation, migration and invasion of HCC cells. **A.** LINC00265 overexpression plasmids and si-LINC00265 were transfected into Hep3B and BEL-7402 cells, respectively. The transfection efficiency was examined by qRT-PCR. **B-D.** After transfection, CCK-8 and EdU assays were used to detect proliferation of Hep3B and BEL-7402 cells. **E, F.** After transfection, Transwell assay was used to detect migration and invasion of Hep3B and BEL-7402 cells (scale bars: 50 μm). All experiments were repeated three times with three replicates for each repeat. HCC; Hepatocellular carcinoma, qRT-PCR; Quantitative real-time polymerase chain reaction, *; P<0.05, **; P<0.01, and ***; P<0.001.

Interaction of LINC00265 with E2F1

Data from the LncMAP database (http://bio-bigdata.hrbmu.edu.cn/LncMAP/) predicted that LINC00265 could promote *CDK2* transcription by recruiting E2F1 to the promoter region of *CDK2* gene (Fig.3A). qRT-PCR showed that LINC00265 mainly existed in the nucleus of HCC cells (Fig.3B), suggesting it may function as a transcriptional regulator. Then, we searched catRAPID database to predict binding domain of LINC00265 and E2F1. It was determined that LINC00265 might interact with E2F1 (Fig.3C, D). RNA pull-down assay indicated that E2F1 was highly expressed in the LINC00265 biotinylated protein group, but not in the NC-biotinylated group (Fig.3E). RIP assay showed that LINC00265 was remarkably enriched by anti-E2F1 antibody both in Hep3B and BEL-7402 cells, compared to the IgG group (Fig.3F). Collectively, these data suggested that LINC00265 could interact with E2F1 to regulate its biological function.

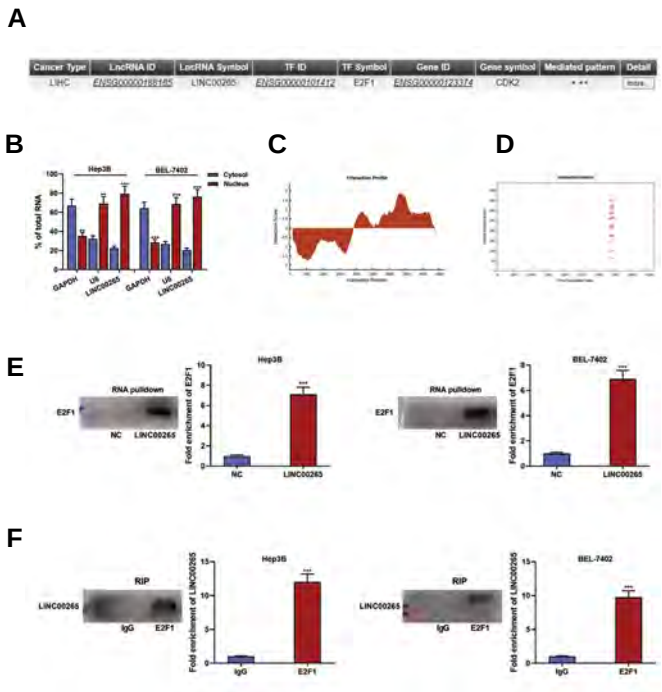

Fig.3: Interactions of LINC00265 with E2F1. **A.** LncMAP database was adopted to predict the binding relationship among LINC00265, E2F1 and *CDK2*. **B.** Subcellular localization of LINC00265 in BEL-7402 and Hep3B cells was detected by qRT-PCR. **C.** Interaction profiles between LINC00265 and E2F1 were predicted by catRAPID database. **D.** Interaction matrix between LINC00265 and E2F1 was predicted by catRAPID database. **E.** Interaction between LINC00265 and E2F1 in BEL-7402 and Hep3B cells was detected by RNA pull-down assay. **F.** Interaction between LINC00265 and E2F1 in BEL-7402 and Hep3B cells was validated by RIP assay. All experiments were repeated three times with three replicates for each repeat. qRT-PCR; Quantitative real-time polymerase chain reaction, **; P<0.01, and ***; P<0.001.

LINC00265 promoted *CDK2* transcription by recruiting E2F1

We then analyzed Promo Database and found that E2F1 could bind to the *CDK2* promoter sequence (Fig.4A). The data in StarBase database (http://starbase.sysu.edu.cn/) showed that, in HCC samples, E2F1 expression was positively interrelated with *CDK2* expression and LINC00265 was positively regulated by expressing *CDK2* (Fig.4B, C). To clarify whether E2F1 can promote *CDK2* transcription, we used E2F1 specific antibody to conduct CHIP-qPCR in Hep3B and BEL-7402 cells. Findings demonstrated that there was a remarkable

enrichment of *CDK2* promoter sequence in the protein-DNA complex containing E2F1 (Fig.4D). In addition, LINC00265 overexpression in HCC cells enhanced binding between E2F1 and *CDK2* (Fig.4E). Next, the binding sequence was truncated or mutated, and dual-luciferase reporter gene assay highlighted that site 3 was the specific site for the binding relationship between E2F1 and *CDK2* promoter region (Fig.4F, G). Western blot and qRT-PCR authenticated that, in Hep3B cells, LINC00265 overexpression could markedly increase *CDK2* expression, while knocking-down of E2F1 counteracted promoting effects of LINC00265 overexpression on *CDK2* expression (Fig.4H, I), in BEL-7402 cells, LINC00265 depletion repressed CKD2 expression, which was partly reversed by E2F1 overexpression. These data suggested that LINC00265 positively regulated *CDK2* expression via modulating E2F1.

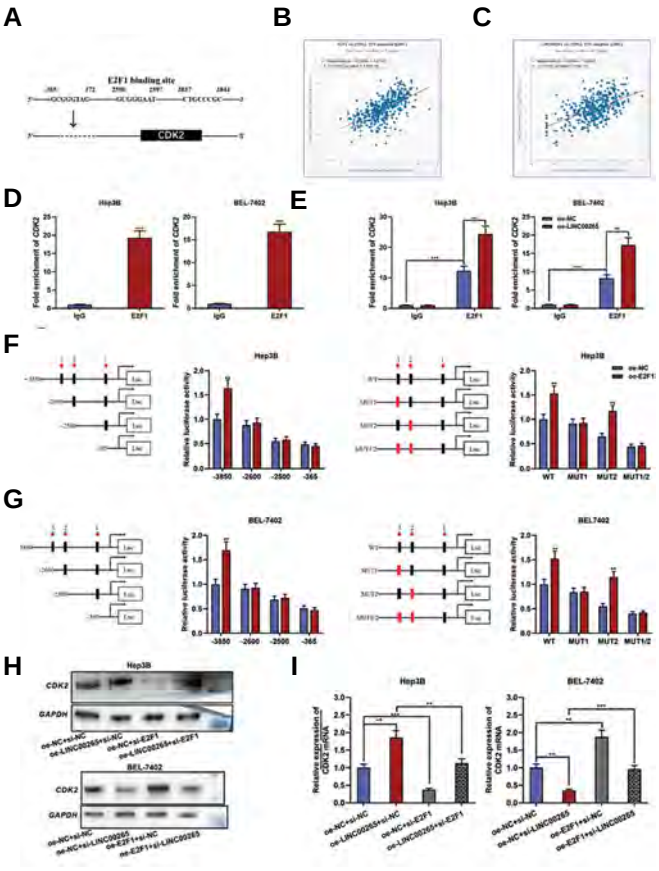

Fig.4: Effects of LINC00265/E2F1 on the expression level of *CDK2* in HCC cells. **A.** PROMO databases were used to predict the binding sites between E2F1 and *CDK2* promoter sequences. **B, C.** Correlations between E2F1 and *CDK2* expressions, LINC00265 and *CDK2* expressions were analyzed by the StarBase database. **D.** Binding relationship between E2F1 and *CDK2* promoter region in Hep3B and BEL-7402 cells was detected with ChIP-qPCR assay. **E.** Effects of LINC00265 on the binding between E2F1 and *CDK2* in Hep3B and BEL-7402 cells were detected by ChIP-qPCR assay. **F.** Dual-luciferase reporter assay was used to detect the specific binding sites between E2F1 and the *CDK2* promoter region in Hep3B cells (3, 2 and 1 respectively indicated site 3, site 2 and site 1). **G.** Dual-luciferase reporter assay was used to detect the specific binding sites between E2F1 and the *CDK2* promoter region in BEL-7402 cells (3, 2 and 1 respectively indicated site 3, site 2 and site 1). **H, I.** Western blot and qRT-PCR were used to detect regulatory effects of LINC00265 and E2F1 on *CDK2* expression in Hep3B and BEL-7402 cells. All experiments were repeated three times with three replicates for each repeat. HCC; Hepatocellular carcinoma, ChIP-qPCR; Chromatin immunoprecipitation (ChIP)-quantitative polymerase chain reaction (qPCR), **; P<0.01, and ***; P<0.001.

LINC00265 regulated proliferation, migration and invasion of HCC cells through the E2F1/*CDK2* axis

To verify the regulatory function of LINC00265 on proliferation, migration and invasion of HCC cells through E2F1/*CDK2* axis, we transfected LINC00265 overexpression plasmids, si-E2F1 and si-*CDK2* into Hep3B cells and si-LINC00265#1. Moreover, we transfected E2F1 overexpression plasmids and *CDK2* overexpression plasmids into BEL-7402 cells. Western blot and qRT-PCR proved that transfection was successful (Fig.5A, B). CCK-8, EdU and Transwell assays showed that LINC00265 overexpression could dramatically promote proliferation, migration and invasion of Hep3B cells, while knocking-down of E2F1 or *CDK2* could partially weaken these effects. Besides, knocking-down of LINC00265 could significantly inhibit malignant biological behaviors of BEL-7402 cells, while E2F1 or *CDK2* overexpression could partially reverse these effects (Fig.5C-F). These results further validated that biological function of LINC00265 in HCC cells were at least partly dependent on the E2F1/*CDK2* axis.

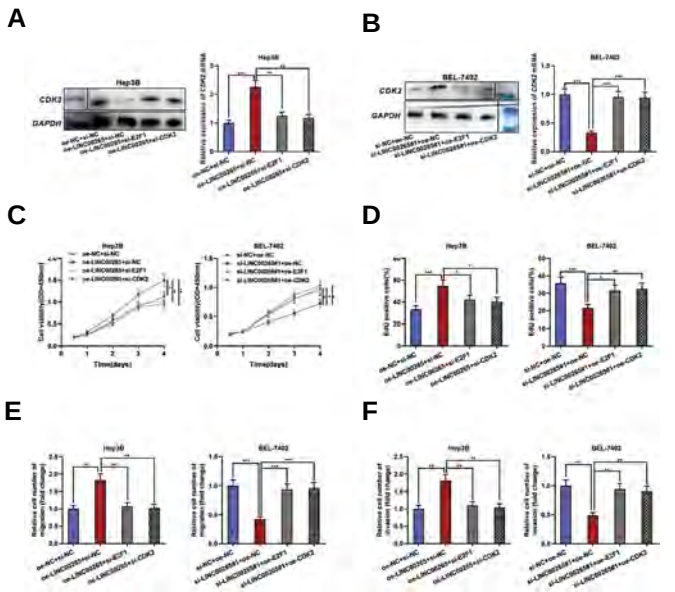

Fig.5: LINC00265 regulates proliferation, migration and invasion of HCC cells via E2F1/*CDK2* axis. **A, B.** LINC00265 overexpression plasmid, si-E2F1 or si-*CDK2* was transfected into Hep3B cells; si-LINC00265#1, E2F1 overexpression plasmid or *CDK2* overexpression plasmid was transfected into BEL-7402 cells. Transfection efficiency was detected by Western blot and qRT-PCR. **C, D.** After transfection, CCK-8 and EdU assays were used to detect proliferation of BEL-7402 and Hep3B cells. **E, F.** After transfection, migration and invasion of BEL-7402 and Hep3B cells were detected by Transwell assay. All experiments were repeated three times with three replicates for each repeat. HCC; Hepatocellular carcinoma, qRT-PCR; Quantitative real-time polymerase chain reaction, *; P<0.05, **; P<0.01, and ***; P<0.001.

Discussion

lncRNAs cannot encode protein due to the lack of open reading frame (16). LncRNAs were initially considered as "transcriptional noise". However, recent studies report that lncRNAs are crucial regulators in both physiological and pathological processes (17-19). Dysfunction of lncRNA features prominently in the pathogenesis of HCC (20).

LINC00265 expression is up-regulated in osteosarcoma, which is associated with the poor prognosis of patients; overexpression of LINC00265 promotes proliferation, migration, invasion and angiogenesis of osteosarcoma cells via up-regulating vav guanine nucleotide exchange factor 3 *(VAV3)* (21). Additionally, LINC00265 was highly expressed in the bone marrow and serum of patients with acute myeloid leukemia; LINC00265 overexpression could promote malignant biological behaviors of leukemia cells via activating the PI3K/AKT signaling pathway (22). In colorectal cancer, overexpression of LINC00265 recruited USP7 enzyme by up-regulating expression of *ZMIZ2*. Ubiquitination of USP7 enzyme activated β-catenin pathway, thus promoting progression of CRC (23). Furthermore, LINC00265 knock-down can inhibit gastric cancer cell proliferation *in vitro* (24). However, the role of LINC00265 in HCC remained unclear. In the present study, we reported for the first time that LINC00265 expression was elevated in HCC. This was significantly correlated with the unfavorable prognosis of HCC patients. Functionally, LINC00265 overexpression could markedly promote proliferation, migration and invasion of HCC cells, while knocking-down LINC00265 had opposite effects. These demonstrations suggested that LINC00265 was a potential biomarker and therapy target for HCC.

E2F1 is a member of the E2F family of cell cycle-related transcription factors (25). Reportedly, E2F1 functions as an oncogene in cancer biology (26). For example, E2F1 induces transcription of cell division cycle associated 5, thus activating AKT signaling pathway, promoting HCC cell proliferation and inhibiting apoptosis (27). Knocking-down of E2F1 can partially abolish promoting effects of SIRT5 on growth and invasion of HCC cells (28); E2F1 overexpression promoted transcription of *DEAD/H-box helicase 11* and activated PI3K/AKT/mTOR signaling pathway. This promoted the malignant biological behaviors of HCC cells (29). Previous studies reported that some lncRNAs can participate in regulating cancer progression via modulating the function of E2F1. Specifically, lncRNA DLX5-AS1 promoted transcription of *DLX6* by recruiting E2F1 to the promoter region of *DLX6*, and potentiated proliferation and invasion of endometrial cancer cells (30). In this study, we found that LINC00265 could interact with E2F1 and LINC00265 overexpression promoted *CDK2* transcription by recruiting E2F1 to the promoter region of *CDK2*. Our data suggested that LINC00265 is a novel regulator of the E2F1.

In eukaryotic cells, cyclin-dependent kinase (CDK) regulates initiation and progression of cell cycle, proliferation and apoptosis of cells (30, 31). *CDK2* consists of 298 amino acid residues and it can interact with different substances to regulate cell cycle progression (32). Besides, *CDK2* is associated with progression of various cancers (12, 33). For example, *CDK2* expression is up-regulated in gastric cancer, and depletion of *CDK2* expression inhibits the aerobic glycolysis of gastric cancer cells and promotes expression of tumor suppressor *SIRT5* (34); HOXA7 facilitates HCC progression via regulating *cyclin E1/CDK2* (35); suppressing S100P expression triggers down-regulation of *CDK2* expression, thus inhibiting mitosis of HCC cells (36). In this study, we found that overexpression of LINC00265 could enhance binding of E2F1 to the promoter region of *CDK2*. Thus this up-regulates *CDK2* expression and promotes proliferation, migration and invasion of HCC cells. These data partly explained mechanism of *CDK2* dysregulation in HCC.

Conclusion

In this study, we substantiated that LINC00265 expression is highly expressed in HCC, implying poor prognosis of HCC patients. We also demonstrated that LINC00265 regulated E2F1/*CDK2* axis, thereby promoting HCC cell proliferation, migration and invasion. Altogether, our data suggested that LINC00265 may act as a new screening biomarker and potential therapy target for HCC patients.

Acknowledgments

This study was supported by Guangxi Natural Science Foundation (General Program, No. 2020GXNSFAA297115). We also thank Hubei Yican Health Industry Co., Ltd. for its linguistic assistance during the preparation of this manuscript. The data used to support the findings of this study are available from the corresponding author upon request. The authors declare that they have no competing interests.

Authors' Contributions

Q.Ch.; Designed the experiments, the structure and the logical flow of the whole manuscript. B.G., X.Zh., W.Zh.; Conducted the most *in vitro* experiments. Y.M., Zh.S.; Collected the tissue samples. G.X.; Helped with literature reviewing and cell culture. All authors participated in the manuscript drafting. B.G., X.Zh., W.Zh., Q.Ch.; Are the main contributors. B.G., Q.Ch.; Reviewed the completed manuscript and made the final revisions. All authors read and approved the final manuscript.

References

1. Forner A, Reig M, Bruix J. Hepatocellular carcinoma. Lancet. 2018; 391(10127): 1301-1314.
2. Greten TF, Lai CW, Li G, Staveley-O'Carroll KF. Targeted and immune-based therapies for hepatocellular carcinoma. Gastroenterology. 2019; 156(2): 510-524.
3. Yang JD, Hainaut P, Gores GJ, Amadou A, Plymoth A, Roberts LR. A global view of hepatocellular carcinoma: trends, risk, prevention and management. Nat Rev Gastroenterol Hepatol. 2019; 16(10): 589-604.
4. Dahariya S, Paddibhatla I, Kumar S, Raghuwanshi S, Pallepati A, Gutti RK. Long non-coding RNA: Classification, biogenesis and functions in blood cells. Mol Immunol. 2019; 112: 82-92.
5. Dykes IM, Emanueli C. Transcriptional and post-transcriptional gene regulation by long non-coding RNA. Genomics Proteomics Bioinformatics. 2017; 15(3): 177-186.
6. Sanchez Calle A, Kawamura Y, Yamamoto Y, Takeshita F, Ochiya T. Emerging roles of long non-coding RNA in cancer. Cancer Sci. 2018; 109(7): 2093-2100.
7. Chi Y, Wang D, Wang J, Yu W, Yang J. Long non-coding RNA in the

pathogenesis of cancers. Cells. 2019; 8(9): 1015.
8. Chen Z, Zhang Z, Zhao D, Feng W, Meng F, Han S, et al. Long noncoding RNA (lncRNA) FOXD2-AS1 promotes cell proliferation and metastasis in hepatocellular carcinoma by regulating MiR-185/AKT axis. Med Sci Monit. 2019; 25: 9618-9629.
9. Ge H, Yan Y, Yue C, Liang C, Wu J. Long noncoding RNA LINC00265 targets EGFR and promotes deterioration of colorectal cancer: A comprehensive study based on data mining and in vitro vValidation. Onco Targets Ther. 2019; 12: 10681-10692.
10. Sun S, Li W, Ma X, Luan H. Long noncoding RNA LINC00265 promotes glycolysis and lactate production of colorectal cancer through regulating of miR-216b-5p/TRIM44 axis. Digestion. 2020; 101(4): 391-400.
11. Gu Y, Wang X, Liu H, Li G, Yu W, Ma Q. SET7/9 promotes hepatocellular carcinoma progression through regulation of E2F1. Oncol Rep. 2018; 40(4): 1863-1874.
12. Tadesse S, Anshabo AT, Portman N, Lim E, Tilley W, Caldon CE, et al. Targeting CDK2 in cancer: challenges and opportunities for therapy. Drug Discov Today. 2020; 25(2): 406-413.
13. Kawakami M, Mustachio LM, Rodriguez-Canales J, Mino B, Roszik J, Tong P, et al. Next-generation CDK2/9 inhibitors and anaphase catastrophe in lung cancer. J Natl Cancer Inst. 2017; 109(6).
14. Patel P, Tsiperson V, Gottesman SRS, Somma J, Blain SW. Dual inhibition of CDK4 and CDK2 via targeting p27 tyrosine phosphorylation induces a potent and durable response in breast cancer cells. Mol Cancer Res. 2018; 16(3): 361-377.
15. Ling L, Lu HT, Wang HF, Shen MJ, Zhang HB. MicroRNA-203 acts as a potent suppressor in septic shock by alleviating lung injury via inhibition of VNN1. Kidney Blood Press Res. 2019; 44(4): 565-582.
16. Jarroux J, Morillon A, Pinskaya M. History, discovery, and classification of lncRNAs. Adv Exp Med Biol. 2017; 1008: 1-46.
17. Mathy NW, Chen XM. Long non-coding RNAs (lncRNAs) and their transcriptional control of inflammatory responses. J Biol Chem. 2017; 292(30): 12375-12382.
18. Grote P, Boon RA. LncRNAs coming of age. Circ Res. 2018; 123(5): 535-537.
19. Wu T, Du Y. LncRNAs: From basic rresearch to Mmedical application. Int J Biol Sci. 2017; 13(3): 295-307.
20. Yang Y, Chen L, Gu J, Zhang H, Yuan J, Lian Q, et al. Recurrently deregulated lncRNAs in hepatocellular carcinoma. Nat Commun. 2017; 8: 14421.
21. Xiao Y, Li C, Wang H, Liu Y. LINC00265 targets miR-382-5p to regulate SAT1, VAV3 and angiogenesis in osteosarcoma. Aging (Albany NY). 2020; 12(20): 20212-20225.
22. Ma L, Kuai WX, Sun XZ, Lu XC, Yuan YF. Long noncoding RNA LINC00265 predicts the prognosis of acute myeloid leukemia patients and functions as a promoter by activating PI3K-AKT pathway. Eur Rev Med Pharmacol Sci. 2018; 22(22): 7867-7876.
23. Zhu Y, Gu L, Lin X, Cui K, Liu C, Lu B, et al. LINC00265 promotes colorectal tumorigenesis via ZMIZ2 and USP7-mediated stabilization of β-catenin. Cell Death Differ. 2020; 27(4): 1316-1327.
24. Yang Z, OuYang X, Zheng L, Dai L, Luo W. Long intergenic noncoding RNA00265 promotes proliferation of gastric cancer via the microRNA-144-3p/Chromobox 4 axis. Bioengineered. 2021; 12(1): 1012-1025.
25. Denechaud PD, Fajas L, Giralt A. E2F1, a novel regulator of ,etabolism. Front Endocrinol (Lausanne). 2017; 8: 311.
26. Sun CC, Zhou Q, Hu W, Li SJ, Zhang F, Chen ZL, et al. Transcriptional E2F1/2/5/8 as potential targets and transcriptional E2F3/6/7 as new biomarkers for the prognosis of human lung carcinoma. Aging (Albany NY). 2018; 10(5): 973-987.
27. Chen H, Chen J, Zhao L, Song W, Xuan Z, Chen J, et al. CDCA5, transcribed by E2F1, promotes oncogenesis by enhancing cell proliferation and inhibiting apoptosis via the AKT pathway in hepatocellular carcinoma. J Cancer. 2019; 10(8): 1846-1854.
28. Chang L, Xi L, Liu Y, Liu R, Wu Z, Jian Z. SIRT5 promotes cell proliferation and invasion in hepatocellular carcinoma by targeting E2F1. Mol Med Rep. 2018; 17(1): 342-349.
29. Yu Y, Zhao D, Li K, Cai Y, Xu P, Li R, et al. E2F1 mediated DDX11 transcriptional activation promotes hepatocellular carcinoma progression through PI3K/AKT/mTOR pathway. Cell Death Dis. 2020; 11(4): 273.
30. Zhao H, Xu Q. Long non-coding RNA DLX6-AS1 mediates proliferation, invasion and apoptosis of endometrial cancer cells by recruiting p300/E2F1 in DLX6 promoter region. J Cell Mol Med. 2020; 24(21): 12572-12584.
31. Liu Q, Gao J, Zhao C, Guo Y, Wang S, Shen F, et al. To control or to be controlled? Dual roles of CDK2 in DNA damage and DNA damage response. DNA Repair (Amst). 2020; 85: 102702.
32. Tadesse S, Caldon EC, Tilley W, Wang S. Cyclin-dependent kinase 2 inhibitors in cancer therapy: an update. J Med Chem. 2019; 62(9): 4233-4251.
33. Abd El-Karim SS, Syam YM, El Kerdawy AM, Abdelghany TM. New thiazol-hydrazono-coumarin hybrids targeting human cervical cancer cells: Synthesis, CDK2 inhibition, QSAR and molecular docking studies. Bioorg Chem. 2019; 86: 80-96.
34. Tang Z, Li L, Tang Y, Xie D, Wu K, Wei W, et al. CDK2 positively regulates aerobic glycolysis by suppressing SIRT5 in gastric cancer. Cancer Sci. 2018; 109(8): 2590-2598.
35. Li Y, Yang XH, Fang SJ, Qin CF, Sun RL, Liu ZY, et al. HOXA7 stimulates human hepatocellular carcinoma proliferation through cyclin E1/CDK2. Oncol Rep. 2015; 33(2): 990-996.
36. Kim JK, Jung KH, Noh JH, Eun JW, Bae HJ, Xie HJ, et al. Targeted disruption of S100P suppresses tumor cell growth by down-regulation of cyclin D1 and CDK2 in human hepatocellular carcinoma. Int J Oncol. 2009; 35(6): 1257-1264.

Original Article

GPX2 and *BMP4* as Significant Molecular Alterations in The Lung Adenocarcinoma Progression: Integrated Bioinformatics Analysis

Mohammad Hossein Derakhshan Nazari, B.Sc.[1#], Rana Askari Dastjerdi, B.Sc.[1#], Parnian Ghaedi Talkhouncheh, B.Sc.[2#], Ahmad Bereimipour, M.Sc.[3], Hamidreza Mollasalehi, Ph.D.[2], Amir Ali Mahshad, B.Sc.[1], Ali Razi, B.Sc.[4], Mohammad Hossein Nazari, M.Sc.[5], Amin Ebrahimi Sadrabadi, Ph.D.[3*], Sara Taleahmad, Ph.D.[3*]

1. Department of Microbiology and Microbial Biotechnology, Faculty of Life Science and Biotechnology, Shahid Beheshti University, Tehran, Iran
2. Department of Cell and Molecular Biology, Faculty of Life Science and Biotechnology, Shahid Beheshti University, Tehran, Iran
3. Department of Stem Cells and Developmental Biology, Cell Science Research Center, Royan Institute for Stem Cell Biology and Technology, ACECR, Tehran, Iran
4. Biophysics Department, Science Faculty, York University, Toronto, Canada
5. V. Zelman Institute for Medicine and Psychology, Novosibirsk State University, Novosibirsk, Russia

Corresponding Address: P.O. Box: 16635-148, Department of Stem Cells and Developmental Biology, Cell Science Research Center, Royan Institute for Stem Cell Biology and Technology, ACECR, Tehran, Iran

Emails: amin.ebrahimi@royaninstitute.org, s.taleahmad@royan-rc.ac.ir

#These authors contributed equally to this work.

Received: 06/January/2021, Accepted: 19/April/2021

Abstract

Objectives: Non-small cell lung adenocarcinoma (NSCLC) is the most common type of lung cancer, which is considered as the most lethal and prevalent cancer worldwide. Recently, molecular changes have been implicated to play a significant role in the cancer progression. Despite of numerous studies, the molecular mechanism of NSCLC pathogenesis in each sub-stage remains unclear. Studying these molecular alterations gives us a chance to design successful therapeutic plans which is aimed in this research.

Materials and Methods: In this bioinformatics study, we compared the expression profile of 7 minor stages of NSCLC adenocarcinoma, including GSE41271, GSE42127, and GSE75037, to clarify the relation of molecular alterations and tumorigenesis. At first, 99 common differentially expressed genes (DEG) were obtained. Then, functional enrichment analysis and protein-protein interaction (PPI) network construction were performed to uncover the association of significant cellular and molecular changes. Finally, gene expression profile interactive analysis (GEPIA) was employed to validate the results by RNA-seq expression data.

Results: Primary analysis showed that *BMP4* was downregulated through the tumor progression to the stage IB and *GPX2* was upregulated in the course of final tumor development to the stage IV and distant metastasis. Functional enrichment analysis indicated that *BMP4* in the TGF-β signaling pathway and *GPX2* in the glutathione metabolism pathway may be the key genes for NSCLC adenocarcinoma progression. GEPIA analysis revealed a correlation between *BMP4* downregulation and *GPX2* upregulation and lung adenocarcinoma (LUAD) progression and lower survival chances in LUAD patients which confirm microarray data.

Conclusion: Taken together, we suggested *GPX2* as an oncogene by inhibiting apoptosis, promoting EMT and increasing glucose uptake in the final stages and *BMP4* as a tumor suppressor via inducing apoptosis and arresting cell cycle in the early stages through lung adenocarcinoma (ADC) development to make them candidate genes to further cancer therapy investigations.

***Keywords*:** Glutathione Peroxidase, In Silico, Microarray, NSCLC, TGF-β Signaling

Cell Journal(Yakhteh), Vol 24, No 6, June 2022, Pages: 302-308

Citation: Derakhshan Nazari MH, Askari Dastjerdi R, Ghaedi Talkhouncheh P, Bereimipour A, Mollasalehi H, Mahshad AA, Razi A, Nazari MH, Ebrahimi Sadrabadi A, Taleahmad S. GPX2 and BMP4 as significant molecular alterations in the lung adenocarcinoma progression: integrated bioinformatics analysis. Cell J. 2022; 24(6): 302-308. doi: 10.22074/cellj.2022.7930.

Introduction

Lung cancer is the leading cause of cancer-related death worldwide. In 2012, approximately 1.8 million cases were diagnosed, and 1.6 million died from lung cancer (1). Besides, 2,093,876 new cases and 1,761,007 deaths were confirmed in 2018, accounting for 18.4 percent of cancer deaths (2). Two main reasons are considered to contribute to the high incidence and mortality of lung cancer. The smoking habit is believed the first reason, because 80 to 90% of diagnosed patients have been reported with a history of smoking (3, 4). And the second one stems from poor diagnosis. Roughly 70% of patients have been diagnosed with locally advanced or metastatic tumors (5). Except for current smoking, some other risk factors such as passive or second-hand smoking, diet, air pollution, alcohol, physical activity, occupational exposure, and genetic

factors have been introduced to have a role in lung cancer progression (5, 6). Lung cancer has two main subtypes: Non-small cell lung cancer (NSCLC) and small cell lung cancer (SCLC) (7). NSCLC makes up approximately 83% of lung cancers (8) and is divided into three main histological subtypes, including squamous cell carcinoma (SCC), large cell carcinoma (LCC), and adenocarcinoma (ADC). NSCLC adenocarcinoma has shown with a higher incidence of NSCLC cases (50%) (9). NSCLC staging, like many cancers, is based on the tumor, nodes and metastasis (TNM) staging system (10) that T stands for the pathological extension of tumor size, N describes the involvement of regional lymph nodes, and M shows distant metastasis (11). Tumor progression, according to the TNM, starts from sub-stage IA (stage I) and end up to stage IV. However, there is a stage 0 called carcinoma in situ (CIS) before sub-stage IA that is usually medicated by an accurate resection. It has been estimated that 5-year survival in NSLCC varies from 73% in stage IA patients to 13% in stage IV patients (12). Selecting a therapeutic method for NSCLC is based on the tumor stage recommending resection for stage I, resection, and adjuvant chemotherapy for stage II, chemotherapy, and radiotherapy for stage III and chemotherapy platinum-based two drugs for stage IV (4, 5). However, recently, targeting molecular events in cancer cells has been implicated as a novel method for cancer therapy (13).

In the process of tumor progression, many genetic alterations can occur, and some researches have been accomplished to elucidate these molecular changes in the NSCLC ADC to treat and prevent cancer progression, but it remains unclear. Genetic alterations, especially expression changes, mediate many biological programs to provide an appropriate statue for malignant cell's rapid proliferation (14). Conclusively, the identification of molecular signature alterations impacting tumor progression that is aimed in this study could be helpful for more investigations for treatment, prognosis, and diagnosis of NSCLC adenocarcinoma.

High-throughput methods such as microarrays have been used for bioinformatics analysis and provided useful information for monitoring biomarkers and discernment of the pathogenic genes in cancer and other diseases that are fundamental for therapeutic targets (15, 16). In this study, we analyzed microarray expression profiles of 3 cohorts with GEO2R based on the R language. Subsequently, functional annotations analysis was performed to uncover the association between molecular alterations and neoplastic cell proliferation.

Materials and Methods

Microarray data analysis

In this bioinformatics study, gene expression profiles of GSE75037, GSE41271, and GSE42127 were extracted from the GEO (https://www.ncbi.nlm.nih.gov/geo/) containing 179, 132, and 82 chips for adenocarcinoma, and then 28, 25, and 22 chips were selected respectively. Gene expression profiles in these series were examined based on the GPL6884 Platform (Illumina Human WG-6V3.0 Expression Bead Chip). ADC samples with the highest similarity in the value distribution in 7 different sub-stages (according to the TNM staging) (11, 12) were divided into six groups in order to screen the molecular alterations in tumor progression (from stage IA to IV) and were subsequently analyzed by GEO2R (Table S1, See Supplementary Online Information at www.celljournal.org). Twelve samples were chosen for stages IIIA, IIB, IB, and IA, and 11, 9, and 7 samples were selected for stage IIA, IIIB, and IV, respectively. Then, comparison of the gene expression profile of stages was performed in 6 groups (Table 1). Using GEO2R, differentially expressed genes (DEGs) were identified in each group with the criterion cut-off $P<0.05$ and $|LogFC| \geq 1$ for statistical significance. Then the DEGs were shared in each group in three data series using the Venn diagram to identify the most predominant molecular alterations. A heatmap was then designed by a web-based tool, Morpheus (https://software.broadinstitute.org/morpheus/), to screen dysregulated genes expression level.

Table 1: Stages samples in each groups

Groups	Stage comparison	Samples count
Group 1	IA vs. IB	12 vs. 12
Group 2	IB vs. IIA	12 vs. 11
Group 3	IIA vs. IIB	11 vs. 12
Group 4	IIB vs. IIIA	12 vs. 12
Group 5	IIIA vs. IIIB	12 vs. 9
Group 6	IIIB vs. IV	9 vs. 7

Functional annotation analysis

Gene ontology (GO) and pathway enrichment analysis were performed using GO Resource (GOR, http://geneontology.org/), Kyoto Encyclopedia of Genes and Genomes (KEGG, https://www.genome.jp/kegg/pathway.html), Database for Annotation, Visualization and Integrated Discovery (DAVID, https://david.ncifcrf.gov/), Wikipathways (https://wikipathways.org/), Reactome (https://reactome.org/) and BioPlanet (https://tripod.nih.gov/bioplanet/). The statistically significant pathways and GOs were defined by $P<0.05$ as the cut-off criterion. Then protein-protein interaction (PPI) network was constructed using the Search Tool for the Retrieval of Interacting Genes (STRING, https://string-db.org/) (17) and a combined score >0.4 was used to identify significant interactions. Next, Cytoscape (version 3.8.0) was used with CentiScape2.2 and CytoHubba plugins to discover hub proteins and visualization of the PPI network.

Candidate genes analysis by GEPIA

GEPIA (http://gepia.cancer-pku.cn/) as a newly developed interactive web server for analyzing the RNA sequencing

expression data using TCGA (https://www.cancer.gov/about-nci/organization/ccg/research/structural-genomics/tcga) and GTEx (https://gtexportal.org/home/) projects was applied for additional analysis of candidate genes in lung adenocarcinoma (LUAD) and comparison with squamous cell carcinoma (LUSC) with the |LogFC| ≥ 1 and P<0.01 as the cut-off criterion. Finally, Kaplan-Meier plot matched to the TCGA data was used to explain the survival rate of patients, according to the expression of candidate genes in GEPIA database.

Results

Identification of differentially expressed genes

A total of 16786 DEGs was identified in the NSCLC adenocarcinoma expression datasets GSE41271, GSE42127, and GSE75037 using GEO2R. Ninety-nine common DEGs in all groups (Table S2, See Supplementary Online Information at www.celljournal.org), including 58 downregulated and 41 upregulated DEGs, were obtained through the Venn diagram (Fig.1A). The group 1 (stage IA vs. stage IB) included most DEGs with 40 downregulated and 29 upregulated genes, indicating that the most molecular alterations have occurred in the early stages. A heatmap of up (blue) and downregulated (red) genes visualized between three different studies (Fig.1B). Top DEGs |LogFC|≥2 between 6 groups are shown in the Table S3 (See Supplementary Online Information at www.celljournal.org). Eventually, our analysis represented *ITLN2*, *CLDN10*, *SLC7A2*, *GFRA3*, and *GPX2* as the most altered genes in the groups 1 to 6, respectively, and among these genes, *GPX2* was the most altered gene with a noticeable 43.56-fold change.

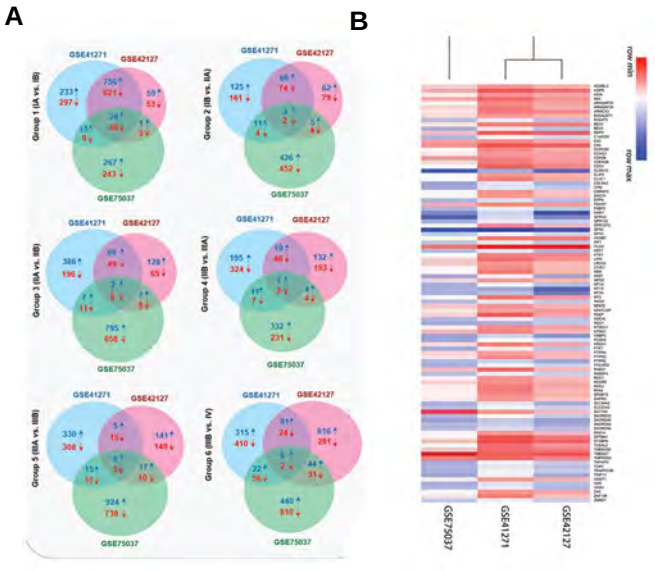

Fig.1: Intersecting genes of GSE41271, GSE42127, and GSE75037 in each sub-stage using a Venn diagram. **A.** Overlapping genes in GSE41271, GSE42127, and GSE75037 in group 1 (IA vs. IB), group 2 (IB vs. IIA), group 3 (IIA vs. IIB), group 4 (IIB vs. IIIA), group 5 (IIIA vs. IIIB), and group 6 (IIIB vs. IV) via Venn diagram ↓ indicates downregulated and ↑ indicates upregulated differentially expressed genes (DEG) respectively. Red numbers refer to downregulated common DEGs and blue numbers are related to the upregulated common DEGs. **B.** A heatmap of differentially expressed genes between three studies. Each row of the heatmap represents a gene that has at least a |LogFC|≥1 between three studies. Red for lower and blue for higher expressions.

Discovering associated gene ontology and pathways

GO was analyzed by Enrichr and DAVID in order to find out enriched BP, MF, and CC. In this manner, for downregulated DEGs smooth muscle tissue development, carbonate dehydratase activity, and endoplasmic reticulum-Golgi intermediate compartment were manifested. Then for upregulated DEGs, cellular response to zinc ion, cysteine-type endopeptidase activator activity involved in the apoptotic process and perinuclear region of cytoplasm were revealed (Fig.2).

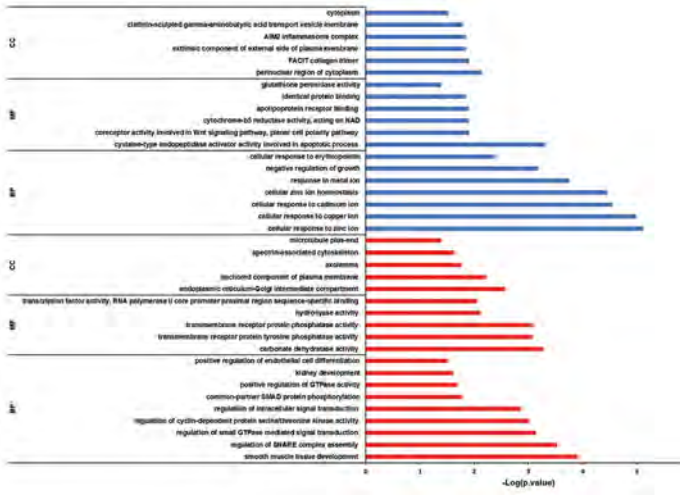

Fig.2: Detecting related gene ontologies. Red and blue columns represent downregulated and upregulated associated. GO, respectively. BP; Biological process, MF; Molecular function, and CC; Cellular component.

Further screening of biological processes, separately in the three data series, revealed an increased rate of the cell cycle and inhibition of apoptosis during tumor progression. In addition, epithelial cells loss of differentiation was observed in the group 6, which seems to contribute to the epithelial-to-mesenchymal transition (EMT) that eventually leads to metastasis. EMT promoter genes were also observed in the GOR (Table S4, See Supplementary Online Information at www.celljournal.org). Next, pathway enrichment analysis was accomplished and indicated Nitrogen metabolism and Mineral absorption in the KEGG. Also, erythrocytes take up oxygen and release carbon dioxide and response to metal ions in the Reactome, Suppression of HMGB1 mediated inflammation by the THBD and Zinc homeostasis in the Wikipathways and Oxygen/carbon dioxide exchange in the erythrocytes and TAp63 pathway in the BioPlanet, were detected as the most disrupted pathways for downregulated and upregulated DEGs respectively (Fig.3A).

Disclosing Hub proteins

To identify key proteins with regulatory impacts, the STRING was used for the PPI network construction, and Cytoscape was used for further analysis, which showed that among all common DEGs, 47 proteins were involved in the network via 37 edges (Fig.3B). Considering the degree and betweenness centrality for the nodes indicated BMP4, NQO1, RHOJ, ZNRD1, and GPX4 as the critical proteins (Table S5, See Supplementary Online Information at www.celljournal.org). Analyzing the network with the CentiScape2.2 and CytoHubba plugins demonstrated BMP4 as the most important protein in this PPI network, which is downregulated in group 1 (Fig.S1, See Supplementary Online Information at www.celljournal.org).

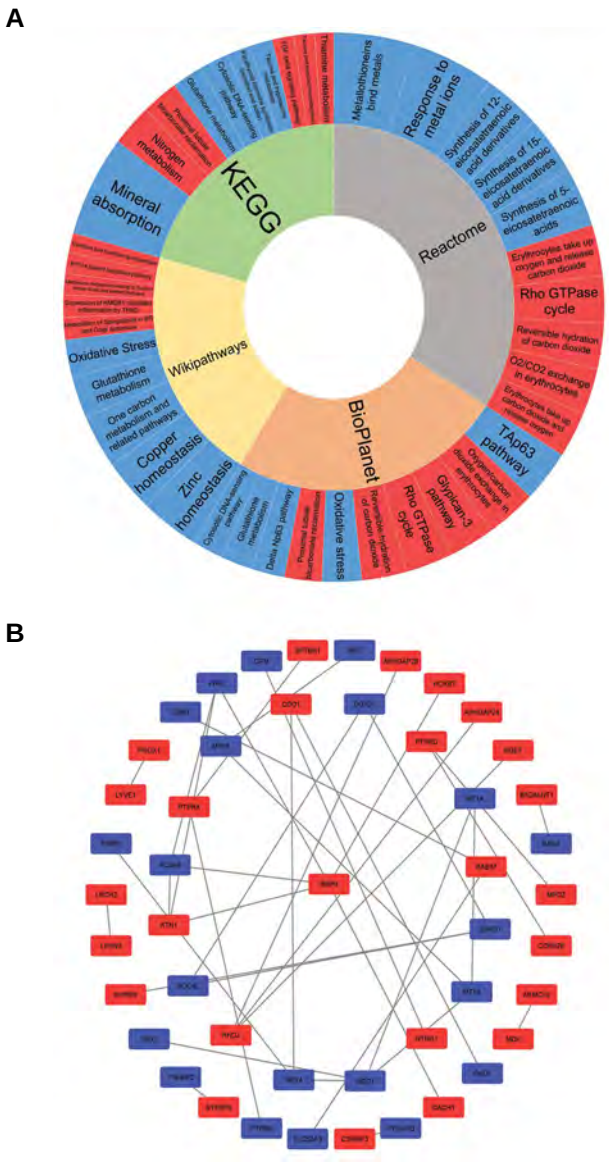

Fig.3: Pathway and network analysis. **A.** Pathway enrichment analysis. Red and blue cells represent downregulated and upregulated pathways, respectively. The most important pathways are those that have bigger cells. **B.** Protein-protein interaction (PPI) network. Red and blue points represent downregulated and upregulated genes.

Accelerate cell cycle and apoptosis arresting during lung adenocarcinoma progression

It seems that the downregulation of *BMP4* during primary tumor progression to stage IB avoids the induction of apoptosis and arresting cell cycle through TGF-β signaling that is needed for tumor progression. Also, the upregulation of *GPX2* through final tumor progression to stage IV (Table S3, See Supplementary Online Information at www.celljournal.org) is correlated with the glutathione metabolism pathway, which maintains the redox balance in the cancer cells against accumulative reactive oxygen species (ROS) and seems to promote EMT, which leads to metastasis. We also found *GPX4* in the glutathione metabolism pathway and *CDKN2B* in the TGF-β signaling that change these pathways in the same way with *BMP4* and *GPX2*. Additionally, screening previous studies on the *GPX2* showed a co-expression relation with *ABCB6* which is involved in the glucose uptake (Fig. S2, See Supplementary Online Information at www.celljournal.org). Hence, upregulation of *GPX2* could result in an increase in the glucose uptake (Fig.4).

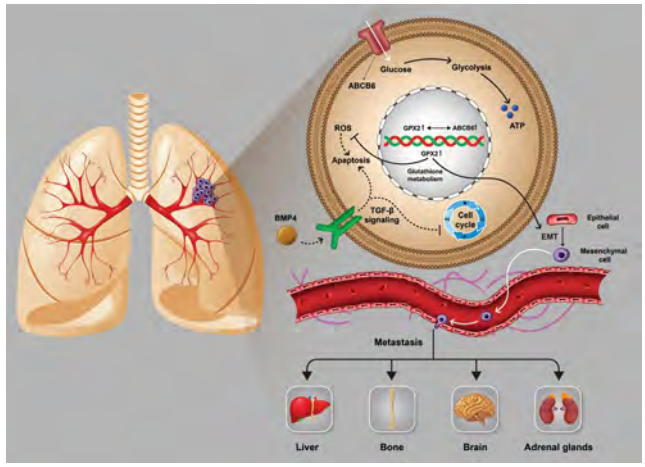

Fig.4: The role of BMP4 in TGF-β signaling and GPX2 in glutathione metabolism in tumor progression.

Verification of *GPX2* and *BMP4* in GEPIA database

Screening the expression changes of *BMP4* according to the normal lung tissue in the TCGA data indicated a significant downregulation in the LUSC and non-significant downregulation in the LUAD by $|LogFC| \geq 1$ and $P<0.01$ as the cut-off criteria. Analyzing the TCGA data for the *GPX2* showed upregulation in the LUAD and LUSC in comparison with the normal lung tissue (Fig.5A). Monitoring expression alterations of *BMP4* and *GPX2* in the TCGA samples in each stage manifested the same results of GEO and confirmed that *BMP4* was downregulated within a

primary tumor progression to stage IB and *GPX2* was upregulated throughout stage IIIB to IV progression (Fig.5B). Kaplan-Mayer analysis illustrated a relation between the downregulation of *BMP4* and upregulation of *GPX2* and the high-risk groups of LUAD patients by considering *GAPDH* as the normalizer gene. Patients with downregulation of *BMP4* approximately between 50-165th month seem to have a lower chance of survival. Contrastingly, upregulation of *BMP4* was correlated with the lower survival rate after 165th. Moreover, upregulation of *GPX2* during the final development of the tumor is related to the high-risk group of patients among approximately 85th month until the 165th month. However, after this period, there was no meaningful difference between the survival chances of LUAD patients, according to the *GPX2* expression (Fig.5C). This information has a predictive potentiality to estimate the life-expectancy of LUAD patients by monitoring their *BMP4* and *GPX2* expression.

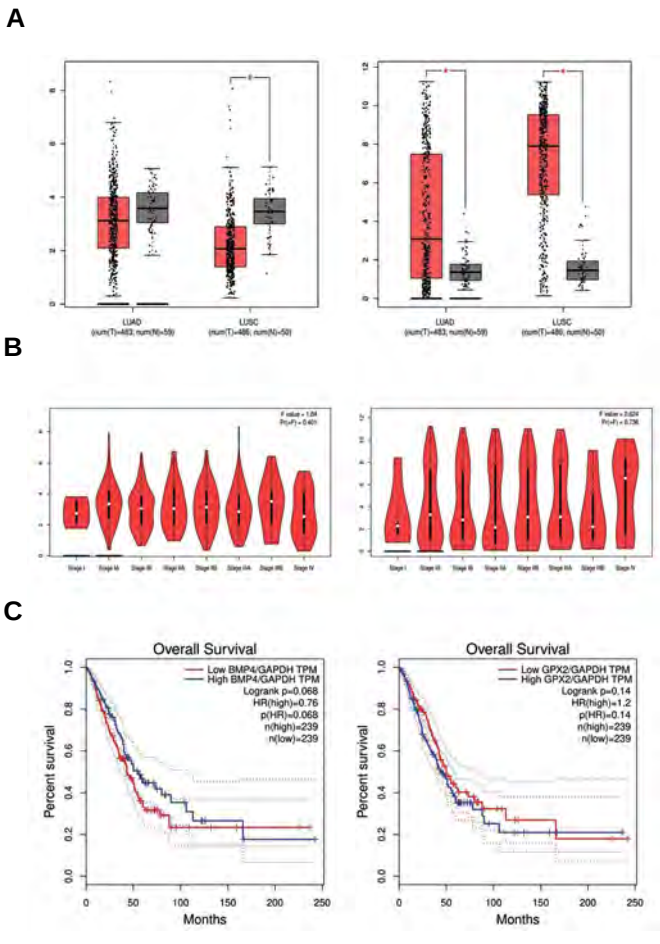

Fig.5: GEPIA analysis of candidate genes. Boxplot of **A.** *BMP4* (left) and *GPX2* (right) in lung adenocarcinoma and lung squamous cell carcinoma. **B.** Stage plot of *BMP4* (left) and *GPX2* (right) in lung adenocarcinoma. **C.** Kaplan-Mayer plotting for survival analysis, divide patients into two groups: high risk and low risk according to *BMP4* downregulation (low TPM) (left) and GPX2 upregulation (high TPM) (right) by recruiting *GAPDH* as the normalizer gene. TPM; Transcription per million.

Discussion

Lung cancer is described as the most common cancer in both women and men worldwide (18), which leads to the death of 84% of patients (2, 4). Among the mentioned subtypes of this cancer, NSCLC adenocarcinoma is the most diagnosed type of lung cancer (19). Recently, molecular alterations have been suggested as a significant factor to be considered for the cancer treatment instead of other invasive therapeutic methods. Hence, identification of molecular alterations in the NSCLC ADC could suggest candidate genes for treatment and diagnosis that is aimed in the present research. Microarray data in GEO provide a platform for analyzing gene expressions useful for considering molecular changes in cancers (20). In the present study, we have analyzed GSE41272, GSE42127, and GSE75037 (based on GPL6884) in 6 groups, and then common DEGs were identified by Venn in each group. Group 1 (stage IA vs. IB) had the highest number of DEGs suggesting that the molecular reprogramming in the LUAD mostly takes place in the early tumorigenesis. Next, pathway enrichment analysis was performed and showed that upregulated DEGs were enriched in mineral absorption, response to metal ions, zinc homeostasis and TAp63 pathway and downregulated DEGs were enriched in nitrogen metabolism, erythrocytes take up oxygen and release carbon dioxide, suppression of HMGB1 mediated inflammation by THBD and Oxygen/carbon dioxide exchange in erythrocytes using KEGG, Reactome, Wikipathways and BioPlanet databases respectively. Considering involved genes in these pathways suggested that the homeostasis of the metal ions and the metabolism of oxygen and carbon dioxide were important pathways for the NSCLC ADC tumor development. This result is consistent with the observation of carbonate dehydratase activity and cellular response to zinc ion for downregulated and upregulated DEGs via GO analysis by DAVID and Enrichr. By analyzing the biological process in three data series separately, we observed promoted cell proliferation and inhibited apoptosis in all stages of NSCLC ADC, which is in agreement with the tumor progression. Also, the undifferentiation of epithelial cells was observed in the final tumor development to stage IV, which seems to contribute to EMT and distant metastasis.

Subsequently, analyzing of the PPI network by CentiScape2.2 indicated *BMP4* as the critical gene in NSCLC ADC tumor development. According to the GEO and TCGA, *BMP4* was downregulated during cancer progression to the stage IB. BMP4 has been identified that can act as a tumor suppressor in many cancers through its anti-proliferative, growth inhibitory, metastasis suppressive, and apoptosis-inducing capability (21). Similarly, research on lung cancer demonstrated overexpression of *BMP4* leads to premature senescence of cancerous cells via the Smad signaling pathway by inducing *BMP4* expression with adriamycin (22). In agreement with this, Wen et al. reported that *BMP4* was suppressed in the NSCLC squamous cell carcinoma. It occurs via Sox2 protein that promotes the SCC cell proliferation (21), which is intriguingly consistent with our results.

BMP4 protein is a member of the TGF-β superfamily that has been reported as both tumor suppressor and tumor promoter pathways. In the early stages, TGF-β has been proven to have tumor suppressor activity via cell cycle arrest and inducing apoptosis (23) that is consistent with the Panther and DAVID results for BP. Thus, the downregulation of BMP4 in the TGF-β signaling pathway seems to be essential for primary cancer progressing to the stage IB, which suggests a tumor suppressor activity of BMP4 in the early stages of NSCLC ADC.

Conversely, Mihajlović et al. (24) indicated a pro-migratory and pro-EMT activity for the BMP4 in the NSCLC within BMP receptor type I SMAD dependent signaling by screening LCLC-103H cells, which is compatible with the tumor promoter activity of TGF-β signaling in the final stages (23).

We also observed *GPX2* as the most upregulated gene (Log FC=6.6). A previous study has suggested *GPX2* as an oncogene due to its capability of inducing tumor initiation, growth, development, and metastasis (25). Besides, *GPX2* overexpression was observed in the breast (26), liver (27), gastric (28), nasopharyngeal (29), and esophageal SCC (30). Although, some other studies have reported a positive correlation between *GPX2* expression and cell proliferation in the colorectal cancer and castration-resistant prostate cancer (31, 32) reduced expression of *GPX2* was associated with advanced tumor status in the patients with urothelial carcinomas of the upper urinary tract and urinary bladder (33). Furthermore, Li et al. (34) showed that *GPX2* expression leads to the *MMP2* and *MMP9* expression via activating the Wnt pathway, which subsequently induces epithelial transition to mesenchymal, metastasis, and tumor invasion in the pancreatic tumor, that is interestingly consistent with the upregulation of *GPX2* during stage IIIB to IV progression, which was attained in our results. A previous study by Naiki-Ito et al. (26) reported that GPX2 played an important role in the mammary carcinogenesis, including humans and rodents. Furthermore, Huang et al. (35) observed that suppression of *GPX2* via YAP pathway relieves lung SCC development. Despite that, a study of the NSCLC cell lines reported that the downregulation of *GPX2* is necessary for EMT induction (36). Moreno Leon et al. (37) found that *GPX2* overexpression increases glucose uptake due to its correlated expression with ABCB6, which was confirmed by GEPIA, suggesting that GPX2 may modulate the metabolic alteration in the LUAD. Evaluated glucose uptake is required for cancer cell metabolism by providing energy via high rated glycolysis (38, 39).

GPX2, which belongs to the family of glutathione peroxidases, is involved in the maintenance of the redox balance in cells, and it can fulfill its function by protecting cancerous cells against ROS that increases in the tumor microenvironment and damages various macromolecules and induces apoptosis, which was approved via Panther (32, 40). ROS reduction is operated via oxidation of glutathione by glutathione peroxidases in the glutathione metabolism pathway (40), which was also observed in our KEGG results. In addition, in previous research, the glutathione metabolism pathway has been implicated to induce EMT in the NSCLC (36) that is compatible with our GO analysis in the Panther and DAVID. Therefore, *GPX2*, in the final stages of NSCLC ADC, may be considered to be an oncogene due to its role in providing excessive glucose for tumor cells and glutathione metabolism pathway by inducing EMT and inhibiting apoptosis.

Conclusion

By the integration of 3 microarrays with bioinformatics analysis, we suggested *BMP4* as a tumor suppressor via inducing apoptosis and arresting cell cycle in the early stages, and *GPX2* as an oncogene by inhibiting apoptosis and promoting EMT in advanced stages. They were the two crucial dysregulated genes in the course of tumor development in experimental design, *in vitro* and *in vivo*, to explore the role of these altered genes and to employ them for therapeutic approaches.

Acknowledgments

We appreciate our colleagues for their helpful effort and valuable comments on this research. The authors confirm that methods were performed in accordance with relevant guidelines and regulations. This research did not receive any specific grant from funding agencies in the public, commercial, or not-for-profit sectors. The authors have declared that they have no conflict of interest.

Authors' Contributions

M.H.D.N., A.E.S., A.B.; Designed the project. S.T., A.E.S.; Project supervisor. M.H.D.N., R.A.D., P.Gh.T.; Bioinformatics data analyzer and manuscript writers. A.B., A.A.M., M.H.N., H.M., A.R.; Helper in cancer biology, lung cancer pathology and molecular biology aspects of the research respectively. A.R.; Edits the main text grammatically and revised it. All authors read and approved the final manuscript.

References

1. Torre LA, Siegel RL, Jemal A. Lung cancer statistics. Adv Exp Med Biol. 2016; 893: 1-19.
2. Bray F, Ferlay J, Soerjomataram I, Siegel RL, Torre LA, Jemal A. Global cancer statistics 2018: GLOBOCAN estimates of incidence and mortality worldwide for 36 cancers in 185 countries. CA Cancer J Clin. 2018; 68(6): 394-424.
3. Collins LG, Haines C, Perkel R, Enck RE. Lung cancer: diagnosis and management. Am Fam Physician. 2007; 75(1): 56-63.
4. Nasim F, Sabath BF, Eapen GA. Lung cancer. Med Clin North Am. 2019; 103(3): 463-473.
5. Molina JR, Yang P, Cassivi SD, Schild SE, Adjei AA. Non-small cell lung cancer: epidemiology, risk factors, treatment, and survivorship. Mayo Clin Proc. 2008; 83(5): 584-594.
6. Ginsberg MS, Grewal RK, Heelan RT. Lung cancer. Radiol Clin North Am. 2007; 45(1): 21-43.
7. de Groot P, Munden RF. Lung cancer epidemiology, risk factors, and prevention. Radiol Clin North Am. 2012; 50(5): 863-876.
8. Rodriguez-Canales J, Parra-Cuentas E, Wistuba II. Diagnosis and molecular classification of lung cancer. Cancer Treat Res. 2016; 170: 25-46.

9. Zheng M. Classification and pathology of lung cancer. Surg Oncol Clin N Am. 2016; 25(3): 447-468.
10. Tsim S, O'Dowd CA, Milroy R, Davidson S. Staging of non-small cell lung cancer (NSCLC): a review. Respir Med. 2010; 104(12): 1767-1774.
11. Detterbeck FC, Boffa DJ, Tanoue LT. The new lung cancer staging system. Chest. 2009; 136(1): 260-271.
12. Woodard GA, Jones KD, Jablons DM. Lung cancer staging and prognosis. Cancer Treat Res. 2016; 170: 47-75.
13. Dachs GU, Dougherty GJ, Stratford IJ, Chaplin DJ. Targeting gene therapy to cancer: a review. Oncol Res. 1997; 9(6-7): 313-325.
14. Garnis C, Buys TP, Lam WL. Genetic alteration and gene expression modulation during cancer progression. Mol Cancer. 2004; 3: 9.
15. Anisimov SV. Application of DNA microarray technology to gerontological studies. Methods Mol Biol. 2007; 371: 249-265.
16. Hanai T, Hamada H, Okamoto M. Application of bioinformatics for DNA microarray data to bioscience, bioengineering and medical fields. J Biosci Bioeng. 2006; 101(5): 377-384.
17. Szklarczyk D, Gable AL, Lyon D, Junge A, Wyder S, Huerta-Cepas J, et al. STRING v11: protein-protein association networks with increased coverage, supporting functional discovery in genome-wide experimental datasets. Nucleic Acids Res. 2019; 47(D1): D607-D613.
18. Romaszko AM, Doboszyńska A. Multiple primary lung cancer: a literature review. Adv Clin Exp Med. 2018; 27(5): 725-730.
19. Cersosimo RJ. Lung cancer: a review. Am J Health Syst Pharm. 2002; 59(7): 611-642.
20. Virtanen C, Woodgett J. Clinical uses of microarrays in cancer research. Methods Mol Med. 2008; 141: 87-113.
21. Fang WT, Fan CC, Li SM, Jang TH, Lin HP, Shih NY, et al. Down-regulation of a putative tumor suppressor BMP4 by SOX2 promotes growth of lung squamous cell carcinoma. Int J Cancer. 2014; 135(4): 809-819.
22. Su D, Zhu S, Han X, Feng Y, Huang H, Ren G, et al. BMP4-Smad signaling pathway mediates adriamycin-induced premature senescence in lung cancer cells. J Biol Chem. 2009; 284(18): 12153-12164.
23. Colak S, Ten Dijke P. Targeting TGF-β signaling in cancer. Trends Cancer. 2017; 3(1): 56-71.
24. Mihajlović J, Diehl LAM, Hochhaus A, Clement JH. Inhibition of bone morphogenetic protein signaling reduces viability, growth and migratory potential of non-small cell lung carcinoma cells. J Cancer Res Clin Oncol. 2019; 145(11): 2675-2687.
25. Du H, Chen B, Jiao NL, Liu YH, Sun SY, Zhang YW. Elevated glutathione peroxidase 2 expression promotes cisplatin resistance in lung adenocarcinoma. Oxid Med Cell Longev. 2020; 2020: 7370157.
26. Naiki-Ito A, Asamoto M, Hokaiwado N, Takahashi S, Yamashita H, Tsuda H, et al. Gpx2 is an overexpressed gene in rat breast cancers induced by three different chemical carcinogens. Cancer Res. 2007; 67(23): 11353-11358.
27. Liu D, Sun L, Tong J, Chen X, Li H, Zhang Q. Prognostic significance of glutathione peroxidase 2 in gastric carcinoma. Tumour Biol. 2017; 39(6): 1010428317701443.
28. Liu T, Kan XF, Ma C, Chen LL, Cheng TT, Zou ZW, et al. GPX2 overexpression indicates poor prognosis in patients with hepatocellular carcinoma. Tumour Biol. 2017; 39(6): 1010428317700410.
29. Liu C, He X, Wu X, Wang Z, Zuo W, Hu G. Clinicopathological and prognostic significance of GPx2 protein expression in nasopharyngeal carcinoma. Cancer Biomark. 2017; 19(3): 335-340.
30. Lei Z, Tian D, Zhang C, Zhao S, Su M. Clinicopathological and prognostic significance of GPX2 protein expression in esophageal squamous cell carcinoma. BMC Cancer. 2016; 16: 410.
31. Emmink BL, Laoukili J, Kipp AP, Koster J, Govaert KM, Fatrai S, et al. GPx2 suppression of H2O2 stress links the formation of differentiated tumor mass to metastatic capacity in colorectal cancer. Cancer Res. 2014; 74(22): 6717-6730.
32. Naiki T, Naiki-Ito A, Asamoto M, Kawai N, Tozawa K, Etani T, et al. GPX2 overexpression is involved in cell proliferation and prognosis of castration-resistant prostate cancer. Carcinogenesis. 2014; 35(9): 1962-1967.
33. Chang IW, Lin VC, Hung CH, Wang HP, Lin YY, Wu WJ, et al. GPX2 underexpression indicates poor prognosis in patients with urothelial carcinomas of the upper urinary tract and urinary bladder. World J Urol. 2015; 33(11): 1777-1789.
34. Li F, Dai L, Niu J. GPX2 silencing relieves epithelial-mesenchymal transition, invasion, and metastasis in pancreatic cancer by down-regulating Wnt pathway. J Cell Physiol. 2020; 235(11): 7780-7790.
35. Huang H, Zhang W, Pan Y, Gao Y, Deng L, Li F, et al. YAP suppresses lung squamous cell carcinoma progression via deregulation of the DNp63-GPX2 axis and ROS accumulation. Cancer Res. 2017; 77(21): 5769-5781.
36. Matadamas-Guzman M, Zazueta C, Rojas E, Resendis-Antonio O. Analysis of epithelial-mesenchymal transition metabolism identifies possible cancer biomarkers useful in diverse genetic backgrounds. Front Oncol. 2020; 10: 1309.
37. Moreno Leon L, Gautier M, Allan R, Ilié M, Nottet N, Pons N, et al. The nuclear hypoxia-regulated NLUCAT1 long non-coding RNA contributes to an aggressive phenotype in lung adenocarcinoma through regulation of oxidative stress. Oncogene. 2019; 38(46): 7146-7165.
38. Vanhove K, Graulus GJ, Mesotten L, Thomeer M, Derveaux E, Noben JP, et al. The metabolic landscape of lung cancer: new insights in a disturbed glucose metabolism. Front Oncol. 2019; 9: 1215.
39. Wang Y, Xia Y, Lu Z. Metabolic features of cancer cells. Cancer Commun (Lond). 2018; 38(1): 65.
40. Bansal A, Simon MC. Glutathione metabolism in cancer progression and treatment resistance. J Cell Biol. 2018; 217(7): 2291-2298.

Original Article

Sodium Selenite Promotes Osteoblast Differentiation via The WNT/ß-Catenin Signaling Pathway

Ashish Ranjan Sharma, Ph.D.[1#], Garima Sharma, Ph.D.[1#], Yeon-Hee Lee, Ph.D.[1#], Chiranjib Chakraborty, Ph.D.[1, 2], Sang-Soo Lee, M.D., Ph.D.[1*], Eun-Min Seo M.D., Ph.D.[1*]

1. Institute for Skeletal Aging and Orthopedic Surgery, Hallym University-Chuncheon Sacred Heart Hospital, Chuncheon-si, Gangwon-do, Republic of Korea

2. Department of Biotechnology, School of Life Science and Biotechnology, Adamas University, Barasat-Barrackpore Rd, Kolkata, West Bengal, India

Corresponding Address: Institute for Skeletal Aging and Orthopedic Surgery, Hallym University-Chuncheon Sacred Heart Hospital, Chuncheon-si, Gangwon-do, Republic of Korea
Emails: 123sslee@gmail.com, seoem@hallym.or.kr

#These authors contributed equally to this work.

Received: 19/October/2021, Accepted: 03/April/2022

Abstract

Objectives: Osteoporosis is regarded as a silent disorder affecting bone slowly, leading to an increased risk of fractures. Lately, selenium has been found to be associated with the acquisition and maintenance of bone health by affecting the bone remodeling process. However, the mechanism of action of selenium on bone is poorly understood. Here, the objective of this study is to examine the protective effects and mechanism of sodium selenite on the differentiation process of osteoblasts as well as under oxidative stress-induced conditions by evaluating the expression of osteoblast differentiation markers in the sodium selenite and/or hydrogen peroxide (H_2O_2)-treated MC3T3-E1 cell line.

Materials and Methods: In this experimental study, we confirmed the inducible osteogenic effect of sodium selenite on MC3T3-E1 cells. Moreover, we investigated the recovery of expression levels of osteogenic markers of sodium selenite in H_2O_2-treated MC3T3-E1 cells.

Results: It was observed that sodium selenite could promote alkaline phosphatase (ALP) activity and collagen synthesis in pre-osteoblasts. Also, sodium selenite enhanced the mRNA expression levels of osteogenic transcriptional factors, like osterix (OSX) and runt-related transcription factor 2 (Runx2). In addition, the terminal differentiation markers, such as osteocalcin (OCN) and collagen 1α (Col1α) were also increased after the treatment of sodium selenite. Also treatment of sodium selenite recused the H_2O_2-induced inhibition of osteoblastic differentiation of pre-osteoblasts cells via the WNT signaling pathway, implicating its antioxidant activity. Furthermore, sodium selenite restored the H_2O_2 repressed β-catenin stability and axin-2 reporter activity in MC3T3-E1 cells.

Conclusion: It may be concluded that sodium selenite can stimulate bone formation and rescue the oxidative repression of osteogenesis by activating WNT signaling pathways. Further detailed studies on the role of selenium and its ability to stimulate bone formation via the WNT signaling pathway may project it as a potential therapeutic intervention for osteoporosis.

Keywords: Osteoblasts, Osteoporosis, Selenium, WNT Signaling Pathway

Cell Journal(Yakhteh), Vol 24, No 6, June 2022, Pages: 309-315

Citation: **Sharma AR, Sharma G, Lee YH, Chakraborty C, Lee SS, Seo EM. Sodium selenite promotes osteoblast differentiation via the wnt/β-catenin signaling pathway. Cell J. 2022; 24(6): 309-315. doi: 10.22074/cellj.2022.8314.**

Introduction

Osteoporosis is the most prominent skeletal disease that increases the risk of osteoporotic fracture by reducing bone density (1). Other complications can also be increased during the osteoporosis progression. Osteoporosis is the net outcome of an imbalance between the resorption and the regeneration of bone tissue. Osteoporosis is regarded as a 'silent disorder' as it progresses slowly and is considered as a major health issue in the world (2). This condition is distinguished by reduced bone weight and bone degeneration, leading to a tendency to fractures. Osteoporosis-related bone fracture is also considered as an age-related bone condition with a high-risk factor in approximately 33% of women and 20% of men (3). At the molecular level, many factors affect the initiation of osteoporosis. One of them is the induction of the secretion of pro-inflammatory cytokines in senescent cells during menopause. The progression of bone loss during osteoporosis has often been associated with the release of inflammatory cytokines like interferon-gamma (IFN-γ), tumor necrosis factor-alpha (TNF-α), interleukin (IL)-1, IL-6, IL-8, and IL-1β (4-6). Growing evidence also suggests that during aging or menopause, increased oxidative stresscontributes to the resorption of bone tissue leading to osteoporosis due to the buildup of free radicals from inflammation or mitochondrial dysfunction (5, 7).

An approach for osteoporosis treatment is the induction of osteoblastogenesis via enhancing proliferation and differentiation of osteoblast cells using anabolic agents, such as estrogens. Another approach for osteoporosis treatment is reducing osteoclastogenesis via inhibition of differentiation of bone-specific multinucleated osteoclasts cells from hematopoietic monocyte precursor cells using anti-resorptive drugs, such as bisphosphonate. Although anabolic agents and anti-resorptive agents are effective against osteoporosis, they are associated with severe side effects, including poor bone quality and carcinogenesis (3). Recent studies

on phytoestrogens having bone stimulatory effects seem promising. However, they suffer bioavailability issue and thus need efficient delivery systems (8-10). Therefore, there is a need to identify novel agents to prevent osteoporosis (3, 11).

The transcription factors, like osterix (OSX) and runt-related transcription factor 2 (Runx2) regulate osteoblast proliferation and differentiation processes at the transcriptional level. At the same time, the bone matrix proteins, such as collagen type I (Col1α), osteocalcin (OCN), alkaline phosphatase (ALP), and osteopontin (OPN), stimulate the bone mineralization process. Thus, these molecules are considered to regulate the bone development and establishment process. In addition, the proliferation and differentiation of both the osteoblast and osteoclast might be modulated by the WNT/β-catenin canonical signaling pathway at multiple levels, leading to an increase in osteoblastogenesis and a decrease in osteoclastogenesis (12). WNTs can promote the differentiation of osteoblast precursors into mature osteoblasts via β-catenin-dependent canonical pathways (13).

Reactive oxygen species (ROS) is often considered as oxidative stress and is shown to induce cellular pathology by degrading proteins, lipids, and DNA (14). Almost most of the sources having oxidative stress generate hydrogen peroxide (H_2O_2) which have the ability to penetrate cellular membranes (15, 16). Treatment of H_2O_2 is shown to exert apoptosis in osteoblasts and suppress differentiation of osteoblasts (17, 18). Hence, H_2O_2 is used to establish *in vitro* cellular model for oxidative stress and evaluate osteonecrosis, proliferation, and osteoblastic differentiation in bone-like cells (19, 20).

Selenium is a micronutrient present as a cofactor in various biologically active enzymes, thus acting as an essential antioxidant in the cellular environment. Not only can selenium reduce oxidative stress, but also it has an inverse correlation between selenium consumption and osteoporosis which has been observed (21). Inadequate selenium intake has been related to a high risk of bone disorders as it is found to be linked to increased turnover of bone and reduced bone mineral density (BMD) (22). It has been observed that sodium selenite induces apoptosis in mature osteoclasts via alterations in mitochondrial signaling pathways (23). However, the signaling mechanism associated with the role of sodium selenite in bone formation is less studied.

Here, we investigate the role of sodium selenite on the MC3T3-E1 cell proliferation and differentiation process. MC3T3-E1 is a pre-osteoblast cell linewhich has been in use to study the proliferation, differentiation process, and mineralization of osteoblasts (24). In addition, we aimed to identify the underlying molecular mechanism of sodium selenite in inducing MC3T3-E1 cell differentiation. Moreover, the antioxidant property of sodium selenium and its effect on osteogenesis in H_2O_2 treated osteoblasts was evaluated.

Materials and Methods

Materials

Cytotoxicity detection kit was purchased from Takara Bio Inc., Japan. CSPD substrate was purchased from Roche, Germany. Trizol reagent, Renilla luciferase thymidine kinase construct, and SuperScript II Reverse Transcriptase were procured from Invitrogen, USA. Phosphate-buffered saline (PBS) was procured from T&I, Korea. SYBR green qPCR MasterMix which was purchased from Bioneer, Korea. Sodium selenite (Na_2SeO_3), 3-(4,5-dimethylthiazol-2yl)-2,5-diphenyl-tetrazolium bromide (MTT), dimethyl sulfoxide (DMSO), Sirius red dye, and Bouin's fluid were procured from Sigma-Aldrich, USA. Penicillin-streptomycin solution (P/S), fetal bovine serum (FBS), and α-minimum essential medium (MEM) were acquired from Gibco, USA.

Cell culture

Mice pre-osteoblast MC3T3-E1 cells (ATCC, CRL-2593) were grown in the α-MEM medium. Cells were cultured at 37˚C in a humidified atmosphere of 95% air and 5% CO_2. The culture medium was supplemented with FBS (10 %), P/S (1 %), L-glutamine (2 mM), sodium pyruvate (1 mM), and non-essential amino acid (0.1 mM).

Cytotoxicity tests (MTT and LDH assay)

MTT assay was performed to evaluate the cell viability of the cells. For this, MC3T3-E1 cells (1×10^4 cells/well) were cultured in 96-wells plate and various doses (0, 0.1, 0.2, 0.4, 0.8, 1.6, 3.2 and 6.4 μM) of Sodium selenite was treated for 24 hours. Insoluble purple MTT formazan crystal produces succinate dehydrogenase in the mitochondria of metabolically active cells. MTT solution (10 μl: 5 mg/ml in PBS) was pipetted in the wells with the cells and further incubated at 37˚C for 2 hours. Afterward, to dissolve MTT, the supernatant was removed, and DMSO (200 μl) added to each well and shaken gently. By using a UV-Vis spectrophotometer, the optical density was recorded (Molecular Devices LLC, USA) at a wavelength of 570 nm. Sodium selenite cytotoxic effect on cells was determined according to the cytotoxicity detection kit protocol.

For the lactate dehydrogenase (LDH) assay, the cells were cultured similarly as described above. The cell culture medium (10 μl) was collected from the cultured wells in a fresh 96-well plate. Next, PBS (40 μl) and LDH reagent (50 μl) was pipetted to every well of the plate and incubated (45 minutes) in the dark at 25˚C. To end the enzymatic reaction, a stop solution (50 μl) was added to each well. Using a UV-Vis spectrophotometer, optical density was noted at 490 nm. For positive control, the optical density of total cell lysate was recorded.

Alkaline phosphatase activity

In 48-wells plates, MC3T3-E1 cells were cultured at a density of 5×10^4 cells/well. Then, sodium selenite with or without hydrogen peroxide (H_2O_2) was treated with various doses (0, 0.2, 0.4, 0.8, 1.6, 3.2, and 6.4 μM) to MC3T3-E1 cells. After incubating for 48 hours, cold PBS was used to wash the cells twice. The cold RIPA buffer (100 μl) was then added to each well and shaked gently. The whole-cell lysate was subjected to centrifugation for 20 minutes at 4˚C and 14,000 rpm. The supernatant (20 μl) was collected and

added to the CSPD substrate (100 µl). The reaction solution was then kept for 30 minutes at room temperature. The luminescence intensity was recorded by using a luminometer (Glomax, Promega, USA). The luminescence of the total cell lysate was used for normalization.

Sirius red staining

In a 48-well plate, the MC3T3-E1 cells were treated for 7 days with 3.2 µM of sodium selenite. The medium, along with sodium selenite was substituted every second day. After treatment, Bouin's fluid was used to fix the cells for 1 hour. Sirius Red dye (1 mg/ml in saturated aqueous picric acid) was then used to stain the cells for 1 hour. To quantitate the Sirius Red dye from the stained cells, 0.1 N sodium hydroxide was added for 30 minutes to the wells. After dissolving the dye, optical density was measured at 550 nm using a spectrophotometer in triplicate cultures (sodium hydroxide (0.1 N) was used as a blank).

Real-time reverse transcription polymerase chain reaction

MC3T3-E1 cells were cultured in a 6-wells plate at a density of 3×10^5 cells/well and were subjected to 3.2 µM of sodium selenite. The cellular RNA was collected using Trizol reagent after 48 hour of treatment. The absorbance ratio (260/280) was measured to determine the quality of the collected RNA. Also, RNA was separated on an agarose gel to observe its integrity. The real-time polymerase chain reaction (PCR) was performed as per our lab protocol (25). By using 2 µg of RNA, SuperScript II Reverse Transcriptase was used to synthesize cDNA. With 1 µl of the synthesized cDNA, real-time PCR was performed using SYBR green qPCR MasterMix and Rotor-Gene 3000 real-time PCR, Corbett, Germany. The qPCR procedure was as follows: an initial step of denaturation for 10 minutes at 95˚C as, and 40-cycles of amplification at 95˚C for 20 seconds, at 60˚C for 20 seconds, and extension at 72˚C for 25 seconds. *GAPDH* was used to standardize the relative expression of mRNAs and was quantified by the double delta CT (ΔΔCT) method. Table 1 shows the list of primer sequences used.

Western blotting

In a 6-wells plate, MC3T3-E1 cells were grown at a 3×10^5 cells/well density. Sodium selenite (3.2 µM) was treated to the cells for 12, 24, and 48 hours. The protein was isolated and loaded on sodium dodecyl sulfate (SDS)-polyacrylamide gel. The separated proteins on the gel were transferred to a polyvinylidene fluoride (PVDF) membrane. 5% skim milk was used to block the membrane for 1 hour, and then it was incubated with antibodies against OSX, β-catenin, Runx2, and β-actin overnight at 4˚C. After that, 1X TBST (Tris-buffered saline, 0.1% Tween 20) was used to wash the membranes and incubated with horseradish peroxidase-conjugated secondary antibodies for 45 minutes at room temperature. Chemiluminescence reagent was used to visualize the target protein bands. As a loading control, β-actin was used. Image J software (NIH, USA) was used to quantify the band intensities.

Table 1: Mouse primers for real-time reverse transcription polymerase chain reaction (RT-PCR)

Gene	Primer sequence (5′-3′)
OSX	F: GGAAAGGAGGCACAAAGAAGCCAT
	R: AGTCCATTGGTGCTTGAGAAGGGA
Col1a	F: TTCTCCTGGCAAAGACGGAC
	R: AGGAAGCTGAAGTCATAACCGCCA
OCN	F: TGCTTGTGACGAGCTATCAG
	R: GAGGACAGGGAGGATCAAGT
Runx2	F: AAGTGCGGTGCAAACTTTCT
	R: TCTCGGTGGCTGGTAGTGA
GAPDH	F: TCGTGGATCTGACGTGCCGCCTG
	R: CACCACCCTGTTGCTGTAGCCGTAT

Statistical analysis

The quantitative statistical analysis was performed using Graphpad Prism 5.0 (San Diego, CA) software utilizing a two-tailed Student's t test. A data value of $P<0.05$ was considered statistically significant.

Results

Sodium selenite induces osteogenic activity in osteoblasts. To assess any effect of sodium selenite on the cell viability and cytotoxicity of MC3T3-E1, various concentrations (0, 0.1, 0.2, 0.4, 0.8, 1.6, and 3.2 µM) of sodium selenite was treated to the cells for 24 hours. MTT and LDH assays were used to evaluate the cell viability and cytotoxicity of MC3T3-E1, respectively. Various concentrations of sodium selenite demonstrated no effect on cell viability and cytotoxicity of osteoblasts (Fig.1A, B).

To assess any osteogenic effect of sodium selenite on osteoblasts, various concentrations (0, 0.1, 0.2, 0.4, 0.8, 1.6, and 3.2 µM) of sodium selenite were treated to MC3T3-E1 cells for 48 hours, and ALP activity was analyzed. ALP is an enzyme found in osteoblasts and is regarded as a marker of osteoblast differentiation. The sodium selenite-treated osteoblasts showed significantly increased ALP activity at a concentration of 1.6 and 3.2 µM compared to control; however, a remarkable decrease in the ALP activity of MC3T3-E1 cells was observed at a dose of 6.4 µM (Fig.1C).

Further, the osteogenic effect of sodium selenite was confirmed by the mRNA expression levels of osteogenic markers. Sodium selenite (3.2 µM) was treated to the MC3T3-E1 cells for 24 hours. The mRNA levels of master regulator for osteogenesis (*OSX*), osteoblast differentiation transcriptional factor (*Runx2*), and terminal differentiation

markers *Col1α* and *OCN* were detected through real-time qRT-PCR. Sodium selenite induced the mRNA expression of *OSX* (~2 folds), *Runx2* (~2 folds), *Col1α* (~2 folds), and *OCN* (~2 folds) in comparison with control (Fig.1D). As evidenced by Sirius red staining, Collagen depositions were increased by ~1.8 folds in 3.2 µM of sodium selenite-treated osteoblasts compared to control (Fig.1E). In conclusion, sodium selenite can induce osteogenic differentiation in osteoblasts.

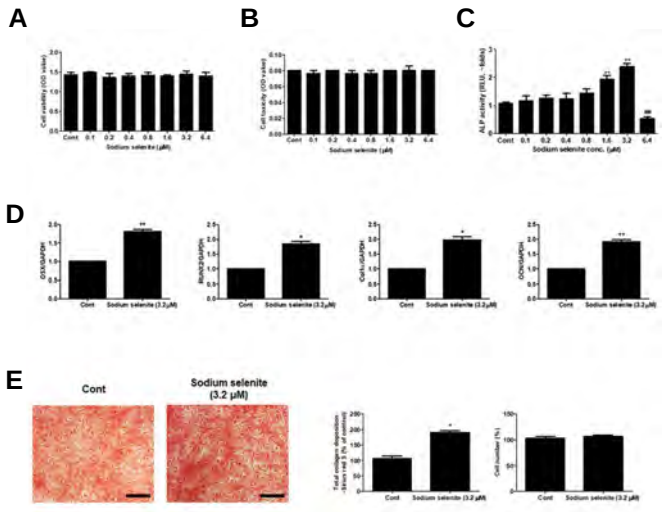

Fig.1: Effect of sodium selenite in osteoblasts. Sodium selenite was treated various concentration (0, 0.1, 0.2, 0.4, 0.8, 1.6, and 3.2 µM) in osteoblasts. **A.** Cell viability and **B.** Cell cytotoxicity of sodium selenite were evaluated through MTT and LDH assay, respectively. **C.** The osteogenic activity of sodium selenite was confirmed through ALP activity. **D.** Genes expression of the osteogenic markers (*OSX*, *Runx2*, *Col1*α, and *OCN*) in sodium selenite (3.2 µM)-treated osteoblasts. Results are represented as a fold increase relative to *GAPDH* expression. All data are shown as the mean ± SD. Similar results were obtained in three independent experiments. *; P≤0.05, **,##; P≤0.01 compared to the control, MTT; 3-(4,5-Dimethylthiazol-2-yl)-2,5-diphenyltetrazolium bromide, LDH; Lactate dehydrogenase, ALP; Alkaline phosphatase, Cont; Control, and OD; Optical density.

Sodium selenite recovered the osteoblast differentiation in H_2O_2-stimulated osteoblasts.

Previous studies have reported that H_2O_2 induces oxidative stress and contributes to the suppression of the differentiation process of osteoblasts (17). To confirm the osteogenic effect of sodium selenite in H_2O_2-stimulated osteoblasts, H_2O_2 (100 µM) was treated alone or with sodium selenite (3.2 µM) to osteoblasts at various concentrations (0, 0.1, 0.2, 0.4, 0.8, 1.6, and 3.2 µM) for 48 hours. Alone treatment of H_2O_2 notably decreased the ALP activity of osteoblasts. However, decreased ALP activity was significantly recovered to a level similar to that of the control when 1.8 and 3.2 µM of sodium selenite was co-treated (Fig.2A). Further, H_2O_2 (100 µM) was treated alone or with sodium selenite (3.2 µM) to osteoblasts for 48 hours. Collected protein lysate was analyzed for the expression of osteogenic transcriptional factors for osteoblasts by western blotting. Treatment of H_2O_2 decreased the expression of osteogenic transcriptional factors (Runx2 and OSX) at the protein levels. However, decreased expression levels of Runx2 and OSX were recovered with a co-treatment of 3.2 µM of sodium selenite (Fig.2B). Our results showed that sodium selenite treatment to MC3T3-E1 cells could mask the suppressive effect of H_2O_2 on the osteogenesis process. Thus, the ability of sodium selenite to affect bone-forming signaling might be expected.

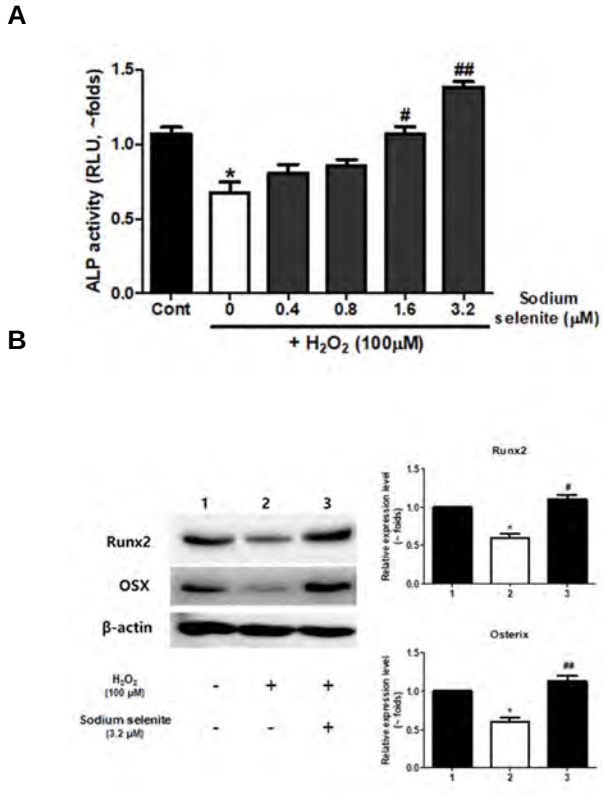

Fig.2: Effect of sodium selenite in H_2O_2-stimulated osteoblasts. **A.** Sodium selenite (3.2 µM) was pretreated to osteoblasts for 24 hours, and after that, H_2O_2 (100 µM) was treated for 48 hours. After 48 hours of incubation, ALP activity was analyzed. **B.** The osteogenic markers protein level was detected after 48 hours of sodium selenite (3.2 µM) treatment. To normalize the densitometry of western blot bands, β-actin was used as a loading control. All data are shown as the mean ± SD. Similar results were obtained in three independent experiments. *,#; P≤0.05 compared to the control, ##; P≤0.01 compared to the H_2O_2-stimulated osteoblasts, ALP; Alkaline phosphatase, and RLU; Relative luminescence units.

Sodium selenite recovers the suppressed WNT/β-catenin signaling pathway in H_2O_2-stimulated osteoblasts

WNT/β-catenin signaling pathway is crucial for the differentiation of osteoblast and bone formation (12). We next assessed the involvement of the WNT/β-catenin signaling pathway in the induction of osteogenesis in osteoblasts by sodium selenite in H_2O_2-stimulated osteoblasts. For this, *Axin-2* luciferase reporter construct was transfected to osteoblasts for 24 hours using Genefectine reagent (Genetrone Biotech, Korea), and the cells were treated with H_2O_2 (100 µM) alone or with 3.2 µM of sodium selenite for 12 and 24 hours. Compared to control, the Axin-2 luciferase activity was found decreased by H_2O_2 in both the treatments for 12 and 24 hours. While co-treatment of sodium selenite with H_2O_2 for 24 hours significantly recovered the reduced Axin-2 reporter activity, suppressed by H_2O_2 (Fig.3A).

Upon activation of the WNT signaling pathway, β-catenin gets localized to the nucleus and stabilizes. β-catenin then binds to the TCF/LEF family of DNA-binding proteins and regulates osteogenesis by targeting WNT-mediated genes (13). Therefore, osteoblasts were treated with H_2O_2 (100 μM) alone or with sodium selenite (3.2 μM) for 12 and 24 hours, and western blotting was performed to analyze the stability of β-catenin molecules. H_2O_2 decreased stabilization of β-catenin molecules after 12 and 24 hours of treatment, but sodium selenite was able to significantly recover the reduced β-catenin stabilization level by H_2O_2 after treatment of 24 hours (Fig.3B). Taken together, through WNT/β-catenin signaling, sodium selenite recovers the osteogenic activity reduced by H_2O_2 in osteoblasts.

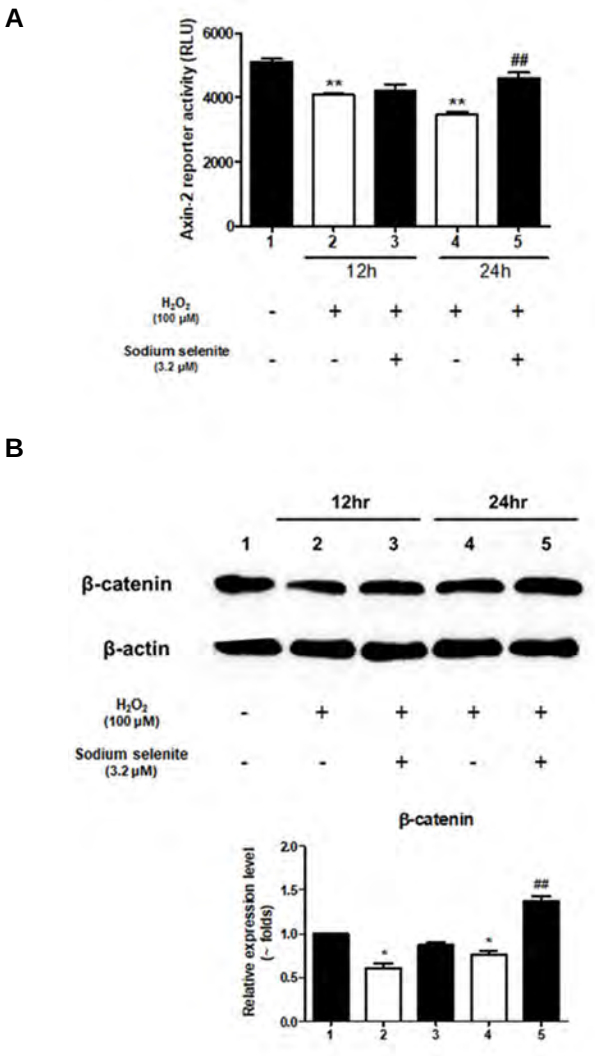

Fig.3: Sodium selenite activates the WNT/β-catenin signaling pathway in H_2O_2-stimulated osteoblasts. **A.** Axin-2 reporter plasmid was transfected to osteoblast for 24 hours. Sodium selenite (3.2 μM) was pretreated to MC3T3 E-1 cells for 24 hours followed by H_2O_2 (100 μM) treatment for 48 hours. As described in materials and methods, luciferase activities were measured in cell lysates. Renilla luciferase activity was used to normalize the luciferase activity of the cell lysates. **B.** Sodium selenite (3.2 μM) was pretreated to MC3T3 E-1 cells for 24 hours followed by H_2O_2 (100 μM) treatment for 12 and 24 hours. After 12 and 24 hours, protein lysates were collected, and western blotting was performed. To normalize the densitometry of western blot bands, β-actin was used as a loading control. Data are shown as the mean ± SD of three independent experiments. *; P≤0.05 compared to the control, **, ##; P≤0.01 compared to the H2O2-stimulated osteoblasts, and hr; Hours.

Discussion

Selenium is a vital trace element and is an essential constituent of selenocysteine (SeCys) residues. It has been known to modulate the functioning of various selenocysteine-containing intracellular selenoproteins (26). Selenium is an essential constituent of several antioxidant enzymes which plays a vital role in scavenging the free radicals released during normal oxygen metabolism (27). Lately, a case-control study on the elderly population showed a decreased risk of osteoporotic hip fracture in people with high selenium intake. However, it was also largely dependent on smoking status (28). Moreover, a bone phenotype showing poorly developed cortical and trabecular mineralization in rodents was due to low dietary selenium intake (22). Also, selenium as sodium selenite has been shown to regulate OCN expression in osteoblasts, required for the formation of a mineralized matrix of bone (29). Thus, we tried to observe the effect of selenium on the osteogenic differentiation process of osteoblasts. Our results showed that in MC3T3-E1 cells sodium selenite stimulated the ALP activity. Additionally, induction in the expression levels of mRNAs of osteogenic transcriptional factors (*OSX* and *Runx-2*), osteogenic markers *(Col1α* and *OCN*) and increased collagen synthesis further confirmed the stimulatory ability of sodium selenite on the osteogenic activity of MC3T3-E1 cells.

Varied environmental conditions or agents or even the normal cellular metabolism may produce ROS, which has been found responsible for the pathogenesis of various pathologies, including osteoporosis (30). H_2O_2, being a member of the ROS family has the ability to diffuse across biological membranes and cause varied kinds of biological activities. It has been reported that exogenous treatment of H_2O_2 inhibits osteoblastic differentiation in MC3T3-E1 and bone marrow stromal cells (MSCs) cells (31-34). Previously, sodium selenite has been shown to protect bone MSCs against H_2O_2-induced inhibition of osteoblastic differentiation. The study observed that the effect of sodium selenite was associated with oxidative stress inhibition and the Mitogen-activated protein kinase (MAPK) signaling pathway (17). Hence, in MC3T3-E1 cells, we tried to confirm the effect of H_2O_2 and, at the same time, observed the rescue effect of sodium selenite, if any, on the osteogenic activity (ALP activity). It was observed that the treatment of sodium selenite (3.2 μM) significantly rescued the adverse effect of H_2O_2 on the osteogenic differentiation marker (ALP activity) in pre-osteoblast cells. This rescued effect of sodium selenite on H_2O_2 suppressed ALP activity in MC3T3-E1 cells was due to rescuing the repressed expression of osteogenic transcription factors (*OSX* and *Runx-2*). Lately, it has been observed that in postmenopausal women with osteoporosis, oxidative stress is negatively associated with BMD of total femora (35). Moreover, in ovariectomized rats, H_2O_2 and the levels of lipid peroxidation were increased, while enzymatic antioxidants like glutathione S transferase (GST), superoxide dismutase (SOD),

glutathione peroxidase (GPx) were reduced in femora tissue homogenates (36). In osteoblasts and bone MSCs, various types of selenoproteins or selenoenzymes, including thioredoxin reductases, GPx, selenoprotein P, and types 2 iodothyronine deiodinases are known to be expressed. In bone MSCs, the expression of the antioxidant enzyme GPx is required to protect against the oxidative damage induced by H_2O_2 (37). Liu et al. (17) also observed that the pretreatment of sodium selenite to bone MSCs effectively suppressed H_2O_2-induced oxidative stress by increasing the total antioxidant capacity (TAOC) and decreased glutathione (GSH) levels and suppressing intracellular ROS levels and lipid peroxidation. Thus, it might be expected that pretreatment of sodium selenite was able to rescue the inhibitory role of the H_2O_2 on the osteoblastic differentiation process by enhancing the expression of antioxidant enzymes like GPx, as observed by the previous researchers.

The WNT/β-catenin signaling pathway is essential for bone formation by regulating the various processes of osteoblastogenesis like proliferation, differentiation, and mineralization (12). Since sodium selenite was able to attenuate the decrease in osteogenic markers and ALP activity in MC3T3-E1 cells treated with H_2O_2, we next tried to examine the role of the WNT/β-catenin signaling pathway in the rescue effect mediated by sodium selenite. Treatment of H_2O_2 decreased the *Axin-2* reporter activity after 12 and 24 hours. A similar decrease in β-catenin stability was observed in H_2O_2 treated MC3T3-E1 cells. Co-treatment of sodium selenite along with H_2O_2 to MC3T3-E1 cells significantly recovered the suppressed *Axin-2* reporter activity after 24 hour of treatment. This was further established by increased stability of β-catenin after the co-treatment of sodium selenite with H_2O_2 to MC3T3-E1 cells. An increase in β-catenin stability and *Axin-2* reporter activity after sodium selenite treatment implicates the involvement of the WNT signaling pathway in osteoblasts. The stimulatory effect of sodium selenite on the WNT signaling pathway might explain the rescue effect of sodium selenite on the osteogenic activity of H_2O_2 stimulated MC3T3-E1 cells. MAPKs play an essential role in bone formation. Studies have shown that the ERK1/2 signaling pathway is responsible for the inhibitory effect of H_2O_2 on osteoblastic differentiation (31, 32). Though other MAPKs like (JNK and p38) have also been implicated in the physiological processes mediated by oxidative stress (38) but their role in H_2O_2-induced inhibition of osteoblastic differentiation is not clearly understood (31, 32). Lately, it was observed that H_2O_2-mediated adverse effect on osteoblastic differentiation of bone MSCs was inhibited by selenium. The effect was due to a decrease in oxidative stress and partly stimulation of the ERK signaling pathway (17). Previous studies have highlighted a crosstalk between MAPKs and WNT signaling pathways during the osteoblast differentiation process, largely decided by the kind of stimuli (25, 39). Thus, future studies are essential to understand any physical crosstalk of MAPKs with the WNT signaling pathway under the influence of selenium in the induction of osteogenic activity in osteoblasts.

Conclusion

Our study demonstrates the osteogenic stimulatory ability of selenium in osteoblasts. Sodium selenite was able to exert induction in the differentiation of osteoblasts as represented by elevation in ALP activity, increased mRNA levels of *OSX*, *Runx2*, *Col1α*, and *OCN*, and enhanced collagen synthesis. Moreover, sodium selenite was able to rescue the H_2O_2-mediated suppression of osteoblastic differentiation in osteoblasts. Sodium selenite was able to achieve this by activating WNT signaling pathway in osteoblasts. With these findings, it may be concluded that the role of selenoproteins in bone formation has just been recognized, and further detailed studies may validate them as potential therapeutic interventions for osteoporosis.

Acknowledgments

This study was supported by Hallym University Research Fund 2016 (HURF-2016-51) and by Basic Science Research Program through the National Research Foundation of Korea (NRF) funded by the Ministry of Education (NRF-2020R1C1C1008694 and NRF-2020R1I1A3074575). There is no conflict of interest in this study.

Authors' Contributions

A.R.S., G.S.; Designed the experiments, performed the experiments, generated data, and wrote the manuscript. Y.-H.L.; Performed the experiments, generated data, and wrote the manuscript. C.C.; Helped with results, discussion and interpretations. S.-S.L., E.-M.S.; Provided the facilities and helped drafting the manuscript. All authors have read and approved the final manuscript.

References

1. Rachner TD, Khosla S, Hofbauer LC. Osteoporosis: now and the future. Lancet. 2011; 377(9773): 1276-1287.
2. Anthamatten A, Parish A. Clinical update on osteoporosis. J Midwifery Womens Health. 2019; 64(3): 265-275.
3. Reid IR. Short-term and long-term effects of osteoporosis therapies. Nat Rev Endocrinol. 2015; 11(7): 418-428.
4. Pacifici R. Cytokines, estrogen, and postmenopausal osteoporosis--the second decade. Endocrinology. 1998; 139(6): 2659-2661.
5. Zhou X, Yuan W, Xiong x, zhang z, liu j, zheng y, et al. Ho-1 in bone biology: potential therapeutic strategies for osteoporosis. Front Cell Dev Biol. 2021; 9: 791585.
6. Luo G, Li F, Li X, Wang ZG, Zhang B. TNFalpha and RANKL promote osteoclastogenesis by upregulating RANK via the NFkappaB pathway. Mol Med Rep. 2018; 17(5): 6605-6611.
7. Manolagas SC. From estrogen-centric to aging and oxidative stress: a revised perspective of the pathogenesis of osteoporosis. Endocr Rev. 2010; 31(3): 266-300.
8. Sharma AR, Nam JS. Kaempferol stimulates WNT/beta-catenin signaling pathway to induce differentiation of osteoblasts. J Nutr Biochem. 2019; 74: 108228.
9. Jagga S, Sharma AR, Kim EJ, Nam JS. Isoflavone-enriched whole soy milk powder stimulates osteoblast differentiation. J Food Sci Technol. 2021; 58(2): 595-603.
10. Ross JA, Kasum CM. Dietary flavonoids: bioavailability, metabolic

effects, and safety. Annu Rev Nutr. 2002; 22: 19-34.
11. Kocijan R, Klaushofer K, Misof BM. Osteoporosis therapeutics 2020. Handb Exp Pharmacol. 2020; 262: 397-422.
12. Baron R, Kneissel M. WNT signaling in bone homeostasis and disease: from human mutations to treatments. Nat Med. 2013; 19(2): 179-192.
13. Karner CM, Long F. Wnt signaling and cellular metabolism in osteoblasts. Cell Mol Life Sci. 2017; 74(9): 1649-1657.
14. Cross CE, Halliwell B, Borish ET, Pryor WA, Ames BN, Saul RL, et al. Oxygen radicals and human disease. Ann Intern Med. 1987; 107(4): 526-545.
15. Forman HJ, Torres M. Redox signaling in macrophages. Mol Aspects Med. 2001; 22(4-5): 189-216.
16. Nordberg J, Arner ES. Reactive oxygen species, antioxidants, and the mammalian thioredoxin system. Free Radic Biol Med. 2001; 31(11): 1287-1312.
17. Liu H, Bian W, Liu S, Huang K. Selenium protects bone marrow stromal cells against hydrogen peroxide-induced inhibition of osteoblastic differentiation by suppressing oxidative stress and ERK signaling pathway. Biol Trace Elem Res. 2012; 150(1-3): 441-450.
18. Yang Y, Su Y, Wang D, Chen Y, Wu T, Li G, et al. Tanshinol attenuates the deleterious effects of oxidative stress on osteoblastic differentiation via Wnt/FoxO3a signaling. Oxid Med Cell Longev. 2013; 2013: 351895.
19. Liang D, Xiang L, Yang M, Zhang X, Guo B, Chen Y, et al. ZnT7 can protect MC3T3-E1 cells from oxidative stress-induced apoptosis via PI3K/Akt and MAPK/ERK signaling pathways. Cell Signal. 2013; 25(5): 1126-1135.
20. Lean JM, Jagger CJ, Kirstein B, Fuller K, Chambers TJ. Hydrogen peroxide is essential for estrogen-deficiency bone loss and osteoclast formation. Endocrinology. 2005; 146(2): 728-735.
21. Wang Y, Xie D, Li J, Long H, Wu J, Wu Z, et al. Association between dietary selenium intake and the prevalence of osteoporosis: a cross-sectional study. BMC Musculoskelet Disord. 2019; 20(1): 585.
22. Moreno-Reyes R, Egrise D, Neve J, Pasteels JL, Schoutens A. Selenium deficiency-induced growth retardation is associated with an impaired bone metabolism and osteopenia. J Bone Miner Res. 2001; 16(8): 1556-1563.
23. Sun JY, Hou YJ, Fu XY, Fu XT, Ma JK, Yang MF, et al. Selenium-containing protein from selenium-enriched spirulina platensis attenuates cisplatin-induced apoptosis in MC3T3-E1 mouse preosteoblast by inhibiting mitochondrial dysfunction and ROS-mediated oxidative damage. Front Physiol. 2018; 9: 1907.
24. Lee SS, Sharma AR, Choi BS, Jung JS, Chang JD, Park S, et al. The effect of TNFalpha secreted from macrophages activated by titanium particles on osteogenic activity regulated by WNT/BMP signaling in osteoprogenitor cells. Biomaterials. 2012; 33(17): 4251-4263.
25. Nam JS, Sharma AR, Jagga S, Lee DH, Sharma G, Nguyen LT, et al. Suppression of osteogenic activity by regulation of WNT and BMP signaling during titanium particle induced osteolysis. J Biomed Mater Res A. 2017; 105(3): 912-926.
26. Allan CB, Lacourciere GM, Stadtman TC. Responsiveness of selenoproteins to dietary selenium. Annu Rev Nutr. 1999; 19: 1-16.
27. Maleki N, Safavi A, Doroodmand MM. Determination of selenium in water and soil by hydride generation atomic absorption spectrometry using solid reagents. Talanta. 2005; 66(4): 858-862.
28. Zhang J, Munger RG, West NA, Cutler DR, Wengreen HJ, Corcoran CD. Antioxidant intake and risk of osteoporotic hip fracture in Utah: an effect modified by smoking status. Am J Epidemiol. 2006; 163(1): 9-17.
29. Sun L, Yu F, Xu Z, Zeng X, Ferreri M, Han B. Alteration of osteocalcin mRNA expression in ovine osteoblasts in dependence of sodium fluoride and sodium selenite medium supplementation. Acta Biol Hung. 2010; 61(1): 52-63.
30. Finkel T, Holbrook NJ. Oxidants, oxidative stress and the biology of ageing. Nature. 2000; 408(6809): 239-247.
31. Bai XC, Lu D, Bai J, Zheng H, Ke ZY, Li XM, et al. Oxidative stress inhibits osteoblastic differentiation of bone cells by ERK and NF-kappaB. Biochem Biophys Res Commun. 2004; 314(1): 197-207.
32. Xu ZS, Wang XY, Xiao DM, Hu LF, Lu M, Wu ZY, et al. Hydrogen sulfide protects MC3T3-E1 osteoblastic cells against H2O2-induced oxidative damage-implications for the treatment of osteoporosis. Free Radic Biol Med. 2011; 50(10): 1314-1323.
33. Mody N, Parhami F, Sarafian TA, Demer LL. Oxidative stress modulates osteoblastic differentiation of vascular and bone cells. Free Radic Biol Med. 2001; 31(4): 509-519.
34. Kim WK, Meliton V, Bourquard N, Hahn TJ, Parhami F. Hedgehog signaling and osteogenic differentiation in multipotent bone marrow stromal cells are inhibited by oxidative stress. J Cell Biochem. 2010; 111(5): 1199-1209.
35. Sendur OF, Turan Y, Tastaban E, Serter M. Antioxidant status in patients with osteoporosis: a controlled study. Joint Bone Spine. 2009; 76(5): 514-518.
36. Muthusami S, Ramachandran I, Muthusamy B, Vasudevan G, Prabhu V, Subramaniam V, et al. Ovariectomy induces oxidative stress and impairs bone antioxidant system in adult rats. Clin Chim Acta. 2005; 360(1-2): 81-86.
37. Ebert R, Ulmer M, Zeck S, Meissner-Weigl J, Schneider D, Stopper H, et al. Selenium supplementation restores the antioxidative capacity and prevents cell damage in bone marrow stromal cells in vitro. Stem Cells. 2006; 24(5): 1226-1235.
38. McCubrey JA, Lahair MM, Franklin RA. Reactive oxygen species-induced activation of the MAP kinase signaling pathways. Antioxid Redox Signal. 2006; 8(9-10): 1775-1789.
39. Guo C, Yang RJ, Jang K, Zhou XL, Liu YZ. Protective effects of pretreatment with quercetin against lipopolysaccharide-induced apoptosis and the inhibition of osteoblast differentiation via the MAPK and Wnt/beta-Catenin pathways in MC3T3-E1 cells. Cell Physiol Biochem. 2017; 43(4): 1547-1561.

Original Article

Comparison of Skin Transcriptome between Responder and Non-Responder Vitiligo Lesions to Cell Transplantation: A Clinical Trial Study

Hadis Abdolahzadeh, M.Sc.[1, 2], Parvaneh Mohammadi, Ph.D.[1], Mahshid Ghasemi, M.D.[3], Seyed Ahmad Mousavi, M.Sc.[1], Amir Bajouri, M.D.[3, 4], Leila Ataei-Fashtami, M.D.[3], Mehdi Totonchi, Ph.D.[1, 5], Mohammad Rezvani, M.D.[3], Nasser Aghdami, M.D., Ph.D.[3*], Saeed Shafieyan, M.D.[3*]

1. Department of Stem Cells and Developmental Biology, Cell Science Research Center, Royan Institute for Stem Cell Biology and Technology, ACECR, Tehran, Iran
2. Department of Molecular and Cellular Biology, Faculty of Basic Sciences and Advanced Technologies in Biology, University of Science and Culture, ACECR, Tehran, Iran
3. Department of Regenerative Biomedicine, Cell Science Research Center, Royan Institute for Stem Cell Biology and Technology, ACECR, Tehran, Iran
4. Skin and Stem Cell Research Center, Tehran University of medical Sciences, Tehran, Iran

5. Department of Genetics, Reproductive Biomedicine Research Center, Royan Institute for Reproductive Biomedicine, ACECR, Tehran, Iran

Corresponding Address: P.O.Box: 16635-148, Department of Regenerative Biomedicine, Cell Science Research Center, Royan Institute for Stem Cell Biology and Technology, ACECR, Tehran, Iran
Emails: nasser.aghdami@royaninstitute.org, sshafiiyan@yahoo.com

Received: 13/December/2020, Accepted: 28/April/2021

Abstract

Objective: Autologous transplantation of epidermal cells has been used increasingly to treat vitiligo patients and is a simple, safe, and relatively efficient method. However, the outcome is not always satisfactory, and some patients show less or no response to this treatment. This study was evaluated to identify genes expressed differently among responders and non-responders to cell transplantation to find potential markers that could predict 'patients' responses to this type of cell therapy.

Materials and Methods: Eleven stable vitiligo patients who received autologous epidermal cell transplantation were included in this clinical trial study. Before cell transplantation, skin samples were obtained from the recipient's vitiligo lesions. After epidermal cell transplantation, patients were followed for at least six months to assess the response to epidermal cell injection. RNA sequencing was used to determine potential gene expression profile differences between responder and non-responder vitiligo patients.

Results: The RNA sequencing results showed differences in expression levels of 470 genes between the skin specimens of responder versus non-responder patients. There were 269 up-regulated genes and 201 down-regulated genes. Upregulated genes were involved in processes, such as Fatty Acid Omega Oxidation. Down-regulated genes were related to PPAR signaling pathway, and estrogen signaling pathway. Among the most differentially expressed genes (DEGs) with the most altered RNA expression levels in responders versus non-responder patients, we selected three genes (up-regulated genes *KRTAP10-11* and down-regulated genes *IP6K2* and *C9*) as potential biomarkers, which are involved in associated pathways.

Conclusion: Based on our findings, it is estimated that proposed genes might predict the response of vitiligo patients to cell therapy. However, further studies are required to clarify the role of these genes in pathogenesis and to characterize gene expression in a larger number of vitiligo patients in the context of epidermal cell transplantation therapy (registration number: IRCT201508201031N16).

Keywords: Cell Therapy, Prediction, RNA Sequencing, Vitiligo

Cell Journal(Yakhteh), Vol 24, No 6, June 2022, Pages: 316-322

Citation: **Abdolahzadeh H, Mohammadi P, Ghasemi M, Mousavi SA, Bajouri A, Ataei-Fashtami L, Totonchi M, Rezvani M, Aghdami N, Shafieyan S. Comparison of skin transcriptome between responder and non-responder vitiligo lesions to cell transplantation: a clinical trial study. Cell J. 2022; 24(6): 316-322. doi: 10.22074/cellj.2022.7893.**

Introduction

Vitiligo is a relatively common skin disease that appears as hypopigmented or depigmented skin lesions affecting 0.5-1% of the population worldwide. Although vitiligo is not life-threatening, it can lead to social avoidance and reduce the 'patients' quality of life (1, 2). Various surgical and non-surgical therapies are currently available to treat this disease. Surgical methods such as skin grafting are not suitable for large skin lesions and may not always be applicable for areas such as the lips, eyelids, and genital areas which are commonly affected. Complications include heterogeneity of texture and color with the surrounding recipient skin and infection of the graft site (3).

On the other hand, medical treatments are often less effective than surgical procedures and are associated with relatively high recurrence rates following their discontinuation (4). Phototherapy is another treatment option. However, there is concern on whether ultraviolet (UV) exposure predisposes patients to skin cancer (5-7), but current scientific literature shows conflicting results

(8). In recent decades, cell therapy has been introduced as a novel therapeutic choice for patients with stable vitiligo, particularly those resistant to other available treatments (9). However, response to treatment is not seen in all patients and is not predictable. For instance, in Orouji et al. (10) study, a total of 1060 patches in 300 stable vitiligo patients were treated with intra-lesional epidermal cell suspension; however, 22.3% of the patients did not respond to the treatment after 30 months of follow-up.

Considering the risk of local adverse effects on the donor site, such as hypopigmentation and scar formation, the treatment cost, and the psychological problems resulting from poor treatment outcomes, it is necessary to find markers and develop reliable methods to predict the response rate to cell transplantation in vitiligo patients.

Here, we compared the skin transcriptome between responder and non-responder patients treated with epidermal cell suspension to find molecular biomarkers that could potentially predict response to cell transplantation.

Materials and Methods

Case selection

Vitiligo patients were recruited with informed consent from the Dermatology Clinic at Royan Institute between February 2017 and September 2017. Inclusion criteria included focal or generalized vitiligo patients aged 18-50 years old, with clinical stability of at least one year before recruitment to the study, and at least one vitiligo lesion on the trunk or limbs. Pregnant or lactating women, patients with active infectious diseases or undergoing any kind of cell therapy, and patients with a history of UV or laser therapy, or previous treatment with immunosuppressive or cytotoxic medications within six months before entry to the study, were excluded. Vitiligo lesions on the trunk or limbs were selected to obtain biopsy specimens, and none of the biopsies were taken from facial lesions due to aesthetic concerns.

This clinical trial study was approved by the Ethics Committee of the Royan Institute. The trial was registered with the United States National Library of Medicine Clinical Trials.gov (NCT00631865). The clinical trial was also registered with the Iranian Registry of Clinical Trials (IRCT201508201031N16). The Research Ethics Committee of Royan Institute approved skin biopsies for RNA sequencing (IR.ACECR.ROYAN.REC.1396.196).

Skin sampling, cell preparation, and transplantation

Skin sampling, cellular suspension separation techniques, and cell transplantation techniques were adapted from Khodadadi et al. (11) study. Briefly, the skin sample was obtained from the thigh-buttock junction as a donation site, with about one-third to the one-seventh surface area. The skin pieces were incubated with dispase II until the epidermis separated from the dermis. Subsequently, epidermal cells were separated from each other by trypsin/EDTA. The cell suspension was injected intralesionally by a trained dermatologist one day after the skin biopsy.

Obtaining skin biopsy

Selected vitiligo lesions were disinfected and anesthetized by a local injection of 0.2-0.3 ml of 1% lidocaine by the dermatologist. Before cell transplantation, two 2.5 mm diameter punch biopsy samples were obtained from the vitiligo area. The biopsy specimens were immersed inside liquid nitrogen for 30 seconds, and then transferred to the -80˚C freezer until the RNA was extracted.

Assessment of repigmentation

The percentage of repigmentation in the treated lesions was assessed subjectively by a dermatologist before and at 2, 4, and 6 months after the treatment. Grades 0, I, II, III and IV were assigned to patches with 0, 1-24%, 25-49%, 50-74% and 75-100% of repigmentation. Repigmentation was assessed based on lesion color and size changes in photographs. Patches with repigmentation of $\geq 25\%$ were considered as "responder" patches (10).

RNA extraction

Total RNA was extracted from skin biopsies stored at the -80˚C freezer using the TRIzol reagent (Invitrogen, 15596-018) and RNeasy micro kit Cat No. /ID: 74004. RNA quantity and quality were measured using Agilent Technologies 2100 Bioanalyzer (or 2200 TapeStation).

Whole transcriptome RNA sequencing and data analysis

Total RNA was extracted from 11 samples for library preparation, and the library was constructed using the TruSeq RNA Access Library Prep Kit. Sequencing was done using the NovaSeq Sequencer. The quality of produced data was determined using the FastQC V-0.11.8 software. The reads were filtered based on sequencing quality with the Trimmomatic V-0.36. Trimmed reads were then mapped to reference genome GRCh V-38 using HISAT2 V-2.1.0. Finally, the number of reads aligning to each gene was determined using htseq-count V-0.11.2 based on gene annotation file GTF V-91. Normalization and differential expression analysis were done using the DESeq2 package in R statistical software. We used $P<0.05$, $1.5 \leq$ fold change ≤ -1.5. Pathway enrichment analysis of the DEGs was performed by Enrichr database (12). RNA sequencing data has been published in NCBI GEO, accession number PRJNA633437.

Results

Patients characteristics

Skin biopsies were obtained from 11 patients with stable vitiligo (5 females and 6 males) with a mean age of 28.63 years. None of the patients reported any family history of autoimmune diseases such as vitiligo and thyroid diseases.

Clinical outcomes

The follow-up visits were performed at 2, 4, and 6 months after cell transplantation. Six months after cell therapy, based on clinical assessment of treated patches by one dermatologist, 6 patients were considered responders to treatment with repigmentation of 25-49% (grade II) while 5 patients were considered unresponsive with repigmentation of 1-24% (grade 1) (Table 1). Figure 1 shows the extent of repigmentation changes in two responder and non-responder patients.

Transcriptome profiling and identification of biomarker(s)

We examined differentially expressed genes (DEGs) between responder (n=6) and non-responder (n=5) vitiligo patients. There were 470 DEGs, including 269 up-regulated and 201 down-regulated genes in responder versus non-responder patients (Fig.2A). Up-regulated genes were associated with processes, such as Fatty Acid Omega Oxidation (Fig.2B1). Down-regulated genes were involved in PPAR signaling pathway, and estrogen signaling pathway (Fig.2B2).

Ten up-regulated and ten down-regulated DEGs with the most altered RNA expression levels are presented in Tables 2 and 3. Among these genes, we selected three candidate genes, i.e, *KRTAP10-11*, *IP6K2*, and *C9* that were involved in related pathways. *KRTAP10-11* is an up-regulated gene involved in keratinization, while *IP6K2* is a down-regulated gene that contributes to the regulation of apoptotic processes, and *C9* is another down-regulated gene that regulates C9 in the complement cascade.

Table 1: Characteristics of patients

Patient ID	Age (Y)	Sex	Recipient site	Response	Recipient size (cm^2)	Injected cells count /cm^2
P15	25	Male	Back	R	5	69333
P18	26	Male	Elbow	R	30	85714
P20	32	Male	Hand	R	70	93333
P25	34	Female	Leg	R	5	63063
P26	21	Female	Back	R	9	220000
P27	32	Female	Hand	R	12	104545
P1	18	Female	Elbow	N	3	200000
P9	25	Female	Leg	N	80	34574
P10	26	Male	Thigh	N	80	121951
P17	28	Male	Leg	N	30	107142
P24	48	Male	Leg	N	70	136363

R; Responder and N; Non-responder.

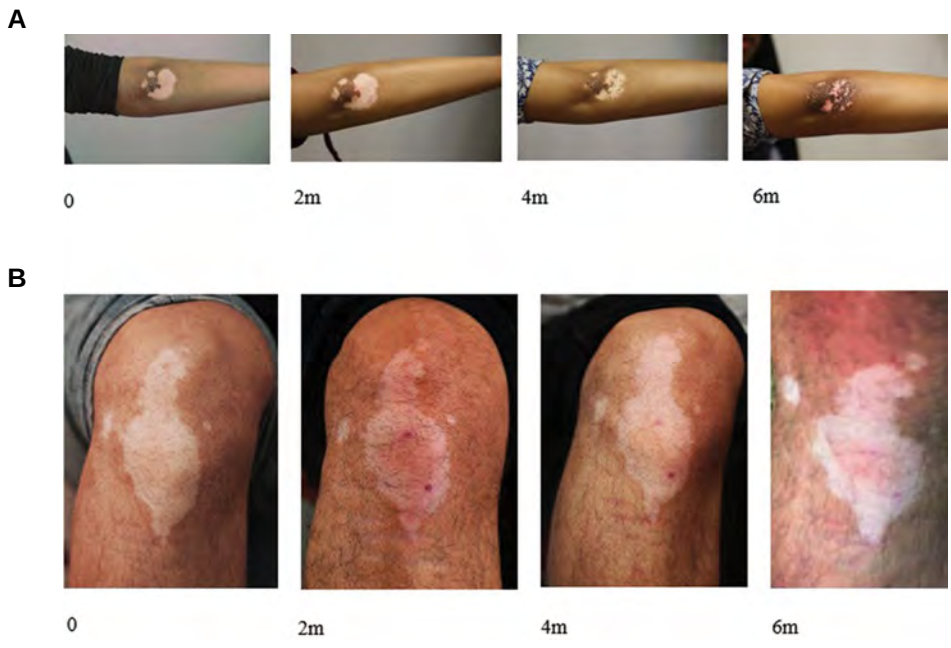

Fig.1: Vitiligo lesions. **A.** Responder and **B.** Non-responder. m; Months post-transplantation.

Table 2: Ten up-regulated differentially expressed genes (DEGs) with the most altered RNA expression levels in responder patients versus non-responder patients

Gene symbol	Gene title	P value	Fold change	Gene ontology (molecular function)
ZNF486	Zinc finger protein 486	0.00002	2.85	DNA binding; metal ion binding
KRTAP10-13P	Keratin associated protein 10-13	0.0001	2.60	Pseudogene
KRTAP10-11	Keratin-associated protein 10-11	0.0001	2.54	Keratinization
ZDHHC20	Palmitoyltransferase ZDHHC20	0.0002	2.47	Palmitoyltransferase activity; protein-cysteine S-palmitoyltransferase activity; zinc ion binding
PGAM1P4	Phosphoglycerate mutase 1 pseudogene 4	0.0003	2.46	Unknown
AC002454.1		0.0006	2.34	Unknown
AC005550.3		0.0007	2.32	Unknown
RIOX1	Ribosomal oxygenase 1	0.0008	2.30	Histone demethylase activity (H3-K36 specific); histone demethylase activity (H3-K4 specific); iron ion binding; oxidoreductase activity, acting on paired donors, with incorporation or reduction of molecular oxygen, 2-oxoglutarate as one donor, and incorporation of one atom each of oxygen into both donors
C2CD6	C2 Calcium Dependent Domain Containing 6	0.0006	2.23	Unknown
GBX1	Homeobox protein GBX-1	0.0008	2.23	RNA polymerase II transcription factor activity, sequence-specific DNA binding; sequence-specific DNA binding

Table 3: Ten down-regulated differentially expressed genes (DEGs) with the most altered RNA expression levels in responder patients versus non-responder patients

Gene symbol	Gene title	P value	Fold change	Gene ontology (molecular function)
AL691447.3		0.0001	2.62	Unknown
AC022182.3		0.0006	2.30	Unknown
WAPL	Wings apart-like protein homolog	0.0003	2.25	Cell division; meiotic chromosome segregation; mitotic sister chromatid cohesion; negative regulation of chromatin binding; negative regulation of DNA replication; negative regulation of sister chromatid cohesion; positive regulation of fibroblast proliferation; protein localization to chromatin; regulation of chromosome condensation; regulation of cohesion loading; response to toxic substance; viral process
HOXA11	Homeobox protein Hox-A11	0.0006	2.20	RNA polymerase II transcription factor activity, sequence-specific DNA binding; sequence-specific DNA binding
IP6K2	Inositol hexakisphosphate kinase 2	0.0014	2.10	ATP binding; inositol-1,3,4,5,6-pentakisphosphate kinase activity; inositol 5-diphosphate pentakisphosphate 5-kinase activity; inositol diphosphate tetrakisphosphate kinase activity; inositol heptakisphosphate kinase activity; inositol hexakisphosphate 1-kinase activity; inositol hexakisphosphate 3-kinase activity; inositol hexakisphosphate 5-kinase activity; inositol hexakisphosphate kinase activity
ZNF652	Zinc finger protein 652	0.001	2.10	DNA binding; metal ion binding; RNA polymerase II transcription factor activity, sequence-specific DNA binding
MISP3	Uncharacterized protein MISP3	0.002	2.08	Unknown
ANKRD28	Ankyrin Repeat Domain 28	0.001	2.05	Unknown
C9	Complement C9	0.0006	2	Complement system
PCDHA3	Protocadherin alpha-3	0.0026	1.96	Calcium ion binding

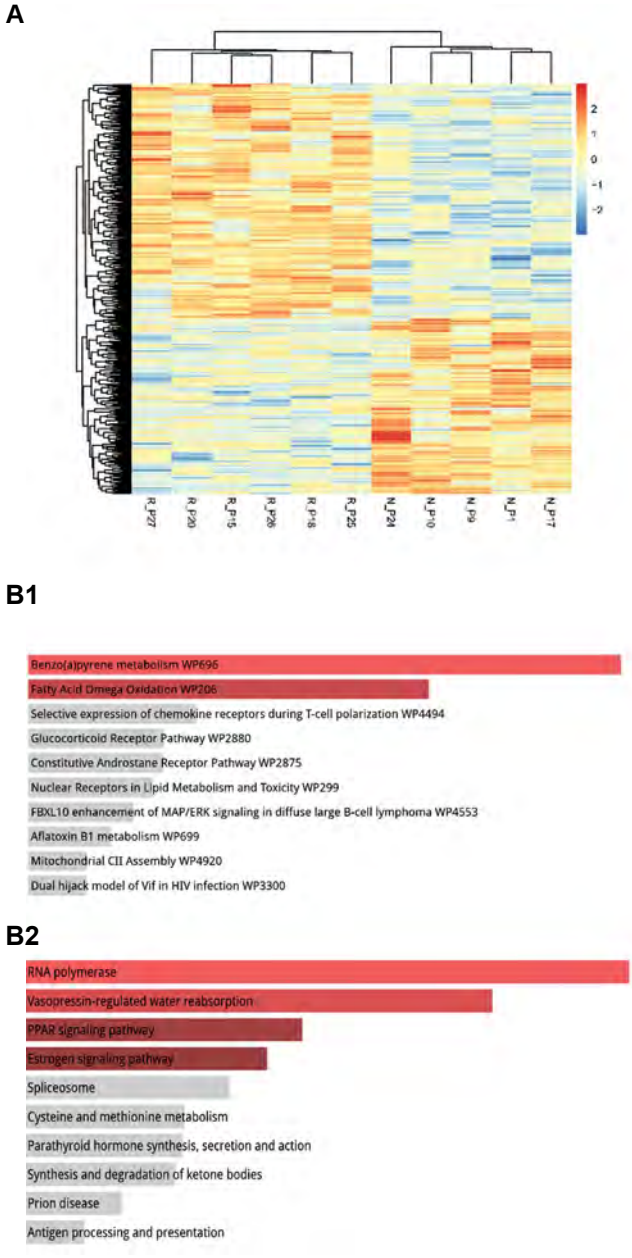

Fig.2: Differential expression of genes in responder versus non-responder patients. **A.** Hierarchical clustering of a heatmap for (DEGs). Different colors indicate up-regulated (red); down-regulated (blue) genes. **B.** Pathway enrichment analysis results by Enrichr. **B1.** Up-regulated; **B2.** Down-regulated genes in responder versus non-responder patients. R; Responder, N; Non-responder and P; Patient.

Discussion

Biomarkers have been one of the most common tools for predicting prognosis or response to treatment in different diseases. RNA biomarkers have several advantages in contrast to other biomarkers such as DNA or protein, and they transmit genetic and regulatory information compared to DNA biomarkers. Compared to protein biomarkers, they reflect cellular states and are more sensitive and specific. Moreover, the cost of finding RNA biomarkers is much lower than protein because specific antibodies are required to detect each protein individually (13).

Transcriptomics technology is often used for biomarker discovery. Among transcriptome analysis methods, RNA sequencing assesses the quantified gene expression measurements at the whole transcriptome level. Moreover, RNA-sequencing provides novel transcript/gene discovery, alternative splicing, gene fusion, and higher sensitivity in expression level (14, 15).

Numerous studies have been conducted on the potential of using RNA-sequencing technology to discover biomarkers for various biological conditions. In 2017, Wright et al. (16) identified a biomarker panel that can predict response to tumor necrosis factor inhibitors (TNFi) therapy in rheumatoid arthritis using RNA sequencing. A study in 2018 by Moreno-Torres et al. (17) conducted transcriptome profiling for response prediction in treating multiple sclerosis patients with fingolimod. They showed that evaluating differential gene expression before treatment might be useful as a biomarker.

No biomarker has been discovered to predict the response to autologous epidermal cells transplantation in vitiligo patients.

Sequencing results of our study showed that the expression of 470 genes (269 up-regulated, 201 down-regulated) were different in responder vitiligo patients compared to non-responders.

Up-regulated genes in responders were involved in fatty acid omega oxidation. Fatty acids regulate tyrosinase synthesis and degradation, and thus regulate pigmentation (18).

As for pathways related to down-regulated genes in responders, PPARs belong to the nuclear hormone receptors subfamily (19). We found decreased PPARs signaling pathway responders' expression and increased expression of non-responders. PPARα, as an E3 ubiquitin ligase induces Bcl-2 (anti-apoptotic protein) ubiquitination and leads to apoptotic death (20). A previous study has shown that levels of Bcl-2 expression are lower in lesional skin compared to normally pigmented skin in vitiligo patients (21). Genes related to the estrogen signaling pathway are also down-regulated in responders. Generation of H_2O_2 by estrogens can cause DNA damage in peripheral blood lymphocytes of vitiligo patients (22). Studies have shown that there are increased levels of H_2O_2 in the skin and blood cells of vitiligo patients, thus resulting in accumulation of free radical mediated melanocyte degeneration (23-25).

Also, according to most DEGs and associated terms, three genes were chosen. *KRTAP10-11* was up-regulated, and *IP6K2* and *C9* were down-regulated in responder versus non-responder patients.

The sequencing results demonstrated increased expression level of *KRTAP10-11* in responders compared to non-responder patients (FC=2.54, $P<0.05$). KRTAP10-11 is a gene that encodes keratin-associated protein 10-11 and is involved in keratinization (26). Keratin 10 is a differentiated keratinocyte marker and

is expressed in the differentiating suprabasal layers of the epidermis (27). Thus, up-regulation of this gene in responder patients could show its role in keratinization and distribution of received melanin from melanocytes into the epidermis. *IP6K2* was also found up-regulated in non-responders compared to responders (FC=-2.1, P<0.05). The role of inositol pyrophosphates (IPs) has been identified in many biological processes (28-30). In response to stress, IP6K2 binds to the tumor suppressor p53 and modulates cell death. p53 inhibits the expression of proarrest target genes or activates pro-apoptotic target genes. IP6K2 selectively modulates inhibiting the induction of p53 proarrest pathway, thus augmenting the p53 response to apoptosis (31). There is no study to date investigating the relation of IP6K2 to vitiligo disease. It seems that the increased expression level of this gene in non-responders may have a role in melanocyte apoptosis.

We showed an increase in *C9* expression in non-responders compared with responder patients (FC=-2, P<0.05). *C9* is an essential member of the complement system membrane attack complex (MAC), which creates pores on the cell membrane of target pathogens resulting in their destruction (32). Furthermore, in vitiligo, anti-pigment cell antibodies can induce melanocyte damage by complement activation and (ADCC) (33). Although no study has previously reported the effects of *C9* expression on vitiligo, the increased activity of this gene in non-responder patients could be attributed to the role of this gene in melanocytes destruction.

Regarding the unknown role of these genes in the pathogenesis of vitiligo, further studies are required to reveal the underlying mechanisms of the gene expression differences.

Conclusion

We proposed candidate biomarkers *KRTAP10-11*, *IP6K2*, and *C9* that potentially may be used as diagnostic tools in the pathogenesis and prediction of vitiligo patients responses to epidermal cell transplantation. These preliminary data are promising; however, further biomarker screening with larger sample sizes and analyses of candidate genes protein expression patterns are required to predict the response of vitiligo patients to cell transplantation.

Acknowledgments

This study was funded by a grant from Royan Institute. We express our appreciation to all members of the Skin Program at Royan Institute and the Department of Regenerative Medicine for their helpful deliberations and consultations during this work. The authors have no conflict of interest to declare.

Authors' Contributions

H.A.; Performed all experimental work, data, and statistical analyses, as well as wrote the manuscript. S.Sh., N.A.; Were responsible for overall supervision and provided scientific advice throughout the project and preparation of the manuscript. P.M., M.Gh.; Participated in study design, data interpretation, and proofreading the manuscript. S.A.M., M.T.; Contributed to data and statistical analyses. A.B.; Was involved in sample collection and interpretation. L.A.-F., M.R.; Contributed to skin sample collection for RNA sequencing. All authors read and approved the final manuscript.

References

1. Grimes PE. New insights and new therapies in vitiligo. JAMA. 2005; 293(6): 730-735.
2. Whitton ME, Ashcroft DM, González U. Therapeutic interventions for vitiligo. J Am Acad Dermatol. 2008; 59(4): 713-717.
3. Falabella R. Surgical approaches for stable vitiligo. Dermatol Surg. 2005; 31(10): 1277-1284.
4. Passeron T. Medical and maintenance treatments for vitiligo. Dermatol Clin. 2017; 35(2): 163-170.
5. Nijsten TE, Stern RS. The increased risk of skin cancer is persistent after discontinuation of psoralen+ultraviolet A: a cohort study. J Invest Dermatol. 2003; 121(2): 252-258.
6. Valejo Coelho MM, Matos TR, Apetato M. The dark side of the light: mechanisms of photocarcinogenesis. Clin Dermatol. 2016; 34(5): 563-570.
7. Rodrigues M. Skin cancer risk (nonmelanoma skin cancers/melanoma) in vitiligo patients. Dermatol Clin. 2017; 35(2): 129-134.
8. Bae JM, Ju HJ, Lee RW, Oh SH, Shin JH, Kang HY, et al. evaluation for skin cancer and precancer in patients with vitiligo treated with long-term narrowband UV-B phototherapy. JAMA Dermatol. 2020; 156(5): 529-537.
9. Gauthier Y, Surleve-Bazeille JE. Autologous grafting with noncultured melanocytes: a simplified method for treatment of depigmented lesions. J Am Acad Dermatol. 1992; 26(2 Pt 1): 191-194.
10. Orouji Z, Bajouri A, Ghasemi M, Mohammadi P, Fallah N, Shahbazi A, et al. A single-arm open-label clinical trial of autologous epidermal cell transplantation for stable vitiligo: a 30-month follow-up. J Dermatol Sci. 2018; 89(1): 52-59.
11. Khodadadi L, Shafieyan S, Sotoudeh M, Dizaj AV, Shahverdi A, Aghdami N, et al. Intraepidermal injection of dissociated epidermal cell suspension improves vitiligo. Arch Dermatol Res. 2010; 302(8): 593-599.
12. Kuleshov MV, Jones MR, Rouillard AD, Fernandez NF, Duan Q, Wang Z, et al. Enrichr: a comprehensive gene set enrichment analysis web server 2016 update. Nucleic Acids Res. 2016; 44(W1): W90-W97.
13. Strimbu K, Tavel JA. What are biomarkers? Curr Opin HIV AIDS. 2010; 5(6): 463-466.
14. Wang Z, Gerstein M, Snyder M. RNA-Seq: a revolutionary tool for transcriptomics. Nat Rev Genet. 2009; 10(1): 57-63.
15. Dillies MA, Rau A, Aubert J, Hennequet-Antier C, Jeanmougin M, Servant N, et al. A comprehensive evaluation of normalization methods for Illumina high-throughput RNA sequencing data analysis. Brief Bioinform. 2013; 14(6): 671-683.
16. Wright HL, Cox T, Moots RJ, Edwards SW. Neutrophil biomarkers predict response to therapy with tumor necrosis factor inhibitors in rheumatoid arthritis. J Leukoc Biol. 2017; 101(3): 785-795.
17. Moreno-Torres I, González-García C, Marconi M, García-Grande A, Rodríguez-Esparragoza L, Elvira V, et al. immunophenotype and transcriptome profile of patients with multiple sclerosis treated with fingolimod: setting up a model for prediction of response in a 2-year translational study. Front Immunol. 2018; 9: 1693.
18. Ando H, Watabe H, Valencia JC, Yasumoto K, Furumura M, Funasaka Y, et al. Fatty acids regulate pigmentation via proteasomal degradation of tyrosinase: a new aspect of ubiquitin-proteasome function. J Biol Chem. 2004; 279(15): 15427-15433.
19. Sertznig P, Seifert M, Tilgen W, Reichrath J. Peroxisome proliferator-activated receptors (PPARs) and the human skin: importance of PPARs in skin physiology and dermatologic diseases. Am J Clin Dermatol. 2008; 9(1): 15-31.
20. Gao J, Liu Q, Xu Y, Gong X, Zhang R, Zhou C, et al. PPARα induces cell apoptosis by destructing Bcl2. Oncotarget. 2015; 6(42): 44635-44642.

21. Lee AY, Youm YH, Kim NH, Yang H, Choi WI. Keratinocytes in the depigmented epidermis of vitiligo are more vulnerable to trauma (suction) than keratinocytes in the normally pigmented epidermis, resulting in their apoptosis. Br J Dermatol. 2004; 151(5): 995-1003.
22. Schallreuter KU, Chiuchiarelli G, Cemeli E, Elwary SM, Gillbro JM, Spencer JD, et al. Estrogens can contribute to hydrogen peroxide generation and quinone-mediated DNA damage in peripheral blood lymphocytes from patients with vitiligo. J Invest Dermatol. 2006; 126(5): 1036-1042.
23. Schallreuter KU, Moore J, Wood JM, Beazley WD, Gaze DC, Tobin DJ, et al. In vivo and in vitro evidence for hydrogen peroxide (H2O2) accumulation in the epidermis of patients with vitiligo and its successful removal by a UVB-activated pseudocatalase. J Investig Dermatol Symp Proc. 1999; 4(1): 91-96.
24. Shalbaf M, Gibbons NC, Wood JM, Maitland DJ, Rokos H, Elwary SM, et al. Presence of epidermal allantoin further supports oxidative stress in vitiligo. Exp Dermatol. 2008; 17(9): 761-770.
25. Arican O, Kurutas EB. Oxidative stress in the blood of patients with active localized vitiligo. Acta Dermatovenerol Alp Pannonica Adriat. 2008; 17(1): 12-6.
26. Kartasova T, Roop DR, Holbrook KA, Yuspa SH. Mouse differentiation-specific keratins 1 and 10 require a preexisting keratin scaffold to form a filament network. J Cell Biol. 1993; 120(5): 1251-1261.
27. Ivanyi D, Ansink A, Groeneveld E, Hageman PC, Mooi WJ, Heintz AP. New monoclonal antibodies recognizing epidermal differentiation-associated keratins in formalin-fixed, paraffin-embedded tissue. Keratin 10 expression in carcinoma of the vulva. J Pathol. 1989; 159(1): 7-12.
28. Saiardi A, Sciambi C, McCaffery JM, Wendland B, Snyder SH. Inositol pyrophosphates regulate endocytic trafficking. Proc Natl Acad Sci U S A. 2002; 99(22): 14206-14211.
29. Illies C, Gromada J, Fiume R, Leibiger B, Yu J, Juhl K, et al. Requirement of inositol pyrophosphates for full exocytotic capacity in pancreatic beta cells. Science. 2007; 318(5854): 1299-1302.
30. Morrison BH, Bauer JA, Kalvakolanu DV, Lindner DJ. Inositol hexakisphosphate kinase 2 mediates growth suppressive and apoptotic effects of interferon-beta in ovarian carcinoma cells. J Biol Chem. 2001; 276(27): 24965-24970.
31. Koldobskiy MA, Chakraborty A, Werner JK Jr, Snowman AM, Juluri KR, Vandiver MS, et al. p53-mediated apoptosis requires inositol hexakisphosphate kinase-2. Proc Natl Acad Sci USA. 2010; 107(49): 20947-20951.
32. Dudkina NV, Spicer BA, Reboul CF, Conroy PJ, Lukoyanova N, Elmlund H, et al. Structure of the poly-C9 component of the complement membrane attack complex. Nat Commun. 2016; 7: 10588.
33. Norris DA, Kissinger RM, Naughton GM, Bystryn JC. Evidence for immunologic mechanisms in human vitiligo: patients' sera induce damage to human melanocytes in vitro by complement-mediated damage and antibody-dependent cellular cytotoxicity. J Invest Dermatol. 1988; 90(6): 783-789.

Original Article

Expression of *TRPV1* as A Heat Sensitive Voltage-Dependent Ion Channel and Oxidative Stress in Sperm Samples of Infertile Men with Varicocele: A Case-Control Study

Sahar Salahshouri, M.Sc.[1, 2], Fahimeh Akbarian, M.Sc.[1], Marziyeh Tavalaee, Ph.D.[1*], Seyed Morteza Seifati, Ph.D.[2], Mohammad Hossein Nasr-Esfahani, Ph.D.[1*]

1. Department of Animal Biotechnology, Reproductive Biomedicine Research Center, Royan Institute for Biotechnology, ACECR, Isfahan, Iran

2. Department of Biology , Medical Biotechnology Research Center, Ashkezar Branch, Islamic Azad University, Ashkezar, Yazd, Iran

Corresponding Address: P.O.Box: 8165131378, Department of Animal Biotechnology, Reproductive Biomedicine Research Center, Royan Institute for Biotechnology, ACECR, Isfahan, Iran
Emails: m.tavalaee@royan-rc.ac.ir, mh.nasr-esfahani@royaninstitute.org

Received: 09/April/2021, Accepted: 02/August/2021

Abstract

Objectives: Transient receptor potential vanilloid 1 (TRPV1) is a heat-activated nonselective cation channel that plays important role in the spermatogenesis, capacitation, acrosome reaction and sperm/oocyte fusion. Considering the high testicular temperature and oxidative stress in varicocele condition, we aimed to assess expression of TRPV1 in sperm of infertile men.

Materials and Methods: In this case-control study, twenty-five men with varicocele (grade II and III) as well as twenty-five fertile were recruited. Sperm parameters, protamine deficiency (Chromomycin A3), DNA damage (TUNEL), lipid peroxidation (BODIPY), *TRPV1* gene expression (real time polymerase chain reaction), TRPV1 protein (flowcytometry and immunocytochemical techniques), and acrosome reaction were assessed between fertile and varicocele groups.

Results: We observed a significant decrease in the sperm parameters, and also, an increased DNA damage, lipid peroxidation, and protamine deficiency in varicocele group. Although, the mRNA expression of *TRPV1* was similar between varicocele and fertile groups, its expression at the protein level was significantly decreased in the varicocele group in comparison with fertile group. Additionally, the TRPV1 localization was changed from the equatorial region to the acrosomal region of the head, especially in the acrosomal region, which was more significant in the fertile group than the varicocele group after inducing acrosome reaction.

Conclusion: In addition to the quality of sperm parameters, and chromatin integrity that were lower significantly in varicocele group, the expression of TRPV1 protein was also lower in varicocele condition that could be associated with reduced capacitation, acrosome reaction and sperm/oocyte fusion and thereby infertility.

Keywords: Acrosome Reaction, Capacitation, Semen Parameters, TRPV1, Varicocele

Cell Journal(Yakhteh), Vol 24, No 6, June 2022, Pages: 323-329

Citation: Salahshouri S, Akbarian F, Tavalaee M, Seifati SM, Nasr-Esfahani MH. Expression of TRPV1 as a heat sensitive voltage-dependent ion channel and oxidative stress in sperm samples of infertile men with varicocele: a case-control study. Cell J. 2022; 24(6): 323-329. doi: 10.22074/cellj.2022.8038.

Introduction

Varicocele is regarded as one of the main causes of male infertility which accounts for about 40% of primary male factor infertility and 80% of secondary male factor infertility (1, 2). Varicocele is characterized by the abnormally enlarged veins of the spermatic cord pampiniform plexus inside the scrotum which is proven to be associated with low sperm count, motility, and viability as well as high abnormal sperm morphology and DNA fragmentation (3).

Although, the exact underlying mechanisms of varicocele pathophysiology are not well-recognized, the induced hyperthermia following the reflux of abdominal warm blood to the pampiniform plexus due to incompetent valves have long been acknowledged to affect spermatogenesis and compromise the fertility in affected ones (2). Impaired or arrested spermatogenesis is among the observed consequences of heat stress due to the fact that germ cells and Sertoli cells are extremely sensitive to hyperthermia (3). As a temperature-sensitive procedure, spermatogenesis takes place at 35-37˚C which is 2-3˚C below the core body temperature, while the scrotum temperature rises by 2.6˚C higher than the optimal temperature in varicocele condition (2).

Elevated oxidative stress and reactive oxygen species (ROS), as well as apoptosis, are among the most destructive consequences of heat stress, which are likely to be induced a change in the composition of the protective or regulative proteins at the level of RNA, protein, post-translational modification and/or its location (2, 4).

Endocannabinoids (ECs) are involved in various physiological and pathological functions including addictive behavior, food intake, inflammation, immunomodulation, analgesia, cancer, epilepsy as well as in reproduction. In reproduction, ECs are considered as evolutionary check points. Anandamide (AEA) and 2-arachidonoylglycerol (2-AG), are the two main components of ECs. Receptors of these components (CB1, CB2, and TRPV1) play a crucial role during

spermiogenesis as well as sperm capacitation, acrosome reaction, thermotaxis, and sperm/oocyte fusion. Recent studies, animal model and human, showed that TRPV1 receptor is affected by hyperthermia (1, 5-8).

Vanilloid compounds like capsaicin and cations, as well as noxious stimuli such as protons and heat (>42˚C), are potential activators of TRPV1. TRPV1 showed a protective effect against apoptosis in the seminiferous tubules of high-temperature exposed mice (9). In a mouse model capsaicin, an agonist of TRPV1, proved to be a protective agent against apoptosis in the spermatogenic cells subsequent to scrotal hyperthermia (5). In several studies, the expression levels of proteins and enzymes of ECs and their components, such as AEA and 2-AG, have been assessed and significant difference has been observed between fertile and infertile men. Infertility in these cases has been attributed to distorted capacitation and acrosome reaction (10, 11). In this regard, Perruzza et al. (10) took the advantage of neural networking system. They assessed different components of ECs in the induced varicocele rats and showed that the only component of ECs that its expression had a predicate value, based on the mean number of new born following two consecutive mating was TRPV1. Therefore, based on these findings, we aimed to assess whether TRPV1, principal component of ECs, is differentially expressed in infertile men with grade II and III varicocele in comparison with fertile men and its relation to the different sperm parameters.

Materials and Methods

Design of Study

This case-control study was approved by the Institutional Review Board from the Royan Institute, Tehran, Iran (IR.ACECR.ROYAN.REC.1398.003). Informed written consent was provided by all the candidates. Fifty in two equal groups of men with varicocele affected and fertile male, who referred to Isfahan Fertility and Infertility Center (IFIC), Iran, were recruited in this study. These participants that made our varicocele and fertile groups, respectively, had less than 40 years old. All members of the fertile group were fertile men who were candidate for family balancing panel. The case group contains, infertile men who suffered from left varicocele of grade II or III. Diagnosis of varicocele grade was performed by a urologist. When vein was palpable during Valsalva maneuver, patient categorize in grade I, not a visible vein palpable at rest made, grade II, and visible, palpable at rest vein was considered as a grade III. Infertile men with grade I varicocele, leukocytospermia, abnormal hormonal profiles, fever nearly 90 days prior to the semen, azoospermia, and urogenital infections were excluded from this study. The fertile men who suffered of varicocele or showed any sign of infertility were excluded from the study. Also, they were excluded if in their semen samples possessed higher than 1 million per ml leukocytes, and/or low quality of sperm parameters and comprised an abnormal hormonal profile.

Semen collection and analysis

Semen samples were obtained in sterile containers through masturbation after 3-5 days of sexual abstinence. Sperm parameters were assessed within 30 minutes after ejaculation (12). Sperm concentration was evaluated using a sperm counting chamber (Sperm processor, Garkheda, Aurangabad, India). Sperm motility and morphology were assessed by computer-assisted semen analysis (CASA) software, and Diff quick staining (Hooshmand Fanavar, Tehran, Iran) based on the fifth version of World Health organization (WHO) protocol, respectively.

Sperm protamine assay

Chromomycin A3 (CMA3) staining was carried out for analyzing the replacement of histones by protamine during spermatogenesis process (13). Briefly, 40 µL of washed semen with phosphate-buffered saline (PBS, Sama Tashkhis, Iran) was smeared and fixed with Carnoy solution (3 methanol:1 glacial acetic acid, Cat No:1.00063, Merck, Darmstadt, Germany) at 4˚C for 5 minutes on slides and stained with 150 µL CMA3 solution (0.25 mg/ml, Cat No: C2659, Sigma-Aldrich, United States) for 20 minutes. Slides were subsequently rinsed with PBS and about 500 spermatozoa per slide were analyzed using an Olympus fluorescent microscope (BX51, Tokyo, Japan) for distinguishing the CMA3 positive spermatozoa from CMA3 negative ones which are stained bright yellow and dull yellow based on the level of protamine level which is reported as a percentage.

Evaluation of sperm DNA damage

In this study, terminal deoxynucleotidyl transferase dUTP nick end labeling (TUNEL) assay was applied to evaluate the DNA damage by fluorescence microscope as described previously (14). Briefly, the sperm sample was fixed using 4% paraformaldehyde (Cat No:158127; Sigma, USA) and permeabilized with 0.2% Triton X-100 (Cat No: 108643, Merck, Darmstadt, Germany). A DNA fragmentation detection kit (Cat No: G3250, Apoptosis Detection System Fluorescein, Promega, Mannheim, Germany) was used according to the manufacturer's instructions. DNA damage was evaluated in about 500 sperms using an Olympus fluorescent microscope (BX51, Tokyo, Japan) for distinguishing the positive TUNEL spermatozoa (with fragmented DNA) from negative TUNEL ones (with intact DNA) which are stained green and red, respectively.

Evaluation of sperm lipid peroxidation

We assessed the percentage of sperm membrane lipid peroxidation according to Aitken et al. (15). Briefly, 5 mM of BODIPY 581/591 C11 (D3861, Molecular Probes, United States) was incubated with 2×10^6 concentrations of spermatozoa at 37˚C for 30 minutes and lipid peroxidation was determined by FACSCalibur flow cytometer (Becton Dickinson, San Jose, CA, USA) and reported as "percentage of lipid peroxidation.

Evaluation of TRPV1 protein by Flowcytometry and Immunocytochemical techniques

Briefly, 12-15×10^6 isolated spermatozoa were washed with PBS at 3000 rpm and fixed with 4% paraformaldehyde (Cat No:158127; Sigma, USA) for 30 minutes. The sample was rinsed twice with PBS (at 3000 rpm, for 5 minutes). The sperm pellet was re-suspended in 500 mL of PBS and treated with Triton X-100 (Cat No: 108643, Merck, Darmstadt, Germany) followed by twice washing with PBS. In the next step, the sample was divided into two portions of the test and control and incubated with 3% bovine serum albumin (BSA, Cat No: A3311, Sigma-Aldrich, USA) for blocking the non-specific binding sites. Following the centrifugation at 3000 rpm and removal of the supernatant, test and control tubes were incubated overnight at 4˚C with rabbit polyclonal anti-TRPV1 antibody (Cat No:ACC030 , Alomone labs, Jerusalem BioPark, Israel) and 1% BSA solution, respectively. After twice washing with PBS, test and control tubes were incubated with secondary antibody (Goat Anti-Rabbit-IgG- FITC, Cat: F1262, Sigma-Aldrich, USA) at 37˚C for 1 hour. After twice washing with PBS, 400 µL of the test and control samples were transferred to a flow cytometric tube and readout with FACSCalibur flow cytometer (Becton Dickinson, San Jose, CA, USA). A similar procedure was used to TRPV1 protein immunocytochemical assay in sperm on the slides. To detect the location of the TRPV1 protein, the microscopic analysis was performed using a fluorescence microscope (BX51, Tokyo, Japan) which about 400 sperm per slide were evaluated. In addition, TRPV1 protein was also assessed before and after the acrosome reaction by immunocytochemical technique.

Acrosome reaction induction

For acrosome reaction induction, semen samples (n=5 of each group) before and after induction of acrosome reaction by calcium sample were processed by density gradient centrifugation (DGC) procedure, and incubated with 10 µM calcium ionophore (Cat: A23187, Sigma-Aldrich, USA) diluted in Dimethylsulfoxide (DMSO, Cat No: D8418, Merck, Germany) at a final concentration for 30 minutes (16). Then, chlortetracycline (CTC, Cat No: 26430, Sigma-Aldrich, USA) staining (17) was used for assessment of capacitation ionophore. CTC method is based on the differential pattern of staining in sperm head for intact or non-capacitated (Non-Cap), capacitated (Cap) and acrosome reacted (AR), sperm.

Evaluation of *TRPV1* gene expression

Total RNA was extracted from washed sperms samples of our both groups using YTzol pure RNA (Cat No:YT9064, Yekta Tajhiz Azama, Iran) according to the manufacturer's protocol, followed by cDNA Synthesis using Yekta Tajhiz cDNA Synthesis Kit (Cat No: YT4500, Yekta Tajhiz Azama, Iran). Expression of *TRPV1* gene at the mRNA level in sperm cells was analyzed through real-time polymerase chain reaction (PCR) in StepOnePlus Real-Time PCR System (Model No: 4376357, Applied Biosystems, Foster City, USA) using YTA SYBR Green qPCR MasterMix 2X (Cat No: yt2551, Yekta Tajhiz Azama, Iran) according to the manufacturer's instruction. Specific primers were designed for *TRPV1*-

F: 5′GGCTGTCTTCATCATCCTGCT3′
R: 5′GTTCTTGCTCTCCTGTGCGATCTT3′ (accession number: NM_080705.4, NM_080704.4, NM_080706.3, NM_018727.5).

We also used F: 5′-CCACTCCTCCACCTTTGACG-3′ and R: 5`-CCACCACCCTGTTGCTGTAG-3′ primers for the *GAPDH* housekeeping gene as an internal control for normalization (accession number: NM_001357943.2, NM_001256799.3,NM_001289745.3,NM_001289746.2, NM_002046.7). The relative expression of *TRPV1* at the RNA level was calculated through the $^{2\text{-}\Delta\Delta ct}$ method.

Statistical analysis

Data analysis was performed by statistical package for the social sciences for windows, version 26 (SPSS, Inc., Chicago, IL, USA) software using Independent T-test and Two-tailed Pearson correlation. The graphs are plotted using 8.4.3 (GraphPad Software, Inc., San Diego, CA). Real-time PCR data were evaluated using the $2^{-\Delta\Delta ct}$ method. Data were presented as mean± standard error of the mean (SEM), and $P<0.05$ was assumed as significant.

Results

Sperm parameters, sperm DNA damage, sperm lipid peroxidation, and sperm protamine deficiency

As shown in Table 1, the mean sperm concentration and sperm motility were significantly lower in the varicocele group than the fertile group. Additionally, the mean percentage of sperm DNA damage, membrane lipid peroxidation, and protamine deficiency were significantly higher in the varicocele group than the fertile group.

TRPV1 expression analysis

As shown in Figure 1A, the percentage of sperm TRPV1 protein in men with varicocele (31.00 ± 3.54) was significantly lower than fertile individuals (60.61 ± 3.45, P=0.001) which are presented in Figure 1B and C in more detail, however, comparison of *TRPV1* at the RNA level between fertile and varicocele groups showed no significant difference (Fig.1D). Also, immunofluorescence staining revealed the presence of the TRPV1 protein in the neck, flagellum, and different areas of the sperm head (equatorial and post acrosome regions) (Fig.1E).

Table 1: Comparison of conventional sperm parameters

Parameters	Fertile (n=25)	Varicocele (n=25)	P value
Sperm concentration (10^6/mL)	83.46 ± 7.36	51.74 ± 5.56	0.002
Sperm motility (%)	55.83 ± 2.7	44.61 ± 2.68	0.008
Abnormal sperm morphology (%)	96.36 ± 0.27	97.20 ± 0.17	0.013
Sperm DNA damage (%)	4.64 ± 0.53	9.62 ± 1.19	0.002
Sperm lipid peroxidation (%)	18.23 ± 2.20	43.80 ± 2.75	0.001
Sperm Protamine deficiency (%)	14.12 ± 1.05	27.70 ± 1.75	0.001

Values are expressed as mean ± standard error of the mean (SEM).

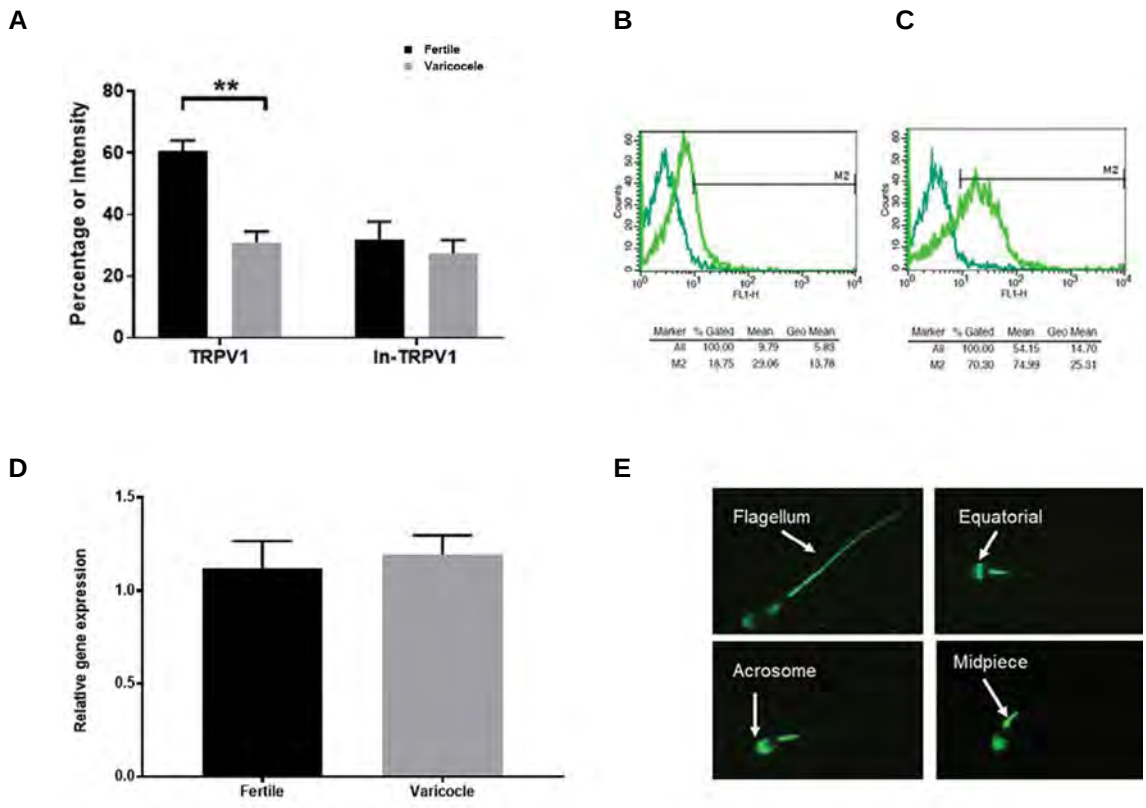

Fig.1: Assessment of sperm TRPV1 at RNA and protein levels. **A.** Comparison of mean percentage (P=0.001) and intensity of TRPV1 (In-TRPV1) proteins between varicocele (n=25) and fertile groups (n=25). In-TRPV1 show relative fluorescence intensity of TRPV1 in sperm sample. **B.** Flow cytometric plot of TRPV1 protein in a fertile man and **C.** An infertile man with varicocele. **D.** Comparison of gene expression analysis of the *TRPV1* gene relative to *GAPDH* gene (housekeeping gene as an internal control) between fertile and varicocele groups. **E.** Localization of TRPV1 protein in the sperms of fertile individuals. Values are expressed as mean ± standard error of the mean (SEM). The significant difference is presented as ** P<0.01.

Acrosome reaction and capacitation rate

Acrosome reaction and capacitation analysis in varicocele and fertile groups before and after of induced acrosome reaction are presented in Figure 2. While acrosome reaction and capacitation were not significantly different between the two groups, the percentage of sperm with reacted acrosome was significantly lower in the varicocele group (56.48 ± 2.06) than fertile ones (67.32 ± 2.52, P=0.006). Additionally, the percentage of non-capacitated (20.94 ± 1.57, P=0.02) and capacitated (22.64 ± 1.12, P=0.03) sperms were significantly higher in the varicocele group.

TRPV1 Localization before and after induction of acrosome reaction

Using immunochemistry, the percentage of TRPV1 positive sperm was evaluated before and after induction of acrosome reaction. The after induction of acrosome reaction results indicated that, the mean percentages of TRPV1 positive sperm in the acrosomal region (Fig.3A) were significantly higher than equatorial region (Fig.3B) in both groups. Also, it was significantly higher than "before" state in our groups. Comparison of the degree of localization

changes is significantly lower in the varicocele group in comparison with the fertile group before induction of acrosome reaction.

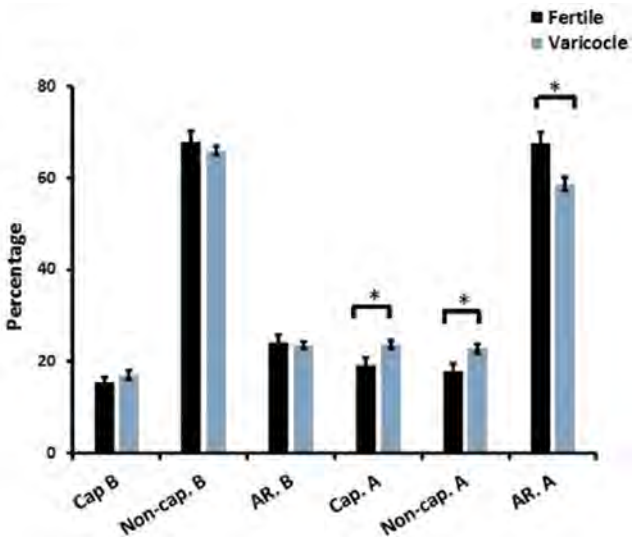

Fig.2: Comparison of the percentage of capacitated (Cap) and not capacitated (Non-Cap) sperms, as well as percentage of acrosome reacted sperms (AR) between fertile and varicocele groups before (B) and after (A) induction of acrosome reaction with calcium ionophore. Values are expressed as mean ± standard error of the mean (SEM). The significant difference is presented as *; P<0.05.

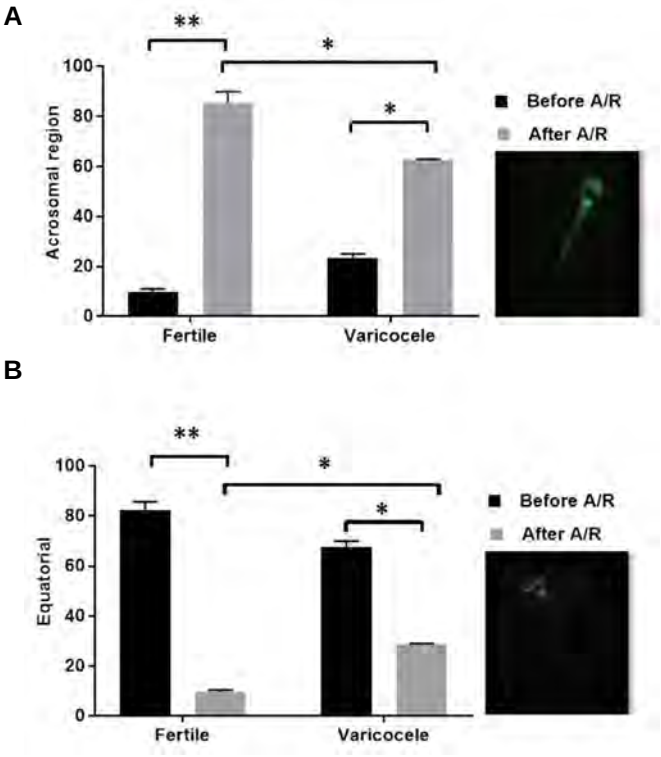

Fig.3: Comparison of TRPV1 protein localization between fertile and varicocele groups, before and after induction of acrosome reaction using the calcium ionophore at **A.** Acrosomal and **B.** Equatorial region. Values are expressed as mean ± standard error of the mean (SEM). The significant difference is presented as *; P<0.05 and **; P<0.01. A/R; Acrosom reaction.

Discussion

TRPV1 is a voltage-dependent ion channel that is sensitive to noxious stimuli like heat and oxidative stress, which are two main features of varicocele pathogenesis (10). *TRPV1* expression at the mRNA level in all male genital tissues has been reported previously (18). Similar to Lewis et al. (1) study in infertile men, we observed a significantly reduced level of TRPV1 protein in the varicocele group, however, we detected no differences at mRNA level compared to the fertile group. The lack of significant difference in the *TRPV1* expression at the RNA level between our groups may be due to post-transcription modification that might be induced by varicocele state (19, 20). In line with our results, the presence of TRPV1 in the human, bull, and boar spermatozoa, as well as rat Sertoli cells, were reported in previous studies, specifically at acrosomal and post-acrosomal parts of sperm cells (6, 21-25). According to Francavilla et al. (7) study, TRPV1 localization is restricted to the post-acrosomal region in the human sperm head and also, Chen et al. (26) reported TRPV1 receptor expression in the tail and neck regions of zebrafish spermatozoa. We also observed the presence of TRPV1 protein in the tail, equatorial, acrosome, and neck regions in sperm samples of varicocele and fertile groups.

Unlike the capacitation process that was significantly higher in the varicocele group, the mean of sperm reacted acrosome was significantly lower in the varicocele group in comparison with the fertile group.

In addition, the mean percentage of TRPV1 positive sperm in the acrosome region of sperm head significantly reduced following induction of acrosome and remained in the equatorial region of the sperm head in the varicocele group. Therefore, it can be concluded that the physiological role of TRPV1 protein in the acrosomal reaction has faded significantly in the varicocele group due to temperature stress and oxidative stress.

TRPV1 also plays a role in managing temperature-oriented sperm motility in the fallopian tube, known as thermotaxis, through which spermatozoa sense the slight temperature increase from the reservoir to the probable site of fertilization as a guide for moving toward the oocyte via managing calcium trafficking (7, 21). Thermotaxis lays a foundation for selecting sperms with higher TRPV1 expression. Moreover, sperm exposure to the rising temperature drastically affects the structure and fluidity of the plasma membrane, preceding to capacitation and acrosome reaction. At the same time, capacitation intensifies the sperm response to the temperature gradient (21). Of note, sperm motility increases during capacitation and, changes from progressive to a hyperactivated pattern with more bending in flagella with an asymmetric "8" shaped movements in addition to the intense lateral head movements. These features are requisite for penetrating of sperm to the cumulus cells before fertilization and this change in motility pattern is exploited through TRPV1

via calcium influx, membrane depolarization, downstream cAMP and PKA signaling pathway, and subsequent production of ATP by activating mitochondrial machinery (1, 21, 27). Kumar et al. (27) reported the reduced progressive motility following the treatment of bull spermatozoa with Capsazepine, while sperm motility was not affected in *trpv1*$^{-/-}$ zebrafish. We also demonstrated that mean of sperm motility in the varicocele group was significantly lower than the fertile individuals which is likely associated with a decrease in the TRPV1 protein level. In this regard, we recently showed that treatment of varicocelized rats with Capsaicin could recover sperm concentration and motility through the reduction of oxidative stress level (28).

The sensitivity of spermatocytes to heat stress is a pathogenic feature of varicocele, in this case, the TRPV1, a heat transducer, gains more importance (9). Several lines of evidence have identified apoptosis as a major mechanism in removing the damaged, unwanted cells involved in the various diseases (5). TRPV1 activation is proven to play a role in settling the fate of non-neuronal cells, including sperm cells during spermatogenesis by choosing between death and survival of spermatozoa and a decreased level of TRPV1 could result in oligospermia (1, 9). In addition, TRPV1 is involved in the apoptosis or protection of cells at the gonads considering the more drastic depletion of germ cells after hyperthermia in *Trpv1*$^{-/-}$ mouse models (9, 10). In this context, it was found that capsaicin prevented apoptosis of gonadal cells induced by heat shock through antioxidative action by activating TRPV1 (5). Perruzza et al. (10) reported a significant downregulation of the *TRPV1* gene among other components of the endocannabinoid (EC) system in the rat model of experimental varicocele, which correlated positively with fertility status implying the pivotal role of this channel in varicocele. This downregulation could lead to the deprivation of testis from a defensive mechanism in a deleterious milieu like heat and oxidative stress in the varicocele state. In this study, we compared the TRPV1 expression between the sperm of varicocele and fertile groups and we showed unlike RNA and protein expression level are reduced in the varicocele group. Considering the role of TRPV1 in inhibiting premature capacitation and acrosome reaction (11), we observed that despite of an increase in the capacitated sperm, the mean of sperm intact acrosome is reduced in this varicocele group. This result indicates the reduced level of TRPV1 may prone sperm to premature capacitation before sperm reaching the site of fertilization and this may be of the reason for reduced fertility in the varicocele state. Therefore, capsaicin treatment, an activator of TRPV1, of varicocele affected, may have potential therapeutic value (28).

Conclusion

TRPV1 is a voltage-dependent ion channel sensitive to heat and oxidative stress, which plays important roles in the physiological phenomenon such as capacitation, acrosome reaction, sperm-oocyte fusion. In infertile men with varicocele compared to fertile men, the mean of TRPV1 protein, as well as sperm parameters (concentration, motility, morphology), were significantly lower and these reductions were associated with increased oxidative stress and DNA fragmentation, and protamine deficiency. These results could be associated with the high level of heat and oxidative stress in the testis of these individuals.

Acknowledgments

The authors would like to thank the patients for their kind contribution to this project. We would like to express our gratitude to the staff of Fertility and Infertility Center and Royan Institute for Biotechnology due to their full support. There is no financial support and conflict of interest in this study.

Authors' Contributions

S.S.; Patients management, preparation tests, samples collection, and analysis of data. F.A.; Analysis of data and writing the manuscript. M.H.N.-E., M.T.; Study conception and design, data analysis and interpretation. S.M.S.; Data analysis and interpretation. All authors read and approved the final manuscript.

References

1. Lewis SE, Rapino C, Di Tommaso M, Pucci M, Battista N, Paro R, et al. Differences in the endocannabinoid system of sperm from fertile and infertile men. PLoS One. 2012; 7(10): e47704.
2. Panner Selvam MK, Agarwal A. Sperm and seminal plasma proteomics: molecular changes associated with varicocele-mediated male infertility. World J Mens Health. 2020; 38(4): 472-483.
3. Jensen CFS, Østergren P, Dupree JM, Ohl DA, Sønksen J, Fode M. Varicocele and male infertility. Nat Rev Urol. 2017;14(9): 523-533.
4. Durairajanayagam D, Agarwal A, Ong C. Causes, effects and molecular mechanisms of testicular heat stress. Reprod Biomed Online. 2015; 30(1): 14-27.
5. Park SG, YonJM, Lin C, Gwon LW, Lee JG, Baek IJ, et al. Af- iliations expand. Capsaicin attenuates spermatogenic cell death induced by scrotal hyperthermia through its antioxidative and anti-apoptotic activities. Andrologia. 2017; 49(5): e12656.
6. Gervasi MG, Osycka-Salut C, Caballero J, Vazquez-Levin M, Pereyra E, Billi S, et al. Anandamide capacitates bull spermatozoa through CB1 and TRPV1 activation. PLoS One. 2011; 6(2): e16993.
7. Francavilla F, Battista N, Barbonetti A, Vassallo MRC, Rapino C, Antonangelo C, et al. Characterization of the endocannabinoid system in human spermatozoa and involvement of transient receptor potential vanilloid 1 receptor in their fertilizing ability. Endocrinology. 2009; 150(10): 4692-4700.
8. Maccarrone M, Barboni B, Paradisi A, Bernabò N, Gasperi V, Pistilli M G, et al. Characterization of the endocannabinoid system in boar spermatozoa and implications for sperm capacitation and acrosome reaction. J Cell Sci. 2005; 118(Pt 19): 4393-4404.
9. Mizrak SC, van Dissel-Emiliani FM. Transient receptor potential vanilloid receptor-1 confers heat resistance to male germ cells. Fertil Steril. 2008; 90(4): 1290-1293.
10. Perruzza D, Bernabò N, Rapino C, Valbonetti L, Falanga I, Russo V, et al. Arti icial neural network to predict varicocele impact on male fertility through testicular endocannabinoid gene expression pro iles. Biomed Res Int. 2018; 2018: 3591086.
11. Darszon A, Sánchez-Cárdenas C, Orta G, Sánchez-Tusie AA, Beltrán C, López-González I, et al. Are TRP channels involved in sperm development and function? Cell Tissue Res. 2012; 349(3): 7497-7464.
12. World Health Organization. WHO laboratory manual for the examination and processing of human semen. Cambridge: 5th ed.Cam-bridge University Press; 2010.

13. Afiyani AA, Deemeh MR, Tavalaee M, Razi M, Bahadorani M, Shokrollahi B, et al. Evaluation of heat-shock protein A2 (HSPA2) in male rats before and after varicocele induction. Mol Reprod Dev. 2014; 81(8): 766-776.
14. Henkel R, Kierspel E, Hajimohammad M, Stalf Th, Hoogendijk Ch, Mehnert C, et al. DNA fragmentation of spermatozoa and assisted reproduction technology. Reprod Biomed Online. 2003; 7(4): 477-484.
15. Aitken RJ, Wingate JK, De Iuliis GN, McLaughlin EA. Analysis of lipid peroxidation in human spermatozoa using BODIPY C11. Mol Hum Reprod. 2007; 13(4): 203-211.
16. Plante G, Thérien I, Lachance C, Leclerc P, Fan J, Manjunath P. Implication of the human Binder of Sperm Homolog 1 (BSPH1) protein in capacitation. Mol Hum Reprod. 2014; 20(5): 409-421.
17. DasGupta S, Mills C, Fraser L. A possible role for Ca2+-ATPase in human sperm capacitation. J Reprod Fertil. 1994; 102(1): 107-116.
18. Stein RJ, Santos S, Nagatomi J, Hayashi Y, Minnery BS, Xavier M, et al. Cool (TRPM8) and hot (TRPV1) receptors in the bladder and male genital tract. J Urol. 2004; 172(3): 1175-1178.
19. Bettegowda A, Wilkinson MF. Transcription and post-transcriptional regulation of spermatogenesis. Philos Trans R Soc Lond B Biol Sci. 2010; 365(1546): 1637-1651.
20. Brunner AM, Nanni P, Mansuy IM. Epigenetic marking of sperm by post-translational modification of histones and protamines. Epigenetics Chromatin. 2014; 7(1): 2.
21. Toni LD, Garolla A, Menegazzo M, Magagna S, Nisio AD, Šabović I, et al. Heat sensing receptor TRPV1 is a mediator of thermotaxis in human spermatozoa. PLoS One. 2016; 11(12): e0167622.
22. Auzanneau C, Norez C, Antigny F, Thoreau V, Jougla Ch, Cantereau A, et al. Transient receptor potential vanilloid 1 (TRPV1) channels in cultured rat Sertoli cells regulate an acid sensing chloride channel. Biochem Pharmacol. 2008; 75(2): 476-483.
23. Kumar A, Mishra AK, Swain DK, Singh V, Yadav S, Saxena A, et al. Role of transient receptor potential channels in regulating spermatozoa functions: A mini-review. Vet World. 2018; 11(11): 1618-1623.
24. Xu H, Delling M, Jun JC, Clapham DE. Oregano, thyme and clove-derived flavors and skin sensitizers activate specific TRP channels. Nat Neurosci. 2006; 9(5): 628-635.
25. Bernabò N, Pistilli M, Mattioli M, Barboni B. Role of TRPV1 channels in boar spermatozoa acquisition of fertilizing ability. Mol Cell Endocrinol. 2010; 323(2): 224-231.
26. Chen Y, Wang H, Wang F, Chen Ch, Zhang P, Song D, et al. Sperm motility modulated by Trpv1 regulates zebrafish fertilization. Theriogenology. 2020; 151: 41-51.
27. Kumar A, Mishra AK, Singh V, Yadav S, Saxena A, Garg SK, et al. Molecular and functional insights into transient receptor potential vanilloid 1 (TRPV1) in bull spermatozoa. Theriogenology. 2019; 128: 207-217.
28. Hosseini M, Tavalaee M, Rahmani M, Eskandari A, Shaygannia E, Kiani-Esfahani A, et al. Capsaicin improves sperm quality in rats with experimental varicocele. Andrologia. 2020; 52(11): e13762.

Original Article

Plasma-Rich in Growth Factors Ameliorates Detrimental Effects of Cryopreservation on Human Sperm: A Prospective Study

Jafar Mirzaei, M.Sc., Mansoureh Movahedin, Ph.D., Iman Halvaei, Ph.D.*

Department of Anatomical Sciences, Faculty of Medical Sciences, Tarbiat Modares University, Tehran, Iran

***Corresponding Address: Department of Anatomical Sciences, Faculty of Medical Sciences, Tarbiat Modares University, Tehran, Iran**
Email: ihalvaei@modares.ac.ir*

Received: 23/June/2021, Accepted: 08/September/2021

Abstract

Objectives: Sperm cryopreservation results in damage to membrane integrity, sperm viability, sperm motility, and DNA structure. We aimed to evaluate the effect of plasma rich in growth factors (PRGF) on sperm parameters during the freeze-thaw process.

Materials and Methods: In the first phase of this prospective study, after sperm preparation, 10 normozoospermic specimens were cryopreserved by rapid freezing with different concentrations of PRGF including 0, 1, 5, and 10% to find the optimum dose. Sperm motility and viability were assessed in this phase. In the second phase of the study, based on the results of first phase, 25 normal sperm samples were frozen with 1% PRGF. All sperm parameters including motility, viability, acrosome reaction, and DNA integrity were assessed before freezing and after thawing.

Results: The rates of progressive and total sperm motility and viability were significantly higher in 1% PRGF compared to control, 5%, and 10% PRGF in the first phase ($P<0.05$). Supplementation of freezing medium with 1% PRGF could significantly improve all sperm parameters including sperm motility, viability, normal morphology, acrosome integrity, chromatin structure, chromatin integrity, DNA denaturation, and DNA fragmentation in comparison with the control group.

Conclusion: It appears that the supplementation of freezing medium with 1% PRGF could protect human sperm parameters during cryopreservation.

Keywords: Freeze-Thawing, Growth Factor, Plasma Rich in Growth Factors, Platelet

Cell Journal(Yakhteh), Vol 24, No 6, June 2022, Pages: 330-336

Citation: **Mirzaei J, Movahedin M, Halvaei I. Plasma-rich in growth factors ameliorates detrimental effects of cryopreservation on human sperm: a prospective study. Cell J. 2022; 24(6): 330-336. doi: 10.22074/cellj.2022.8119.**

Introduction

Sperm cryopreservation is one of the main procedures routinely used in assisted reproduction technology. Several indications have been proposed for this technique including neoplastic and autoimmune disease, genetic disease affecting spermatogenesis, before vasectomy, gender reassignment, and sperm donors (1). It seems that oocyte and embryo cryopreservation have approximately found their optimum protocols but sperm freezing has remained to be modified to reach the optimum procedure. Cryopreservation could damage the cells via several mechanisms. Reactive oxygen species (ROS) is one of the most important factors that can damage the cells during cryopreservation (2). Sperm is a unique cell with very special features including a high level of polyunsaturated fatty acids in the plasma membrane, and a low level of antioxidants that make it vulnerable to the detrimental effects of cryopreservation. Spermatozoa also have a high number of mitochondria that could be a source of ROS production (3). Sperm cryopreservation can impair different sperm parameters. Different strategies have been recruited for ameliorating the adverse effects of sperm cryopreservation. Adding antioxidants to the cryopreservation medium has shown beneficial effects (4). Growth factors could act as antioxidants along with their roles in cell growth and differentiation (5).

In recent decades, platelets have been considered an important source of growth factors for regenerative medicine. Different methods using autologous platelet concentrates have been introduced including platelet-rich plasma (PRP) (6), plasma-rich in growth factors (PRGF) (7), and platelet-rich fibrin (8). PRGF was introduced in the late 90s for oral surgery (7). PRGF preparation is an easy method that needs simple centrifugation of fresh venous blood with adding anticoagulants and calcium chloride to release a pool of various growth factors (9). In comparison with other platelets concentrations, PRGF does not contain white blood cells (10). PRGF is a kind of plasma enriched by plasma proteins, coagulating agents, and circulating growth factors that later has an important role in tissue regeneration. The platelets contain α-granules that, after activation, release a pool of growth factors. PRGF has an antioxidant effect because it contains epidermal growth factor (EGF), platelet-derived growth factor (PDGF), vascular endothelial growth factor (VEGF), transforming growth factor beta (TGFβ), hepatocyte growth factor (HGF), fibroblast growth factor (FGF), and insulin-like growth factor (IGF-1) (11, 12). Beneficial effects of PRGF on neurobiology (13) and ophthalmology (14) have been previously described. The impacts of growth factors in the PRGF on the male reproductive system and spermatozoa have been solely evaluated in the previous studies. It was

shown that FGF, and VEGF have beneficial effects on sperm motility (15, 16). Beneficial effects of IGF-1 also have been reported in an animal study (17). Recently, it was shown that PRP has a partially protective effect on human sperm parameters during cryopreservation (18).

To the best of our knowledge, the impact of PRGF on sperm cryopreservation has not been assessed. The objective was to evaluate the role of PRGF on the detrimental effects of human sperm cryopreservation.

Materials and Methods

Chemicals

All chemicals were purchased from Sigma (Sigma-Aldrich, Germany) unless otherwise stated. PRGF preparation.

This step was based on a previous publication with a minor modification (10). Blood samples were taken from 5 healthy donors (all men, 27-40 years) who had not been infected with a viral infection during the last six months and screened for blood-borne viruses like human immunodeficiency virus, hepatitis B surface antigen, hepatitis C virus, cytomegalovirus and Epstein–Barr virus. Informed consent was obtained from all donors. The samples were mixed with 3.8% sodium citrate in a conical tube. After centrifugation (8 minutes, 580 g) at room temperature, the whole plasma layer was aspirated avoiding touching or aspirating the buffy coat layer containing leukocytes. 10% calcium chloride was then added to plasma and incubated at 37˚C for 30 minutes. After that, the supernatant was collected and incubated at 56˚C for 60 minutes. The plasma then was filtered, aliquoted, and stored at -80˚C until use.

Semen collection and preparation

In the first phase of this prospective study, ten normozoospermic samples from patients who were referred to the *in vitro* fertilization (IVF) clinic of Gandhi Hospital were recruited. The abstinence period was 2-7 days. Only ejaculated samples were included in this study. Patients who took antioxidants in time of the study, heavy smokers, alcohol abuse, and with a history of varicocele were excluded from the study. This study was performed between June 2019 and October 2019. Informed consent was obtained from all patients. The ethics committee of Tarbiat Modares University has approved all parts of this study (IR.MODARES.REC.1397.055). The sperm preparation method was direct swim-up. The mean male age was 34.9 ± 4.38 years.

Sperm cryopreservation and thawing

In the first phase of study, the effect of different doses of PRGF on sperm motility and viability was evaluated. Beneficial effects of 0.31-10% PRGF on proliferation of human periosteal cells has been evaluated before (19). There was no data available on evaluating the effects of PRGF on sperm cryopreservation. To do this, ten sperm samples were included of which each sample was divided into four aliquots in the cryotubes containing 0 (control), 1, 5, and 10% (V/V) of PRGF. In the second phase of study, the best PRGF dose determined in the first phase was selected for further evaluations. In this phase, the effects of 1% PRGF (V/V) on sperm parameters were evaluated on twenty-five normozoospermic samples. After adjusting the dose of PRGF, 70 µL Life Global sperm freezing medium (life global) was added for each 100 µL sperm solution. After five minutes of equilibration at room temperature, the samples were cryopreserved by the rapid freezing method (20). For thawing, the cryotubes were placed in tap water for five minutes and then specimens were added to the pre-warmed human tubal fluid (HTF) solution supplemented with human serum albumin. The diluted spermatozoa were centrifuged for 15 minutes (300 g). The supernatant was then discarded and the pellet was re-suspended with the HTF medium for further analysis.

Analysis of sperm characteristics

Sperm motility, viability and morphology

Sperm motility was evaluated using a light microscope (400 x). According to WHO guidelines, sperm motility was divided into three categories of progressive motility, non-progressive motility (total motility: progressive+non-progressive), and immotile. At least 200 spermatozoa at 6 microscopic fields were evaluated each time and different categories of sperm motility were reported as percentage. Each sample was evaluated twice by two expert operators and the mean was reported after the calculation of error. Sperm viability was evaluated using the eosin-nigrosin staining method (21). The spermatozoa with red or dark pink heads were considered dead while spermatozoa with white heads were alive (light microscope 1,000x). At least 200 spermatozoa were checked and the rate of sperm viability was reported as percentage. Sperm morphology was assessed using the Papanicolaou staining method (21). Head abnormalities (shape, number, size, presence of vacuoles, and acrosome size), mid-piece abnormalities (insertion, thickness, and excess residual cytoplasm), and tail abnormalities (shape, number, length, and excess residual cytoplasm) were checked for each sample for at least 200 spermatozoa. The rate of normal sperm morphology was reported as percentage.

Aniline blue

Aniline blue (AB) can bind to the lysine amino acids in histone proteins and detects chromatin condensation. After the preparation of smears from the samples, they were fixed by 3% glutaraldehyde in 0.2 M phosphate buffer (pH=7.2, room temperature, 30 minutes). The slides were then stained with AB staining (in 4% acetic acid, pH=3.5, 10 minutes). Spermatozoa with highly condensed chromatin were light blue and abnormal cells were dark blue. At least 200 spermatozoa were evaluated under the light microscope (1,000X) and the results were reported as percentage (22).

Toluidine blue

Toluidine blue (TB) attaches to the phosphate group in

DNA and assesses the chromatin integrity. The air-dried slides were fixed and placed in 0.1 N HCl solution. The slides were then washed with distilled water and stained with 0.05% TB. The sperm heads with dark blue to purple was considered abnormal and light blue spermatozoa were considered normal (light microscope 1,000x) (22).

Acridine orange

Acridine orange (AO) was used to detect DNA denaturation. The air-dried slides were stained by AO in a dark room for 10 minutes after fixing by Carnoy's solution (methanol-glacial acetic acid, 3:1). Green and yellow to red spermatozoa were considered normal and abnormal cells, respectively. At least 200 spermatozoa were evaluated each time and the rate of normal cells was reported as percentage (fluorescent microscope 1,000×, 460 nm filter) (20).

Sperm chromatin dispersion

Sperm chromatin dispersion (SCD) is an indirect method for the evaluation of DNA fragmentation. The sperm samples were mixed with agarose 1% (30 µL: 70 µL). Half of the sample (50 µL) was placed on a pre-coated slide with low melting agarose. After incubating at 4˚C for 5 minutes, the slides were placed in a 0.08 N HCl solution and a lysis solution for 7 and 25 minutes, respectively. Then, the slides were washed with deionized water (5 minutes) and dehydration was performed by serially increased alcohol concentrations. Finally, the slides were stained by Wright color to see under the light microscope (1,000×). The spermatozoa with large or medium halo were considered normal while spermatozoa with small halo and no halo were considered abnormal. At least 200 spermatozoa were evaluated and normal cells were reported as percentage (23).

Acrosome reaction

The smears were prepared from samples after fixing with glutaraldehyde 3% for 30 minutes. Then, the slides were stained with Bismarck Brown and Bengal Rose for 10 and 25 minutes, respectively. Spermatozoa with light pink acrosome were considered intact acrosome and expressed as a percentage. At least 200 spermatozoa were evaluated under a light microscope (1,000×) (20).

Statistical analysis

SPSS software (version 15, Chicago, USA) was used for statistical analysis. The data are expressed as mean ± SD, median (min-max). To evaluate the normality of data, Shapiro-Wilk test was used. One-way ANOVA with Tukey and Kruskal-Wallis with Dunn were used for comparison between different groups for normal- and non-normal distributed data, respectively. The hypothesis was one-sided and the level of significance was set at $P \leq 0.05$.

Results

The freeze-thawing process decreased sperm total and progressive motility and adding PRGF (1%, 5%, and 10%) could increase these parameters. But only 1% PRGF showed a significant difference in comparison with 5% and 10%. Sperm viability was also decreased after thawing and it was only significantly increased in the 1% PRGF group. Our results showed that 1% PRGF had the best results to preserve the sperm motility and viability (Table 1). There was no obvious agglutination or aggregation in each experimental group.

The data of included semen in the second phase of study are shown in Table 2. Sperm motility decreased after thawing compared to before freezing. Adding 1% PRGF significantly increased both total and progressive sperm motility compared to the control group. Sperm viability also decreased after thawing in both groups and it was significantly increased in the 1% PRGF group compared to controls (73.25 ± 5.58 vs. 62.55 ± 4.5, respectively). Sperm normal morphology and intact acrosome had also higher levels in the 1% PRGF group compared to the control group. Regarding the DNA integrity and chromatin packaging, our results showed that the rates of non-denatured DNA, non-fragmented DNA, and chromatin condensation were significantly higher in the 1% PRGF group compared to the control group (Table 3). Figure 1 shows AB and SCD tests.

Table 1: Sperm motility and viability after thawing in different doses of PRGF

Parameters	Before cryopreservation	PRGF concentration			
		0% (control)	1%	5%	10%
Total motility[a]	92.2 ± 2.19	45.4 ± 10.9	59.2 ± 6.4*	46 ± 16.3	48.2 ± 8.6
	93 (88-96)	45 (32-58)	61 (45-65)	50 (25-69)	49 (36-60)
Progressive motility	85 ± 3.08	35.4 ± 6.2	49 ± 5.8*	37.1 ± 17.6	36 ± 9.8
Viability[a]	94.1 ± 3.1	57.8 ± 7.3	67.3 ± 7.1*	58 ± 11.9	59.6 ± 7.8
	95 (89-97)	62 (44-62)	70 (52-75)	60 (40-73)	65 (50-66)

Data are presented as mean ± SD for data with normal distribution. [a]; Data are presented as mean ± SD, median (min-max) for data with non-normal distribution, and *; Significant difference versus control. All of groups had significant difference with before cryopreservation.

Table 2: Semen characteristics included in the second phase of this study

Parameters	Mean	Minimum	Maximum	Standard deviation
Male age (Y)	34.9	24	42	4.38
Count (10^6/mL)	112.6	50	200	26.74
Progressive motility (%)	64.6	50	81	9.66
Non-progressive motility (%)	9.95	2	20	3.78
Total motility (%)	74.55	59	87	9.16
Immotile (%)	25.45	13	41	9.16
Normal morphology (%)	8.46	5	12	1.43
Round cell (10^3/mL)	435	200	700	159.85

Table 3: Sperm parameters before cryopreservation, and after thawing in control and 1% PRGF groups

Parameters	Groups		
	Before cryopreservation	Control	1% PRGF
Progressive motility*	81.10 ± 5.87 [ab]	33.85 ± 5.95 [ac]	47.20 ± 9.31 [bc]
	82 (65-88)	34 (25-44)	46 (30-71)
Total motility	88.65 ± 4.13 [ab]	55.55 ± 6.63 [ac]	64.45 ± 7.06 [bc]
Viability	92.05 ± 3.25 [ab]	62.55 ± 4.5 [ac]	73.25 ± 5.58 [bc]
Normal morphology*	14.4 ± 3.33 [ab]	6.2 ± 1.82 [ac]	9.85 ± 2.66 [bc]
	14 (8-21)	6 (4-10)	10 (6-16)
Intact acrosome*	93.60 ± 2.7 [ab]	88.5 ± 2.6 [ac]	90.35 ± 2.39 [bc]
	93.5 (89-98)	89.5 (84-92)	90.5 (86-95)
Aniline blue (sperm chromatin structure)	87.2 ± 3.65 [ab]	62.55 ± 4.77 [ac]	76.15 ± 4.1 [bc]
Toluidine blue (sperm chromatin integrity)*	87.7 ± 4.61 [ab]	63.3 ± 5.89 [ac]	77.6 ± 5.03 [bc]
	88.5 (74-92)	63.5 (51-76)	79 (65-85)
Non-denaturated DNA (AO)	91.15 ± 3.26 [ab]	71 ± 5.95 [ac]	81.3 ± 3.88 [bc]
Non-fragmented DNA (SCD)*	90.25 ± 4.63 [ab]	63.70 ± 6.19 [ac]	78.25 ± 6.63 [bc]
	90 (75-96)	63 (55-79)	79 (62-87)

Data are presented as mean ± SD for data with normal distribution. AO; Acridine orange, SCD; Sperm chromatin dispersion test, and *; Data are presented as mean ± SD, median (min-max) for data with non-normal distribution. Similar letters have significant difference.

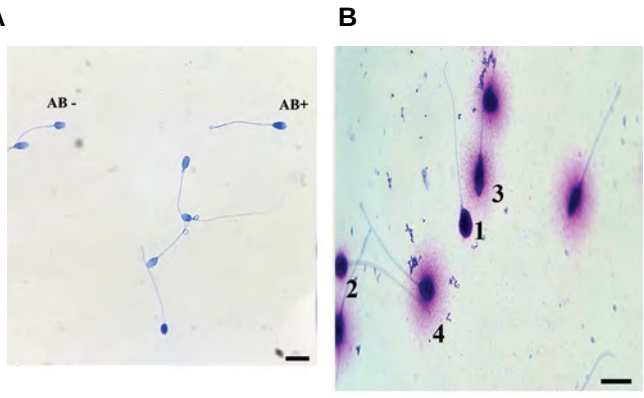

Fig.1: Aniline blue and sperm chromatin dispersion tests. **A.** Aniline blue shows normal light blue spermatozoa with highly condensed chromatin (AB-) and abnormal dark blue spermatozoa (AB+) (scale bar: 10 µm). **B.** Sperm chromatin dispersion test shows DNA fragmentation with four patterns of halos. 1; Abnormal cell with no halo, 2; Abnormal cell with small halo, 3; Normal cell with medium halo, and 4; Normal cell with large halo (1000×) (scale bar: 10 µm).

Discussion

PRGF could be considered as a suitable example of endogenous regenerative medicine in which the patient's own blood plasma and growth factors are used for treatment. PRGF has been introduced as the first 100% autologous PRP. White blood cells are considered as a source of ROS generation in culture media and they are omitted during PRGF preparation. It has several other advantages including the low volume of venous blood needed, it is not time-consuming, easy, inexpensive and safe. PRGF has more beneficial effects on tissue regeneration compared to PRP (19).

To the best of our knowledge, this is the first study that evaluates the protective effects of PRGF on human sperm cryopreservation. Our findings showed that PRGF 1% protects human sperm during cryopreservation. The beneficial effects of PRGF in infertility treatment and assisted reproduction have been previously described. It was shown that PRGF is useful for proliferation and migration of endometrial fibroblast and thickness of endometrium in IVF cycles (24). Also, Chang et al. found that PRP affects endometrial growth and increases pregnancy rate in implantation failure cases (25). An excess amount of ROS is the main candidate for the adverse effects of cryopreservation on spermatozoa. Antioxidant effect of PRGF has been shown on retinal pigment epithelium (5). Besides, PRGF could protect the function of mitochondria. It can increase the level of glutathione, as a major antioxidant molecule, against increasing ROS. PRGF also reduced nuclear factor erythroid 2-related factor 2 (Nrf2) gene expression in the Keap1-Nrf2 pathway (an important antioxidant pathway) (5).

The protective effects of PRGF on cryo-damage are related to its ingredients and growth factors that each of them has been shown to have beneficial effects on sperm parameters. It was found that IGF-I has a receptor on sperm cells (26) and a lower level of IGF-I in serum was associated with abnormal sperm parameters (27). Also, a significant positive correlation was shown between seminal IGF-I and sperm count (28). Miao et al. (29) found that the incubation of normozoospermic samples with IGF-I increases sperm motility. It was also reported that IGF-I can preserve canine sperm motility during hypostorage (4˚C) via acting on mitochondrial membrane potential (30). The protective effect of IGF-I on ovine sperm motility and plasma membrane integrity during cryopreservation has been approved as well (17). Li et al. (31) showed that sperm incubation with IGF-1 decreases sperm DNA damage may be due to its effects on mitochondrial cytochrome c/caspase pathway. EGF, another component of PRGF, also has receptors on sperm cells (32). It was shown that EGF can modulate acrosome reaction via actin polymerization (33). Animal studies showed that EGF improves ram sperm motility and viability during hypostotage at 4˚C (34) and its effect on bovine sperm acrosome reaction has been described (35). The receptor of VEGF has been found in the male reproductive system and this protein was found in spermatids, seminal plasma, Sertoli cells, and Leydig cells. The positive effects of VEGF on sperm motility were shown in the previous study (16). Tohidnezhad et al. (36) found that VEGF ameliorates oxidative stress damage by activating the Nrf2 pathway. TGFβ has anti-inflammatory effects and it was shown that seminal TGFβ has a correlation with sperm motility and affects sperm function (37). FGF2 is the most important member of the FGF family. It was shown that sperm incubation with FGF2 could result in increasing sperm motility (15). FGF receptors have been found on sperm cells and it was proposed that FGF2 can increase FGFR phosphorylation in the sperm tail and modulate the sperm motility through the ERK1/2, PI3K and AKT pathway (38). Using another platelet concentrate, PRP containing similar growth factors, was shown to have positive effects on human sperm parameters. Recently, Bader *et* al. showed that incubation of 2% PRP with sperm increases sperm motility and viability and decreases sperm DNA fragmentation (39). They found that 2% PRP significantly increases sperm motility compared to controls and 5% PRP did not increase the sperm motility while 10% PRP reduced total sperm motility in the non-stressed group and in the stress group (treated with H_2O_2). They concluded that 2% PRP was the best dose for the preservation of sperm motility and viability. In a very recent study with low sample size, Yan *et* al. evaluated the possible effects of PRP on human sperm cryopreservation (18). They showed that 5% PRP preserved sperm motility, viability and integrity of plasma membrane but sperm DNA fragmentation, intracellular ROS and mitochondrial membrane potential were the same between different groups. Osmotic stress that has occurred during cryopreservation may affect sperm morphology. Spermatozoa during cryopreservation are exposed to change in osmolality which may change sperm morphology. Different proteins in the PRGF may have protective effects on osmotic shock and cell membrane during different stages of cryopreservation

(40). All of these factors together may have additive and synergistic effects to ameliorate the detrimental effects of cryopreservation on spermatozoa. It is suggested to evaluate the possible effects on PRGF on poor quality samples in the next step. This study was designed for research purposes that shows PRGF can be used for sperm cryopreservation and would provide new insights for use of autologous PRGF in assisted reproduction in the next studies in the concept of personalized medicine.

Conclusion

It seems PRGF can preserve sperm parameters including motility, viability, morphology, and the integrity of acrosome and DNA during cryopreservation. More studies with larger sample size are required to confirm our results. PRGF as one of the most important sources of growth factors could be a good candidate for adding to the freezing medium to ameliorate the detrimental effects of the freeze-thaw process on sperm parameters.

Acknowledgments

This study was extracted from the M.Sc. thesis of J.M. The authors gratefully thank Tarbiat Modares University for financial support of this project. The authors declare no competing interests.

Authors' Contributions

I.H., M.M.; Conceived and designed the study and revised the manuscript. J.M.; Conducted the study and wrote the manuscript. J.M., M.M., I.H.; Analysed the data. All authors read and approved the final manuscript.

References

1. Paoli D, Dal Canto M, Baldi E, Cervi M, Ciotti PM, Ciriminna R, et al. Cryopreserved gamete and embryo transport: proposed protocol and form templates—SIERR (Italian Society of Embryology, Reproduction, and Research). Biopreserv Biobank. 2021; 19(1): 27-32.
2. Di Santo M, Tarozzi N, Nadalini M,Borini A. Human sperm cryopreservation: update on techniques, effect on DNA integrity, and implications for ART. Adv Urol. 2012; 2012: 854837.
3. Amidi F, Pazhohan A, Nashtaei MS, Khodarahmian M, Nekoonam S. The role of antioxidants in sperm freezing: a review. Cell Tissue Bank. 2016; 17(4): 745-756.
4. Bahmyari R, Zare M, Sharma R, Agarwal A, Halvaei I. The efficacy of antioxidants in sperm parameters and production of reactive oxygen species levels during the freeze-thaw process: a systematic review and meta-analysis. Andrologia. 2020; 52(3): e13514.
5. Suárez-Barrio C, del Olmo-Aguado S, García-Pérez E, de la Fuente M, Muruzabal F, Anitua E, et al. Antioxidant role of PRGF on RPE cells after blue light insult as a therapy for neurodegenerative diseases. Int J Mol Sci. 2020; 21(3): 1021.
6. Marx RE, Carlson ER, Eichstaedt RM, Schimmele SR, Strauss JE,Georgeff KR. Platelet-rich plasma: growth factor enhancement for bone grafts. Oral Surg Oral Med Oral Pathol Oral Radiol Endod. 1998; 85(6): 638-646.
7. Anitua E. Plasma rich in growth factors: preliminary results of use in the preparation of future sites for implants. Int J Oral Maxillofac Implants. 1999; 14(4): 529-535.
8. Choukroun J, Adda F, Schoeffler C,Vervelle A. Une opportunité en paro-implantologie: Le PRF. Implantodontie. 2001; 42: 55-62.
9. Anitua E, Alkhraisat MH ,Orive G. Perspectives and challenges in regenerative medicine using plasma rich in growth factors. J Control Release. 2012; 157(1): 29-38.
10. Anitua E, Aguirre JJ, Algorta J, Ayerdi E, Cabezas A I, Orive G, et al. Effectiveness of autologous preparation rich in growth factors for the treatment of chronic cutaneous ulcers. J Biomed Mater Res B Appl Biomater. 2008; 84(2): 415-421.
11. Anitua E, Orive G. Endogenous regenerative technology using plasma- and platelet-derived growth factors. J Control Release. 2012; 157(3): 317-320.
12. Anitua E, Sánchez M, Orive G, Andia I. Delivering growth factors for therapeutics. Trends Pharmacol Sci. 2008; 29(1): 37-41.
13. Anitua E, Pascual C, Pérez-Gonzalez R, Antequera D, Padilla S, Orive G, et al. Intranasal delivery of plasma and platelet growth factors using PRGF-Endoret system enhances neurogenesis in a mouse model of Alzheimer's disease. PLoS One. 2013; 8(9): e73118.
14. Anitua E, Muruzabal F, Tayebba A, Riestra A, Perez VL, Merayo-s Lloves J, et al. Autologous serum and plasma rich in growth factors in ophthalmology: preclinical and clinical studies. Acta Ophthalmol. 2015; 93(8): e605-614.
15. Garbarino Azúa D J, Saucedo L, Giordana S, Magri M, Buffone MG, Neuspiller F, et al. Fibroblast growth factor 2 (FGF 2) is present in human spermatozoa and is related with sperm motility. The use of recombinant FGF 2 to improve motile sperm recovery. Andrology. 2017; 5(5): 990-998.
16. Iyibozkurt AC, Balcik P, Bulgurcuoglu S, Arslan BK, Attar R, Attar E. Effect of vascular endothelial growth factor on sperm motility and survival. Reprod Biomed Online. 2009; 19(6): 784-788.
17. Padilha R, Magalhães-Padilha D, Cavalcante M, Almeida A, Haag K, Gastal M, et al. Effect of insulin-like growth factor-I on some quality traits and fertility of cryopreserved ovine semen. Theriogenology. 2012; 78(4): 907-913.
18. Yan B, Zhang Y, Tian S, Hu R,Wu B. Effect of autologous platelet-rich plasma on human sperm quality during cryopreservation. Cryobiology. 2021; 98: 12-16.
19. Nishiyama K, Okudera T, Watanabe T, Isobe K, Suzuki M, Masuki H, et al. Basic characteristics of plasma rich in growth factors (PRGF): blood cell components and biological effects. Clin Exp Dent Res. 2016; 2(2): 96-103.
20. Najafi L, Halvaei I, Movahedin M. Canthaxanthin protects human sperm parameters during cryopreservation. Andrologia. 2019; 51(10): e13389.
21. World Health Organization. WHO laboratory manual for the examination and processing of human semen. 5th ed. Geneva, Switzerland: World Health Organization; 2010.
22. Nabi A, Khalili MA, Halvaei I, Ghasemzadeh J, Zare E. Seminal bacterial contaminations: Probable factor in unexplained recurrent pregnancy loss. Iran J Reprod Med. 2013; 11(11): 925-932.
23. Nabi A, Khalili M, Halvaei I, Roodbari F. Prolonged incubation of processed human spermatozoa will increase DNA fragmentation. Andrologia. 2014; 46(4): 374-379.
24. Anitua E, de la Fuente M, Ferrando M, Quintana F, Larreategui Z, Matorras R, et al. Biological effects of plasma rich in growth factors (PRGF) on human endometrial fibroblasts. Eur J Obstet Gynecol Reprod Biol. 2016; 206: 125-130.
25. Chang Y, Li J, Chen Y, Wei L, Yang X, Shi Y, et al. Autologous platelet-rich plasma promotes endometrial growth and improves pregnancy outcome during in vitro fertilization. Int J Clin Exp Med. 2015; 8(1): 1286-1290.
26. Naz R, Padman P. Identification of insulin-like growth factor (IGF)-1 receptor in human sperm cell. Arch Androl. 1999; 43(2): 153-159.
27. Lee HS, Park YS, Lee JS, Seo JT. Serum and seminal plasma insulin-like growth factor-1 in male infertility. Clin Exp Reprod Med. 2016; 43(2): 97-101.
28. Colombo JB, Naz RK. Modulation of insulin-like growth factor-1 in the seminal plasma of infertile men. J Androl. 1999; 20(1): 118-125.
29. Miao ZR, Lin TK, Bongso T, Zhou X, Cohen P, Lee KO. Effect of insulin-like growth factors (IGFs) and IGF-binding proteins on in vitro sperm motility. Clin Endocrinol (Oxf). 1998; 49(2): 235-239.
30. Shin SM, Kim S, Hong JG, Kim YJ. IGF-I improves mitochondrial membrane potential during hypothermic storage of canine spermatozoa. J Vet Med Sci. 2014; 76(7): 1065-1067.
31. Li Y, Higashi Y, Itabe H, Song YH, Du J, Delafontaine P. Insulin-like growth factor-1 receptor activation inhibits oxidized LDL-induced cytochrome C release and apoptosis via the phosphatidylinositol 3 kinase/Akt signaling pathway. Arterioscler Thromb Vasc Biol. 2003; 23(12): 2178-2184.
32. Zitta K, Albrecht M, Weidinger S, Mayerhofer A, Köhn F. Protease activated receptor 2 and epidermal growth factor receptor are involved in the regulation of human sperm motility. Asian J Androl.

2007; 9(5): 690-696.
33. Brener E, Rubinstein S, Cohen G, Shternall K, Rivlin J, Breitbart H. Remodeling of the actin cytoskeleton during mammalian sperm capacitation and acrosome reaction. Biol Reprod. 2003; 68(3): 837-845.
34. Makarevich AV, Spalekova E, Olexikova L, Lukac N, Kubovicova E, Hegedusova Z. Functional characteristics of ram cooling-stored spermatozoa under the influence of epidermal growth factor. Gen Physiol Biophys. 2011: S36-S43.
35. Etkovitz N, Tirosh Y, Chazan R, Jaldety Y, Daniel L, Rubinstein S, et al. Bovine sperm acrosome reaction induced by G protein-coupled receptor agonists is mediated by epidermal growth factor receptor transactivation. Dev Biol. 2009; 334(2): 447-457.
36. Tohidnezhad M, Wruck CJ, Slowik A, Kweider N, Beckmann R, Bayer A, et al. Role of platelet-released growth factors in detoxification of reactive oxygen species in osteoblasts. Bone. 2014; 65: 9-17.
37. Sharkey DJ, Tremellen KP, Briggs NE, Dekker GA, Robertson SA. Seminal plasma transforming growth factor-β, activin A and follistatin fluctuate within men over time. Hum Reprod. 2016; 31(10): 2183-2191.
38. Saucedo L, Buffa GN, Rosso M, Guillardoy T, Góngora A, Munuce J, et al. Fibroblast growth factor receptors (FGFRs) in human sperm: expression, functionality and involvement in motility regulation. PLoS One. 2015; 10(5): e0127297.
39. Bader R, Ibrahim J, Moussa M, Mourad A, Azoury J, Azoury J, et al. In vitro effect of autologous platelet-rich plasma on H2O2-induced oxidative stress in human spermatozoa. Andrology. 2020; 8(1): 191-200.
40. Taher-Mofrad SMJ, Topraggaleh TR, Ziarati N, Bucak MN, Nouri M, Seifi S, et al. Knockout serum replacement is an efficient serum substitute for cryopreservation of human spermatozoa. Cryobiology. 2020; 92: 208-214.

Original Article

Pre-Ischemic Oxytocin Treatment Alleviated Neuronal Injury via Suppressing NF-κB, MMP-9, and Apoptosis Regulator Proteins in A Mice Model of Stroke

Shahein Momenabadi, M.Sc.[1, 2], Abbas Ali Vafaei, Ph.D.[1, 2], Mahdi Zahedi Khorasani, Ph.D.[1, 2], Abedin Vakili, Ph.D.[1, 2*]

1. Research Center of Physiology, Semnan University of Medical Sciences, Semnan, Iran
2. Department of Physiology, Faculty of Medicine, Semnan University of Medical Sciences, Semnan, Iran

Corresponding Address: P.O.Box: 3513138111, Department of Physiology, Faculty of Medicine, Semnan University of Medical Sciences, Semnan, Iran
Email: abvakili@semums.ac.ir

Received: 28/November/2020, Accepted: 09/March/2021

Abstract

Objectives: This study was designed to determine the effects of pre-ischemic administration of oxytocin (OXT) on neuronal injury and possible molecular mechanisms in a mice model of stroke.

Materials and Methods: In this experimental study, stroke was induced in the mice by middle cerebral artery occlusion (MCAO) for 60 minutes and 24 hours of reperfusion. OXT was given as intranasal daily for 7 consecutive days before ischemic stroke. Neuronal damage, spatial memory, and the expression levels of nuclear factor-kappa B (NF-κB), interleukin-1β (IL-1β), tumor necrosis factor-α (TNF-α), matrix metalloproteinase-9 (MMP-9), brain-derived neurotrophic factor (BDNF) and apoptosis were assessed 24 hours after stroke.

Results: Pre-ischemic treatment with OXT significantly reduced the infarct size ($P<0.01$); but did not recover the neurological and spatial memory dysfunction ($P>0.05$). Moreover, OXT treatment considerably decreased the expressions of NF-κB, TNF-α, IL-1β, and MMP-9 ($P<0.001$) and enhanced the level of BDNF protein. OXT treatment also significantly downregulated Bax expression and overexpressed Bcl-2 proteins.

Conclusion: The finding of this study indicated that administration of OXT before ischemia could limit brain injury by inhibiting MMP-9 expression, apoptosis, inflammatory signaling pathways, and an increase in the BDNF protein level. We suggested that OXT may be potentially useful in the prevention and/or reducing the risk of the cerebral stroke attack, and could be offered as a new prevention option in the clinics.

Keywords: Focal Cerebral Ischemia, Mice, Oxytocin, Pre-Ischemic

Cell Journal(Yakhteh), Vol 24, No 6, June 2022, Pages: 337-345

Citation: **Momenabadi S, Vafaei AA, Zahedi Khorasani M, Vakili A. Pre-ischemic oxytocin treatment alleviated neuronal injury via suppressing NF-κB, MMP-9, and apoptosis regulator proteins in a mice model of stroke. Cell J. 2022; 24(6): 337-345. doi: 10.22074/cellj.2022.7884.**

Introduction

Cerebral ischemic stroke is a result of interruption or reduction of blood flow to a part of the brain, which is one of the major causes of mortality and disability worldwide. The policies for acute stroke management are mainly focused on the use of neuroprotective agents and intravenous thrombolysis and/or endovascular thrombectomy, but delay in starting the treatment may diminish their effectiveness. However, the prevention approach is always better than the treatment. Today, in addition to managing the modifiable risk factors, antiplatelet or anticoagulant drugs are used to prevent and/or diminish recurrent ischemic stroke (1). Most of the studies have indicated that the use of neuroprotection agents prior to ischemia has better outcomes than post-treatment (2). However, prophylactic treatment is not practicable for a large group of patients with acute stroke. But some patients may be at the risk of ischemic stroke in the short or long term, and for these groups, the prophylactic approach may be appropriate (1). For example, patients with transient ischemic attacks, atrial fibrillation, and asymptomatic carotid stenosis are at high risk of cerebral stroke attacks (1, 3). These patients may need to use suitable prophylactic neuroprotection for a long time. Therefore, a safe and cheap neuroprotective agent would be an interesting treatment option for prophylactic use in patients with high-risk stroke.

It has been shown that matrix metalloproteinase (MMP, as a protease enzyme), nuclear factor-kappa B (NF-κB, as a regulator of pro-inflammatory gene expression), brain-derived neurotrophic factor (BDNF, as a neurotrophic factor) and apoptosis have key roles in the pathogenesis of ischemic stroke (4-6). Oxytocin (OXT) is a peptide hormone, which is conventionally used as a well-known drug for many years to accelerate labor and lactation in humans (7). It has been shown that short-time use of OXT in humans is safe with no significant side effects (8). Currently, OXT has become an attractive topic for research in social behaviors and its potential usage in the treatment of some psychiatric disorders in human beings (9, 10). Moreover, recent animal studies have shown that post-stroke treatment with OXT reduced ischemic injury via suppressing apoptosis and inflammatory pathways (11-13). In addition, some recent studies showed that exogenous OXT can modulate brain BDNF levels and matrix metalloprotease activity under *in vitro* and *in vivo*

conditions (14, 15).

Although previous limited experimental studies offered that OXT is useful in post-ischemic stroke, the effect of OXT as prophylactic neuroprotection remained unclear. Therefore, this study was designed to determine whether seven days of intranasal daily application of OXT before ischemia could reduce brain injury after stroke in mice. Moreover, interfering with OXT with NF-κB, pro-inflammatory cytokines (TNF-α, IL-1β), MMP-9, BDNF, and apoptosis regulator proteins (Bax and Bcl2) were assessed 24 hours after stroke in the brain tissue.

Material and Methods

Animals

In this experimental study, 46 adult male Swiss albino mice (35-40 g, 3-4 months old) were used that obtained from the animal center of Semnan University of Medical Sciences (SUMS). All procedures were performed in accordance with the ethical policy for laboratory animals and approved by the SUMS institutional Committee of Research Ethics (IR.SUMUMS.REC.1396.241).

Intranasal application of oxytocin

OXT (Sigma-Aldrich, O3251, Germany) or saline, as the vehicle (10 µl), was softly injected into the bilateral nostrils (less than 30 seconds) daily for 7 days prior to ischemic stroke, using a catheter PE-10 that was entered into the nasal cavity. The last dose of OXT was injected 30 minutes before the MCAO. To decline stress reaction, mice experienced 1 week of habituation to the holding position every day before the start of the experiment.

Animal model of stroke

To create the stroke model, mice were anesthetized with chloral hydrate (400 mg/kg, IP) and then under microscopic surgery MCA was occluded using a silicone-coated 8–0 monofilament and Laser Doppler Flowmetry (LDF) monitoring. Blood flow in MCA was blocked for 60 minutes and then flow was restored for 24 hours in the brain ischemic tissue. The Body temperature was checked and preserved in the normal range. Buprenorphine (0.05 mg/kg IP, Temad Co. Active Pharmaceutical Ingredients, Iran) was given approximately 30 minutes before the surgery and once again at 8 hours after MCAO to reduce the surgery pain.

Experimental design and protocols

To examine the preventive effect of intranasal OXT (8 IU/ per mouse intranasal) on brain injury and neurological disorder, 21 mice were randomly divided into three equal groups (n=7, each). In group 1, the sham group, surgery was made without ischemia. Group 2, the control group, received saline (10 µl, intranasal) daily for 7 days prior to ischemia. Group 3, the treatment group, received OXT at a dose (8 IU/ per mouse intranasal), daily for 7 days prior to ischemia. We used the dose of 8 IU/ per mouse of OXT as the therapeutic dose, which was obtained from the data of our previous study (13). At the end of the experiment, neurological impairments and spatial learning and memory were examined, and then infarct size was determined.

For investigating the effect of OXT on the expressions of NF-κB, MMP-9, BDNF, and the level of apoptotic regulator proteins (Bax and Bcl2), 10 mice were divided into 3 groups (Sham=3, saline=4, and OXT=3) with the same interventions as those groups used for brain injury assessment. In all these groups, about 24 hours after ischemia, the animals were euthanized by cervical dislocation, under deep anesthesia, and their brains were isolated and then cut into three equal portions. Then, each part of the brain was used for BDNF measurement using ELISA, NF-κB, and apoptotic regulator proteins (Bax and Bcl2) by western blotting, and MMP-9 using immunohistochemistry methods.

To explore the effect of OXT on the expressions of TNF-α, and IL-1β, 9 mice were randomly divided into 3 equal groups (n=3, each) with the same interventions similar to the groups described above for NF-κB assessment.

Physiological parameters

Physiological parameters were measured in the two separated animal groups 20 minutes before and after MCAO in the mice pretreated with saline (n=3) and/or OXT (n=3). For the measurement of physiologic parameters, the right common carotid artery was cannulated by a polyethylene catheter (PE-50) to record blood pressure and blood sampling for the analysis of arterial blood gas, pH, hemoglobin, and glucose.

Neurobehavioral test

To assess motor and sensory performance, an adjusted neurological severity score was used (16). The neurological scoring was 10-14 for severe; 5-9 for moderate; and 1-4 for mild injury. An individual who was blinded to the animal groups evaluated neurobehavioral tests.

Spatial learning and memory

Spatial learning and memory were estimated using a Radial Arm Water Maze (RAWM) task with six arms. RAWM trials were performed in three situations, habituation (1 day), training (4 days), and probe (1 day). Habituation: Animals were adapted to the atmosphere of the RAWM for 2-3 minutes. Training: Animals received five trials /day with a 30 seconds inter-trial interval for 4 days. During this period, the animals were given 60 seconds to discover the visible platform. If at this time the animal could not discover the platform, it was assisted to find the platform. On the fifth day (probe test), the platform was removed, and animals were dropped from a similar location and permitted to swim for 60 seconds to find the site of the platform. The time to find the platform position and the period spent in the target location was

verified and analyzed (NoldusEtho Vision XT7, the Netherlands).

Infarct size

Twenty-four hours after ischemia animals were deeply anesthetized and euthanized by cervical dislocation, and then the brain was isolated. Using a brain matrix, five 2-mm-thick slices were prepared with triphenyl tetrazolium chloride (TTC) staining (T8877, Sigma, Germany) and measurement of the infarct area. Data of the infarct area of each section was obtained using an image analyzer software (NIH image analyzer). The volume of infarct size was calculated by multiplying the lesion area in the thickness of each section. Total brain injury was calculated by summing the lesion volume of five slices, and finally, the data was presented as infarct volume (mm^3) modified for edema (17).

Western blotting

One week after OXT treatment and 24 hours after ischemia, brain samples were prepared and used to assay the apoptotic regulator proteins (Bax and Bcl2), NF-kB, TNF-α, IL-1β, and Glyceraldehyde-3-phosphate dehydrogenase (GAPDH, ab181602, UK) by western blotting technique. Samples were lysed in the RIPA buffer and a common protease inhibitor (20-188; Merck, Germany). Protein concentration was measured by the Bradford method,then tissues were loaded on SDS-polyacrylamide gel electrophoresis (SDS- PAGE), and protein on the gel was transferred to PVDF membranes (Roth) for 80 minutes at 80 V (Bio-Rad). Proteins were then isolated by polyacrylamide gel electrophoresis (Bio-Rad) via 4-20% gradient polyacrylamide gels containing 0.1% sodium dodecyl sulfate for ~2 hours at 95 V. After blocking with 5% non-fat milk in Tris-buffered saline and Tween 20 (pH=7.6) (TBST), the membranes were incubated with primary antibodies against NF-kB (sc-398442; Santa Cruz, USA), Bax (sc-7480; Santa Cruz, USA), Bcl2 (sc-56018; Santa Cruz, USA), TNF-α (sc-133192; Santa Cruz, USA), IL-1β (orb382131; Biorbyt, UK) and GAPDH at 4˚C overnight. Then, the membranes were incubated with horseradish peroxidase-conjugated secondary anti-rabbit antibodies (HRP, 1:5000, ab6721, UK,) for 1 hour at room temperature. Finally, blots were stained by DAB (3, 3′-diaminobenzidine), imaged, and analyzed using the Image J software. The level of protein expression (Bax, Bcl2, NF-kB, TNF-α, IL-1β) was normalized to the GAPDH (ab181602, UK).

Measurement of BDNF

Seven days after OXT treatment and 24 hours after ischemia, brain tissues were homogenized (1:10 w/v) in cold PBS, and then centrifuged at 30,000×g at 4˚C for 20 minutes. The supernatant was used for measuring the BDNF protein level. The quantity of BDNF was estimated by enzyme-linked immunosorbent assay (ELISA) method and a mouse BDNF ELISA kit (orb409268, biorbyt, UK).

Immunohistochemistry

MMP-9 protein expression was measured by immunofluorescent immunohistochemistry staining in the cortex and hippocampus. The samples were post-fixed overnight and then dehydrated in the ascending alcohol series, rinsed with xylene, and after that infiltrated with paraffin. Subsequently, all of the blocks were cut into 5 μm coronal slices. The slices were incubated in 50% formamide and 2x standard sodium citrate buffer for 2 hours at 65˚C and then incubated twice in 100 mM of sodium borate (pH=8.5). The DNA was then denatured by incubating the sections in 2N HCl at 37˚C, rinsed in phosphate-buffered saline (PBS), and finally blocked with 0.4% Triton X-100 in PBS and goat serum (10%, Gibco™ PCN5000 10098792, UK**)** for 30 minutes. The slices were incubated overnight at 4˚C with primary antibodies for MMP-9 [rabbit anti- MMP-9 (1:100; sc-393859 Santa Cruz, USA)]. The slices were then incubated with secondary antibody FITC anti-rabbit (1:200; ab6785) at 37˚C for 90 minutes in a dark place. Cell nuclei were stained by DAPI (4′, 6-diamidino-2-phenylindole). Tissues were examined under a fluorescence microscope (Olympus, Japan) at 400X magnification. The quantification of the immune-like reactivity of cells was accomplished using Image J software v1.8 (NIH, Wayne Rasband, USA).

Statistical analyses

The normality test was assessed by the Shapiro-Wilk method. Data of infarct size, neurological disorder, spatial learning and memory, apoptosis-related proteins, NF-κB, TNF-α, IL-1β, MMP-9, and BDNF protein were analyzed by one-way ANOVA and Tukey as the posthoc test (Statistical Software, Sigma Stat/ plot 12.3.0,; Jandel Scientific, Erkmiceh, Germany). Data are shown as mean ± SEM. $P<0.05$ was considered statistically significant.

Results

Cerebral blood flow and physiological parameters

Cerebral blood flow (CBF) was monitored by an LDF to assure ischemia. Diminish in local CBF to less than 20% of the basal was a certification for ischemia. In all groups, after ischemia, CBF was reduced to lower than 20% of the initial and preserved during 60 minutes of MCAO (Fig. 1A). There was no significant difference among the groups concerning CBF during 60-minute ischemia and 15 minutes reperfusion ($P>0.05$, Fig.1A).

There is no significant difference among physiological parameters 20 minutes before and after MCAO in animals that were pre-treated with saline and OXT (Table 1).

The effect of pre-ischemic treatment with OXT on the infarct size, neurological function, and spatial learning and memory

The infarct size after 60 minutes of the ischemic event and 24 hours of reperfusion was 150 ± 9 mm^3 in the control (saline) group. Intranasal pre-ischemic treatment with OXT for 7 days significantly reduced the infarct size (111 ± 9 mm^3) compared to the saline (control) group ($P<0.001$, Fig.1B, C). Moreover, OXT pretreatment did not change the neurological function ($P>0.05$, Fig.1D).

Table 1: Physiological parameters 20 minutes before and 20 minutes after MCAO of animals pre-treated with saline and OXT

Parameters	Before-MCAO		After-MCAO	
	Saline	**OXT**	**Saline**	**OXT**
MABP (mmHg)	72 ± 3	67 ± 3	66 ± 3	64 ± 2
Heart rate (per minute)	367 ± 8	373 ± 6	390 ± 6	393 ± 3
pH	7.28 ± 0.02	7.29 ± 0.01	7.22 ± 0.01	7.23 ± 0.01
Arterial pCO_2 (mm Hg)	44 ± 3	47 ± 0.8	51 ± 2	49 ± 1.8
Arterial pO_2 (mm Hg)	98 ± 2	98 ± 1	97 ± 4	96 ± 4
Blood glucose (mg/dl)	143 ± 9	129 ± 4	152 ± 5	147 ± 10
Hb (g/L)	13.68 ± 1	13.1 ± 0.86	13.34 ± 0.3	12.74 ± 0.14

Values are mean ± SEM. Data of physiological parameters between of two groups were analyzed by t test. MABP; Mean arterial blood pressure, Hb; Hemoglobin concentration, MCAO; Middle cerebral artery occlusion, and OXT; Oxytocin.

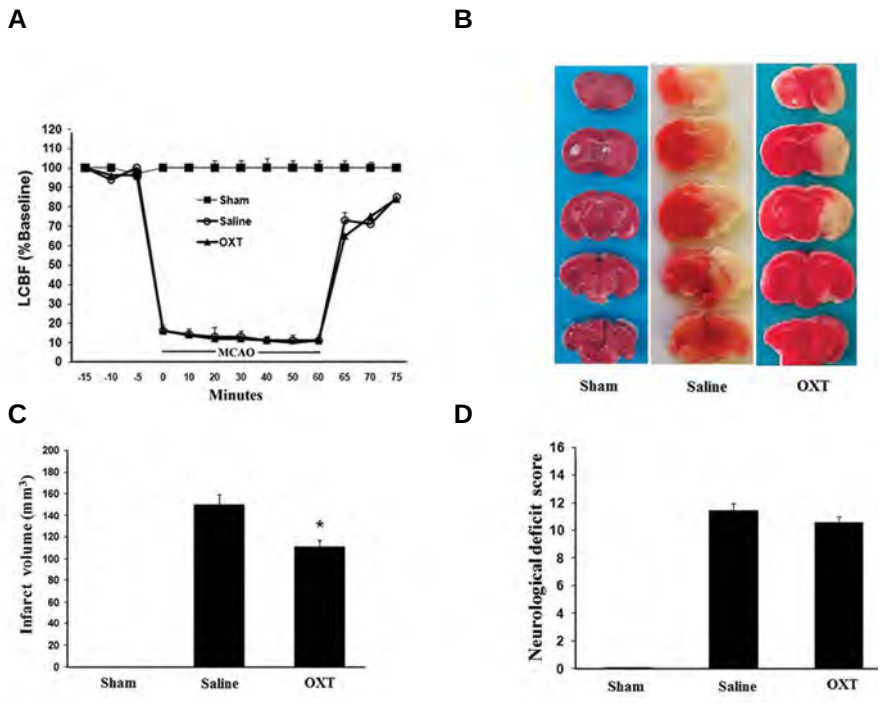

Fig.1: The effect of OXT on the brain injury. **A.** LCBF. **B.** TTC staining image. **C.** Infarct volume. **D.** Neurological deficit scores in the sham operated, saline (control) and OXT groups. White color display damage and red color show normal area. Values are as mean ± SEM (n=7, each). *; P<0.01, compared to the saline (control) group, OXT; Oxytocin, TTC; Triphenyl tetrazolium chloride, and LCBF; Local cerebral blood flow.

The results of spatial memory displayed that in all groups 4 days after training, the time to find the location of the platform (escape latency) was significantly shorter (P<0.01, Fig.2A). After ischemia, the time to find the place of the platform considerably enhanced, and the time spent in the target zone diminished (P<0.01, Fig.2B, C). However, intranasal pre-ischemic administration of OXT for 7 days did not significantly recover these parameters (P>0.05, Fig.2B, C).

The effect of pre-ischemic treatment with oxytocin on the NF-κB, TNF-α, IL-1β, and BDNF proteins

After the interruption of brain blood flow, the level of NF-κB protein considerably increased in the brain compared to the sham groups. OXT pretreatment for 7 days prior to ischemia considerably decreased the

expression of NF-κB protein (P<0.001, Fig.3A).

Twenty-four hours after ischemia, protein levels of TNF-α, and IL-1β were significantly enhanced in the saline (control) group (P<0.001, Fig.3B, C). Pre-treatment with OXT significantly suppressed the synthesis of TNF-α and IL-1β in the brain tissue (P<0.001, Fig. 3B, C).

The ELISA assessment demonstrated that intranasal administration of OXT for one week before ischemia significantly increased the level of BDNF protein in the brain (P<0.001, Fig.3D).

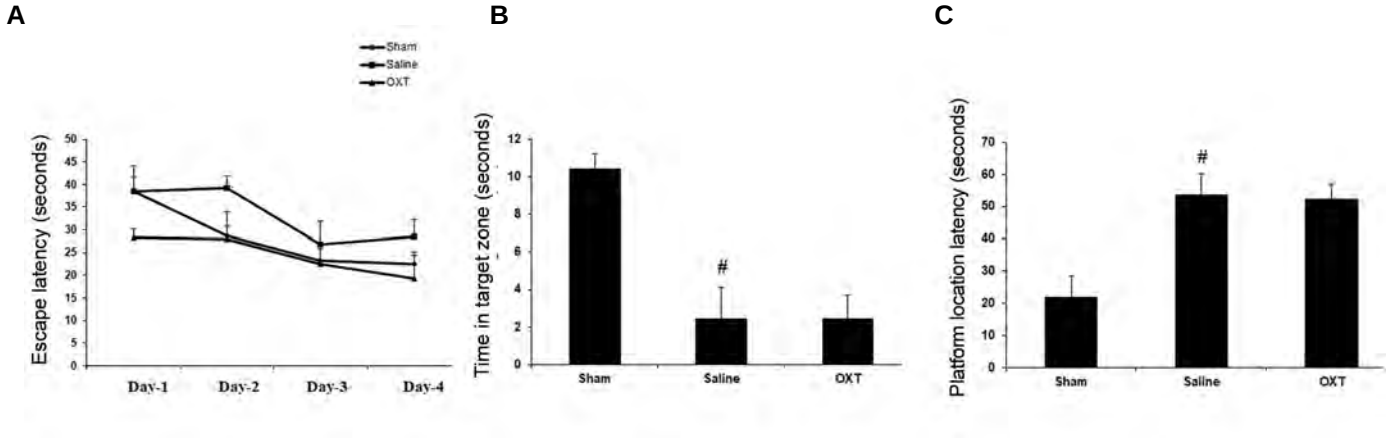

Fig.2: The effect of oxytocin (OXT) on the spatial learning and memory. **A.** Time (second) of 4-days training (escape latency). **B.** Spent in the target zone. **C.** Latency to discovery the platform place in sham-operated, saline (control) and OXT groups. Values are mean ± SEM (n=7, each). #; P<0.001 compared to respective sham-operated group.

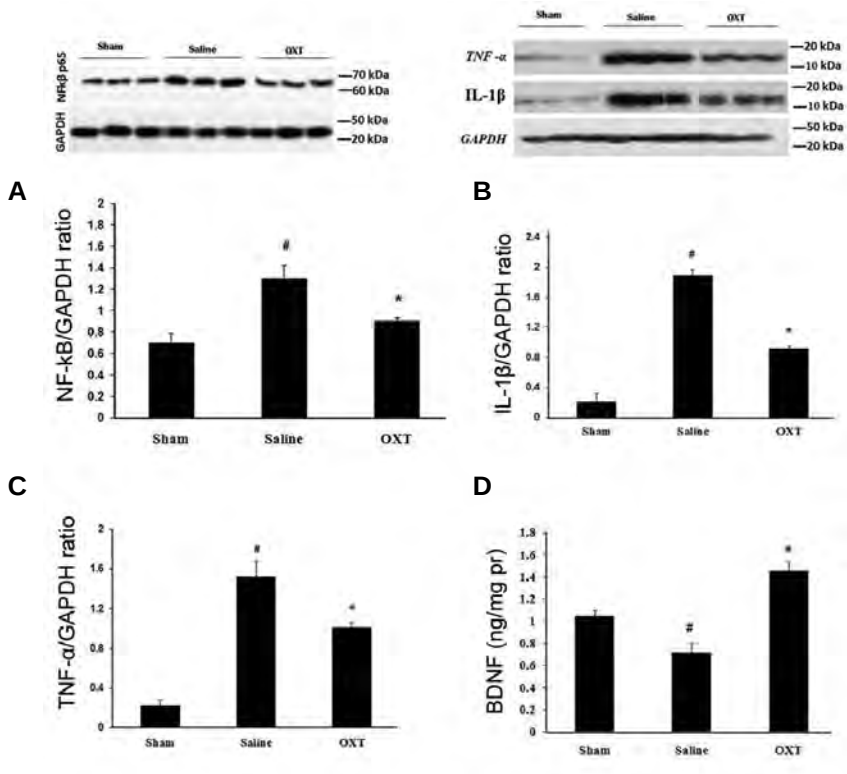

Fig.3: The photograph demonstrates the level of NF-kB, TNF-α, IL-1β and BDNF proteins in the sham-operated and saline (control) and oxytocin (OXT) groups. **A.** The quantitative examination displays as NF-kB/GAPDH. **B.** TNF-α/GAPDH. **C.** IL-1β/GAPDH ratio. **D.** BDNF (ng/mg Pr). Values are mean ± SEM (n=3). *; P<0.001 compared to the saline (control) group and #; P<0.001 compared to respective sham-operated group.

The effect of pretreatment with oxytocin on the expressions of apoptotic regulator proteins

Pro-apoptotic proteins (Bax) significantly increased and anti-apoptotic protein (Bcl2) decreased after an ischemic episode in the brain. Proteins of Bcl-2 were downregulated, and Bcl-2 was significantly upregulated in the group that was pretreated with OXT. The Bcl-2/Bax ratio was also noticeably enhanced in the OXT pre-treated group (P<0.001, Fig.4A-D).

The effect of pre-ischemic treated with oxytocin on the expression of MMP-9

After ischemic stroke, immunohistochemistry analysis showed that the expression of MMP-9 markedly enhanced in the cortex and hippocampus tissues. Intranasal administration of OXT for 7 days prior to ischemia noticeably decreased the expression of MMP-9 protein in these two parts of the brain (P<0.001, Fig.5A, B).

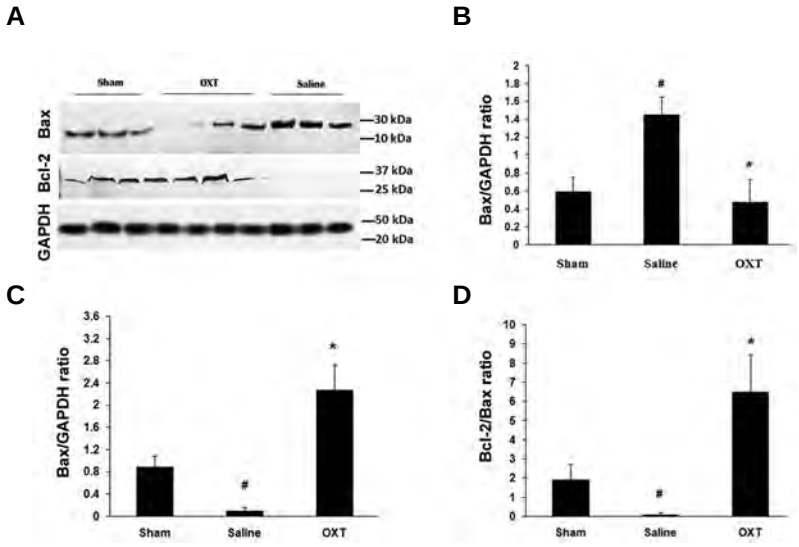

Fig.4: The effect of oxytocin (OXT) on the expressions of apoptotic regulator proteins. **A.** The image demonstrates the levels of Bax and Bcl-2 proteins in the sham-operated and saline (control) and OXT groups as identified by western blotting. **B.** The quantitative analysis illustrated Bax/GAPDH. **C.** Bcl-2/GAPDH. **D.** Bcl-2/Bax ratio in the brain tissue (n=3-4, each). #; P<0.001 from respective sham-operated group and *; P<0.001 compared to the saline (control) group.

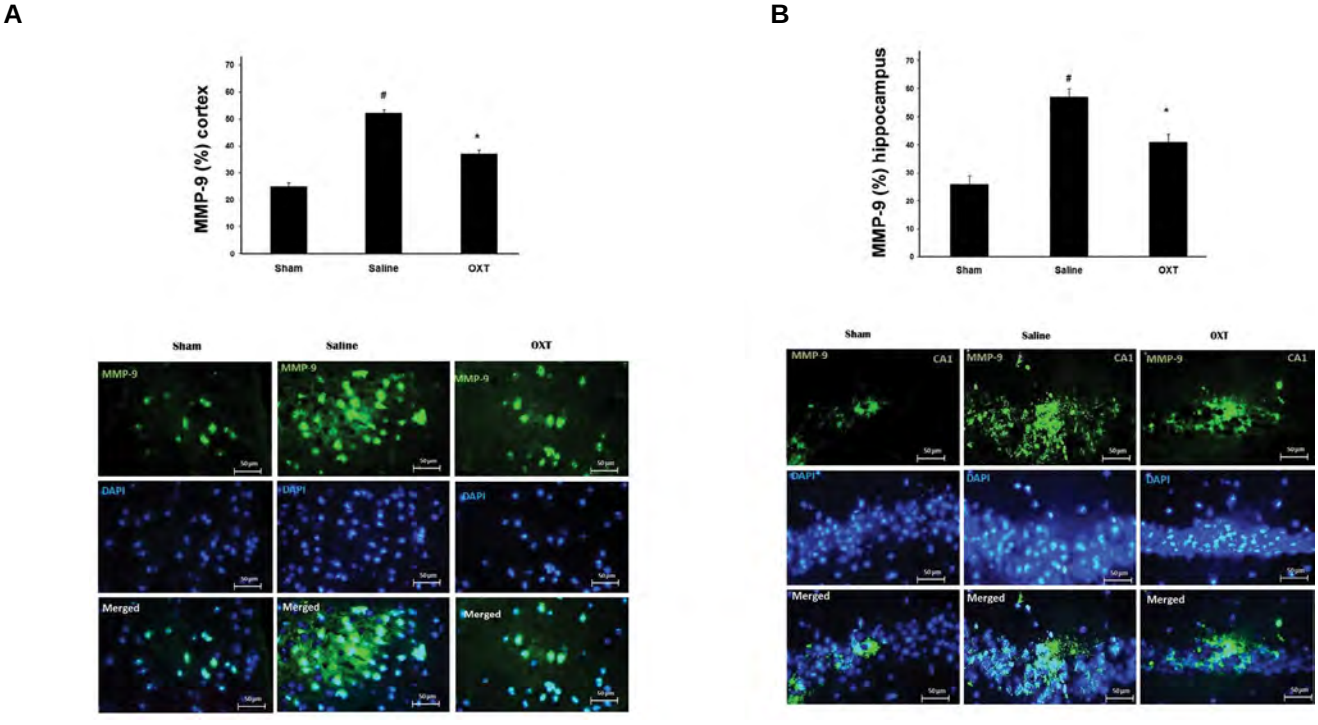

Fig.5: The effect of oxytocin (OXT) on the expression of MMP-9. **A.** Photograph of MMP-9 immune-like reactivity and amount of MMP-9 expression the cortex. **B.** Hippocampus in sham-operated and saline (control) and OXT groups. MMP-9 immune-like reactivity (green) were presented as percentages of the total number of DAPI -stained nuclei (blue) (400× fluorescent microscope). Results presented as mean ± SEM (n=3, each). #; P<0.001 compared to respective sham-operated group and *; P<0.001 compared to the saline (control) group.

Discussion

The principal finding of the current study was that one-week intranasal administration of OXT prior to cerebral ischemia attenuates brain injury by reducing the expressions of NF-κB, pro-inflammatory cytokines (TNF-α, IL-1β), MMP-9, inhibition programmed cell death machinery and enhancing of BDNF protein. Moreover, OXT pretreatment did not correct spatial memory and neurological dysfunction 24 hours after stroke in mice.

Intranasal injection of OXT for 7 days before ischemia declined the infarct size by 26% when compared to the control group; however, it was unable to recover spatial memory and neurological disorders. The reason why OXT pretreatment did not change neurological functions, despite reducing the infarct size, is not clear. According to our previous studies and others (18-20), there is not necessarily a straightforward relationship between the reduction of cerebral damage and improvements in neurological functions. Our previous studies (13, 16, 18) show that in an animal model of stroke improvements in the behavioral disorders mainly occur when an intervention reduces the brain lesion by more than 50%. In the present study, however, our intervention declined brain injury by 25%. This hypothesis is supported by several experimental and clinical studies, which have reported there is not always a direct link between infarct size and neurological outcomes (18-20). However, the possibility of OXT application, as a preventive approach in a high-risk population, needs to be more explored. Therefore, we suggest performing more studies in experimental and clinical trials.

NF-κB is a transcriptional factor, which is activated during the acute phase of cerebral ischemia and plays a detrimental role in stroke pathogenesis by increasing the gene expression of many inflammatory and pro-inflammatory cytokines such as TNF-α and IL-1β (6, 21). It is well established that activation of NF- κB and pro-inflammatory cytokines such as IL-1β and TNF-α in the early stage of stroke could exacerbate brain damage (21, 22). Our findings revealed that pre-treatment with OXT attenuated the expression of pro-inflammatory cytokines (IL-1β and TNF-α) by inhibiting the NF-κB p65 in the brain tissue. This result demonstrates the anti-inflammatory effect of OXT. The anti-inflammatory properties of OXT may be related to the inhibition of nuclear translocation of NF-κB p65 in the microglia or neurons. However, an additional experimental study is required to confirm this hypothesis. Inhibition of NF-κB, TNF-α, and IL-1β by OXT may be responsible for part of its protective effects on cerebral ischemia in the present study. Several *in vitro* and *in vivo* studies have shown that OXT has anti-inflammatory activity by inhibiting the expressions of NF-κB and pro-inflammatory cytokines (11, 23, 24), which confirms our finding.

The apoptotic signaling pathway is controlled by many apoptotic-related proteins including Bcl2 family proteins, Bax, Bad, and Bcl-xL (25). Bcl-2 and Bax family proteins are highly expressed between 12-and 24 hours after cerebral ischemia (26). Overexpression of the anti-apoptotic protein Bcl-2 protects the neuronal cell against apoptosis, while the activation of the apoptotic protein Bax triggers apoptosis and neuronal injury in the acute phase of stroke (27). The results of the current study showed that one week of pre-treatment of mice with OXT reduced the apoptosis by down-regulating pro-apoptotic, BAX, and up-regulation anti-apoptotic, BCL2. Our findings are in agreement with Dalia et al.'s study, which showed that pre-treatment with OXT 7 days before myocardial infarction diminished heart injury via reducing Bax and p53 as makers of apoptosis in rats (28). In addition, several studies have reported that OXT has anti-apoptotic effects in *in vitro* and *in vivo* situations that confirm our results (28-30).

MMPs belong to the family of protease enzymes, and it has an important contribution to physiology and pathological processes such as extracellular matrix remodeling and cerebral ischemia (31, 32). Data obtained from previous preclinical studies indicated that the activation of MMP-9 in the acute phase of stroke plays a destructive role in the pathogenesis of brain trauma, focal, and global cerebral ischemia may be via interrupting blood-brain barrier, edema formation, and myelin injury (4, 31, 32). A clinical study also showed that there is a link between MMP-9 and the risk of ischemic stroke in humans (33). The finding of our study showed that pretreatment with OXT significantly decreased the expression of MMP-9 in the cortex and the hippocampus following cerebral ischemia in mice. Recently, a study indicated that OXT in a dose-dependent manner inhibits TNF-α induced MMP-1 and MMP-13 expressions at the gene and protein levels in isolated human chondrocyte cells (15), which is somewhat in agreement with our findings. There is some evidence that metalloproteases play a significant role in activating the programmed cell death machinery of apoptosis. For instance, Dang et al. (34) showed that inhibition of MMP2/MMP9 attenuates spinal cord injury via diminishing apoptosis in the mouse model. Therefore, we can conclude that OXT by reducing MMP-9 expression and subsequently inhibiting programmed cell death machinery led to diminishing the infarct size in the present study. Previous studies have reported that various types of cells including neurons, microglia, endothelial cells, and neutrophils can express MMP-9 after cerebral ischemia (35, 36). However, the major cellular source of MMP-9 in ischemic stroke is not exactly clear. Experimental evidence has shown that in the ischemic core, MMP-9 is likely produced by both infiltrating neutrophils and microglia (36). In peri-infarct areas, the MMP-9 is mainly produced by microglial cells (36, 37). Although the cellular source of MMP-9 in the present study is not clear, regarding the size of MMP-9 positive cells (about 15-30 μm wide), it can be concluded that the main source of MMP-9 in microglia cells (38).

Neurotrophic factors such as BDNF, play a key role in

the regulation of neuroplasticity, neurogenesis, and also the recovery of brain damage after strokes (5). The present study showed that one week of daily administration of OXT before ischemia resulted in elevated cerebral BDNF protein levels, which were associated with improving brain injury. There is growing evidence indicating that part of the OXT function was done through interaction with the BDNF in various tissues such as the brain (14, 39, 40). For example, Dayi et al. (14) showed that intranasal administration of OXT increased the levels of BDNF in the brain following chronic stress in rats.

Conclusion

The results of this study indicated that intranasal OXT before ischemia limited stroke-induced brain injury by downregulating NF-κB, pro-inflammatory cytokines (IL-1β, TNF-α), MMP-9, and apoptotic mediators Bax proteins and up-regulating anti-apoptotic Bcl-2 and BDNF protein in mice. We suggest that OXT may be potentially useful in the prevention and/or reducing the risk of cerebral stroke attack and can be offered as a new prevention option in the clinics. However, the possibility of using OXT, as a prophylactic agent to reduce the risk of a stroke attack, needs to be clarified.

Acknowledgments

This work was supported by a research grant from the Vice Chancellor for Research of the Semnan University of Medical Sciences (grant number: 1355). We thank Prof. Ali Rashidy-Pour for his help with revising of the manuscript. We also thank Reza Nasr form the Department of Biotechnology, Semnan University of Medical Sciences for his technical assistance. The authors have no conflicting interests to disclose.

Authors' Contributions

A.V., M.Z.K.; Contributed to conception and design research. S.M., A.A.V, M.Z.K., A.V.; Contributed to all experimental work, data and statistical analysis, and interpretation of data. A.V.; Contributed extensively in the interpretation of the data and the conclusion, responsible for overall supervision, molecular experiments were done in Basic Medical Science Research, Histogenotech Company, Tehran, Iran. All authors read and approved the final version of the manuscript.

References

1. Campbell BCV, De Silva DA, Macleod MR, Coutts SB, Schwamm LH, Davis SM, et al. Ischaemic stroke. Nat Rev Dis Primers. 2019; 5(1): 70.
2. Karimipour M, Shojaei Zarghani S, Mohajer Milani M, Soraya H. Pre-treatment with metformin in comparison with post-treatment reduces cerebral ischemia reperfusion induced injuries in rats. Bull Emerg Trauma. 2018; 6(2): 115-121.
3. Famakin BM, Chimowitz MI, Lynn MJ, Stern BJ, George MG. Causes and severity of ischemic stroke in patients with symptomatic intracranial arterial stenosis. Stroke. 2009; 40(6): 1999-2003.
4. Asahi M, Wang X, Mori T, Sumii T, Jung JC, Moskowitz MA, et al. Effects of matrix metalloproteinase-9 gene knock-out on the proteolysis of blood-brain barrier and white matter components after cerebral ischemia. J Neurosci. 2001; 21(19): 7724-7732.
5. Nowacka M, Obuchowicz E. BDNF and VEGF in the pathogenesis of stress-induced affective diseases: an insight from experimental studies. Pharmacol Rep. 2013; 65(3): 535-546.
6. Zhao H, Chen Z, Xie LJ, Liu GF. Suppression of TLR4/NF-κB signaling pathway improves cerebral ischemia-reperfusion injury in rats. Mol Neurobiol. 2018; 55(5): 4311-4319.
7. Prevost M, Zelkowitz P, Tulandi T, Hayton B, Feeley N, Carter CS, et al. Oxytocin in pregnancy and the postpartum: relations to labor and its management. Front Public Health. 2014; 2: 1.
8. Macdonald K, Feifel D. Helping oxytocin deliver: considerations in the development of oxytocin-based therapeutics for brain disorders. Front Neurosci. 2013; 7: 35.
9. Cai Q, Feng L, Yap KZ. Systematic review and meta-analysis of reported adverse events of long-term intranasal oxytocin treatment for autism spectrum disorder. Psychiatry Clin Neurosci. 2018; 72(3): 140-151.
10. Domes G, Ower N, von Dawans B, Spengler FB, Dziobek I, Bohus M, et al. Effects of intranasal oxytocin administration on empathy and approach motivation in women with borderline personality disorder: a randomized controlled trial. Transl Psychiatry. 2019; 9(1): 328.
11. Karelina K, Stuller KA, Jarrett B, Zhang N, Wells J, Norman GJ, et al. Oxytocin mediates social neuroprotection after cerebral ischemia. Stroke. 2011; 42(12): 3606-3611.
12. Etehadi Moghadam S, Azami Tameh A, Vahidinia Z, Atlasi MA, Hassani Bafrani H, Naderian H. Neuroprotective effects of oxytocin hormone after an experimental stroke model and the Possible role of calpain-1. J Stroke Cerebrovasc Dis. 2018; 27(3): 724-732.
13. Momenabadi S, Vafaei AA, Bandegi AR, Zahedi-Khorasani M, Mazaheri Z, Vakili A. Oxytocin reduces brain injury and maintains blood-brain barrier integrity after ischemic stroke in mice. Neuromolecular Med. 2020; 22(4): 557-571.
14. Dayi A, Cetin F, Sisman AR, Aksu I, Tas A, Gönenc S, et al. The effects of oxytocin on cognitive defect caused by chronic restraint stress applied to adolescent rats and on hippocampal VEGF and BDNF levels. Med Sci Monit. 2015; 21: 69-75.
15. Wu Y, Wu T, Xu B, Xu X, Chen H, Li X. Oxytocin prevents cartilage matrix destruction via regulating matrix metalloproteinases. Biochem Biophys Res Commun. 2017; 486(3): 601-606.
16. Behrouzifar S, Vakili A, Bandegi AR, Kokhaei P. Neuroprotective nature of adipokine resistin in the early stages of focal cerebral ischemia in a stroke mouse model. Neurochem Int. 2018; 114: 99-107.
17. Khorasani MZ, Hosseinzadeh SA, Vakili A. Effect of central microinjection of carbenoxolone in an experimental model of focal cerebral ischemia. Pak J Pharm Sci. 2009; 22(4): 349-354.
18. Akhoundzadeh K, Vakili A, Sameni HR, Vafaei AA, Rashidy-Pour A, Safari M, Mohammadkhani R. Effects of the combined treatment of bone marrow stromal cells with mild exercise and thyroid hormone on brain damage and apoptosis in a mouse focal cerebral ischemia model. Metab Brain Dis. 2017; 32(4): 1267-1277.
19. González-Falcón A, Candelario-Jalil E, García-Cabrera M, León OS. Effects of pyruvate administration on infarct volume and neurological deficits following permanent focal cerebral ischemia in rats. Brain Res. 2003; 990(1-2): 1-7.
20. Stroke Therapy Academic Industry Roundtable II (STAIR-II). Recommendations for clinical trial evaluation of acute stroke therapies. Stroke. 2001; 32(7): 1598-1606.
21. Zhang W, Potrovita I, Tarabin V, Herrmann O, Beer V, Weih F, et al. Neuronal activation of NF-kappaB contributes to cell death in cerebral ischemia. J Cereb Blood Flow Metab. 2005; 25(1): 30-40.
22. Jin R, Liu L, Zhang S, Nanda A, Li G. Role of inflammation and its mediators in acute ischemic stroke. J Cardiovasc Transl Res. 2013; 6(5): 834-851.
23. Ahmed MA, Elosaily GM. Role of oxytocin in deceleration of early atherosclerotic inflammatory processes in adult male rats. Int J Clin Exp Med. 2011; 4(3): 169-178.
24. Khori V, Alizadeh AM, Khalighfard S, Heidarian Y, Khodayari H. Oxytocin effects on the inhibition of the NF-κB/miR195 pathway in mice breast cancer. Peptides. 2018; 107: 54-60.
25. Isenmann S, Stoll G, Schroeter M, Krajewski S, Reed JC, Bähr M. Differential regulation of Bax, Bcl-2, and Bcl-X proteins in focal cortical ischemia in the rat. Brain Pathol. 1998; 8(1): 49-62.
26. Zhang W, Meng A. MicroRNA-124 expression in the brains of rats during early cerebral ischemia and reperfusion injury is associated with cell apoptosis involving STAT3. Exp Ther Med. 2019; 17(4): 2870-2876.
27. Asadi Y, Gorjipour F, Behrouzifar S, Vakili A. Irisin peptide protects

brain against ischemic injury through reducing apoptosis and enhancing BDNF in a rodent model of stroke. Neurochem Res. 2018; 43(8): 1549-1560.
28. Mostafa DG, Khaleel EF, Abdel-Aleem GA. Mechanism of action of oxytocin as cardioprotection in rat model of myocardial infarction. IOSR J Dent Med Sci 2015; 14: 25-36.
29. Al-Amran FF, Shahkolahi M. Oxytocin ameliorates the immediate myocardial injury in heart transplant through down regulation of the neutrophil dependent myocardial apoptosis. Heart Views. 2014; 15(2): 37-45.
30. Latt HM, Matsushita H, Morino M, Koga Y, Michiue H, Nishiki T, et al. Oxytocin inhibits corticosterone-induced apoptosis in primary hippocampal neurons. Neuroscience. 2018; 379: 383-389.
31. Lee SR, Tsuji K, Lee SR, Lo EH. Role of matrix metalloproteinases in delayed neuronal damage after transient global cerebral ischemia. J Neurosci. 2004; 24(3): 671-678.
32. Wang X, Jung J, Asahi M, Chwang W, Russo L, Moskowitz MA, et al. Effects of matrix metalloproteinase-9 gene knock-out on morphological and motor outcomes after traumatic brain injury. J Neurosci. 2000; 20(18): 7037-7042.
33. Gao N, Guo T, Luo H, Tu G, Niu F, Yan M, et al. Association of the MMP-9 polymorphism and ischemic stroke risk in southern Chinese Han population. BMC Neurol. 2019; 19(1): 67.
34. Dang AB, Tay BKB, Kim HT, Nauth A, Alfonso-Jaume MA, Lovett DH. Inhibition of MMP2/MMP9 after spinal cord trauma reduces apoptosis. Spine. 2008; 33(17): E576-E579.
35. Rosell A, Cuadrado E, Ortega-Aznar A, Hernández-Guillamon M, Lo EH, Montaner J. MMP-9-positive neutrophil infiltration is associated to blood-brain barrier breakdown and basal lamina type IV collagen degradation during hemorrhagic transformation after human ischemic stroke. Stroke. 2008; 39(4): 1121-1126.
36. Turner RJ, Sharp FR. Implications of MMP9 for blood brain barrier disruption and hemorrhagic transformation following ischemic stroke. Front Cell Neurosci. 2016; 10: 56.
37. Rosell A, Ortega-Aznar A, Alvarez-Sabín J, Fernández-Cadenas I, Ribó M, Molina CA, et al. Increased brain expression of matrix metalloproteinase-9 after ischemic and hemorrhagic human stroke. Stroke. 2006; 37(6): 1399-1406.
38. Könnecke H, Bechmann I. The role of microglia and matrix metalloproteinases involvement in neuroinflammation and gliomas. Clin Dev Immunol. 2013; 2013: 914104.
39. Barker V, Walker RM, Evans KL, Lawrie SM. Methylation of glucocorticoid receptor (NR3C1), BDNF and oxytocin receptor genes in association with childhood maltreatment in schizophrenia and schizoaffective disorder. Schizophr Res. 2020; 216: 529-531.
40. Camerino C, Conte E, Carratù MR, Fonzino A, Lograno MD, Tricarico D. Oxytocin/osteocalcin/IL-6 and NGF/BDNF mRNA levels in response to cold stress challenge in mice: possible oxytonic brain-bone-muscle-interaction. Front Physiol. 2019; 10: 1437.

Original Article

The Effect of Low-Level Laser Therapy in Combination with Leukocyte- and Platelet- Rich Fibrin on Bone Regeneration in Rabbits' Calvarial Defects: Histologic and Histomorphometric Studies

Fereshteh Shanei, D.D.S., M.Sc.[1], Ahad Khoshzaban, D.D.S., Ph.D.[2], Ferial Taleghani, D.D.S., M.Sc.[3]*, Maryam Tehranchi, D.D.S., M.Sc.[3], Mohammad Hossein Tayeed, D.D.S., M.Sc.[3]

1. Department of Periodontics, Faculty of Dentistry, Alborz University of Medical Sciences, Alborz, Iran
2. Iranian Tissue Bank Research Center, Imam Khomeini Medical Complex, Tehran University of Medical Sciences, Tahran, Iran
3. Department of Periodontics, Faculty of Dentistry, Shahed University, Tehran, Iran

Corresponding Address: P.O.Box: 1417755351, Department of Periodontics, Faculty of Dentistry, Shahed University, Tehran, Iran
Email: ferial2002@yahoo.com

Received: 01/December/2020, Accepted: 21/April/2021

Abstract

Objectives: Bone regeneration is a desired treatment outcome in implant dentistry. The primary goal of the current investigation was to assess the joint effect of low-level laser therapy (LLLT) and leukocyte- and platelet-rich fibrin (PRF) on new bone formation.

Materials and Methods: During this experiment study, forty bone defects (8 mm in diameter) were generated in the calvaria of ten New-Zealand white rabbits. defects were filled with autogenous bone defined as the control group, autogenous bone with leukocyte- and PRF (PRF group), autogenous bone and low-level diode laser radiation (LLLT group), and autogenous bone with leukocyte- and PRF and low-level laser radiation (LP group). Laser irradiation was done every second day for 2 weeks after surgery. Five rabbits were randomly selected to be sacrificed on postoperative weeks 4 and 8. On one and two-month post-surgery, histological and histomorphometric parameters including bone formation, fibroblast, and osteoblast were assessed.

Results: The histological panel depicted that the ratio of fresh bone formation increased at one-and two-month post-surgery in all treatment groups compared to the control group. The most favorable results were seen in the LP group, followed by the PRF group. Based on the ANOVA test, bone neoformation was statistically significant in the LP group in comparison with the control group ($P<0.001$). One-month post-surgery, a higher degree of fibroblast was seen in the control group, while the last place was for LP group (118.6 ± 6.9 vs. 24.0 ± 3.2). In the PRF group, the percentage of bone formation was higher than that in the control group (13.2 ± 2.8 vs. 2.0 ± 1.2), but no significant difference when compared to the LP group (13.2 ± 2.8 vs. $19.0 \pm .3.8$).

Conclusion: The combined L-PRF and LLLT was more likely to have a positive effect on accelerating bone regeneration and reducing fibrosis.

Keywords: Bone Regeneration, Leukocyte- and Platelet-Rich Fibrin, Low-Level Laser Therapy

Cell Journal(Yakhteh), Vol 24, No 6, June 2022, Pages: 346-352

Citation: **Shanei F, Khoshzaban A, Taleghani F, Tehranchi M, Tayeed MH. The effect of low-level laser therapy in combination with leukocyte- and platelet- rich fibrin on bone regeneration in rabbits' calvarial defects: histologic and histomorphometric studies. Cell J. 2022; 24(6): 346-352. doi: 10.22074/cellj.2022.7864.**

Introduction

xBone regeneration is a desired treatment outcome. It is well-documented that bone regeneration could be obtained through the grafting of bone (1). The main feature that clinicians are seeking, is to provide osteoinductivity which can be achieved by combining bone grafts with bioactive growth factors or with their containing compounds (2-4).

Platelet-rich plasma (PRP) and platelet-rich fibrin (PRF) have been identified as biological sources encompassing high levels of necessary growth factors for bone regeneration (5). PRF is an autologous blood-derived platelet concentrate created using a simplified procedure that involves no biochemical processing of blood (6). PRF contains a dense fibrin network in which platelets and leukocytes are trapped (7, 8). It seems that the high fibrin content of PRF improves the growth factors and cytokines stability by conserving them from proteolytic degradation and increasing their longevity (9). Finally, leukocyte content can play an essential role in minimizing inflammation and preventing infection (7).

Studies have reported the benefits of PRF including increased vascularization and an increase in graft stability when combining PRF with bone graft material (5, 10). In addition, some studies have suggested that the use of platelet concentrates can accelerate the bone healing process. This could be because these substances contain platelet-derived growth factors and vascular endothelial growth factors which in combination with a suitable scaffold can transfer the required molecules to the bone regeneration region (6, 11). However, limited evidence showed the effect of PRF on the bone regeneration process (5). For instance, one systematic review addressing the effect of PRF indicated that most studies have reported improvement in soft tissue regeneration and reduction in dimensional changes post-extraction (12).

Low-level laser therapy (LLLT) is regarded as a

promising treatment to accelerate bone metabolism. LLLT employs directional non-ionized electromagnetic radiation in a monochromatic and coherent manner. This can lead to stimulation of bone repair via increasing the osteoblasts' activity, vascularization, and organization of collagen fibers (13). Results from in vivo and in vitro investigations have shown that this therapy could induce bone repair by stimulating the secretion of osteogenic factors (14). Additionally, LLLT can provoke cell proliferation as well as angiogenesis which is an essential factor in bone formation in the primary stage of repairing (14, 15). In recent decades, *in vitro* studies addressing the effect of LLLT on bone regeneration have shown an increase in the activity of the alkaline phosphatase enzyme. Thus, increased intracellular calcium concentrations and osteoblastic activity lead to a higher amount of bone formation (16, 17).

The low-level laser therapy has been proved to impact the proliferation and variation of bone cells, reducing the time of osseointegration of dental implants, preimplantitis therapy, and periodontitis as well as accelerating dental orthodontic movement (15). Although positive effects of LLLT have been reported, there are still studies with contradictory results (18). Such discrepancies might be due to components such as standardized radiation protocol for the surgical procedure or the diversity of experimental models (15, 19).

In recent years, the research on the effect of low-level laser and leukocyte- and PRF on bone regeneration has received wide currency, but there is still controversy on the effects of Leukocyte- and Platelet- Rich Fibrin therapy as well as LLLT on bone regeneration. In the present study, we made an effort to address the effect of leukocyte- and PRF therapy in combination with the LLLT. This histomorphometric study aimed to evaluate the effect of low-level laser combined with PRF and could be a step toward improving bone repair treatments, especially in periodontal interventions.

Materials and Methods

Animals

Ten adult male New Zealand white rabbits, aged close to 6 months, weighing about 2.5 to 3 kg, and raised at the Pasteur Institute of Iran-Tehran, were used in this study. They were kept for 4 and 8 weeks in individual cages at the Iranian Tissue Bank and Research Center, Imam Khomeini Medical Complex (Tehran, Iran), and were provided unrestricted access to food and water. In the laboratory, they were housed in a temperature- and humidity-controlled environment with a 12-hour light/dark cycle.

Experimental design

In the present experimental study, the rabbits were randomly selected for operation. The rabbit's Calvaria bone, the matching bone to the human's Mandible (jaw bone), was selected as a model for bone defect, which as well, allowed us to observe the repair process 3 to 4 times faster compared to humans (20). Rabbits are equally divided into two groups; five rabbits were randomly allocated to evaluate histological variables at one-month post-surgery and the rest were used two-monthmonths post-surgery. Four treatment groups were defined: i. Defects filled with autograft bone (control group), ii. Autogenous bone mixed with leukocyte- and PRF (PRF group), iii. Autogenous bone and low-level diode laser radiation (LLLT group) and iv. Autogenous bone with leukocyte- and platelet -rich fibrin and low-level diode laser radiation (LP group). On days 30 and 60 after the operation, histological parameters including the number of fibroblasts, percentage of new bone formation, and osteoblast were measured. Histological analyses were performed by two pathologists independently. The experiment was done during the 10:00-17:00 hours light phase.

Preparation of the leukocyte- and platelet-rich fibrin

The Choukroun protocol was used to prepare PRF. Concisely, the tubes containing 5 ml of blood samples, with the source of cardiac, were centrifuged at 2700 rpm for 8 minutes. Following that, L-PRF was removed from the blood cells, and then it was mixed with the autogenous bone to fill the defects (21).

Surgical procedure

The animals were anesthetized using an intramuscular injection of ketamine hydrochloride (10%, 30 mg/kg) and 2% xylazine (Alafason, Woeden, Holland, 3 mg/kg). The rabbit's heads were shaved and the scalp was prepped with povidone-iodine solution. Using a surgical blade a longitudinal anteroposterior incision (10 cm) was created along the midline of the skull from the midpoint of the base of the ears (No. 15). Before cutting the periosteum, the skin was retracted using a surgical mosquito and then using a periosteal elevator, the periosteum was separated from the bone surface cranial to caudal.

Four defects (8 mm in diameter) were generated in the parietal bone (Fig.1). Defects were on both sides of the sagittal suture without crossing the midline employing an electric 2000 rpm handpiece (Dio company, South Korea) and 8mm in diameter round surgical trephine. The obtaining bone by trephine bur was crushed by the bone mill and used as autograft bone in each defect. The first defect was filled with autograft bone. The autograft bone containing Leukocyte- and Platelet-Rich Fibrin was used in the second defect. The third, was filled with autograft bone and radiated by low-level laser. Finally, a mixture of the autograft bone containing leukocyte- and platelet-rich fibers were placed into the fourth defect before using low-level laser radiation. A clockwise counter was applied with no pressure, to fully avoid the particle's entrance to the meningeal zone while filling the defects. Then, the periosteum and the calvarium skin were sutured with

4-0 simple absorbable sutures and 3-0 silk respectively. When animals were brought to full consciousness, they were placed into cages. To prevent infection, one-day post-operation, cefazolin (20 mg/kg, IM) was injected. Tramadol (20 mg/kg, i.m) was also and administrated to relieve pain. Skin sutures were removed 10 days following the surgery.

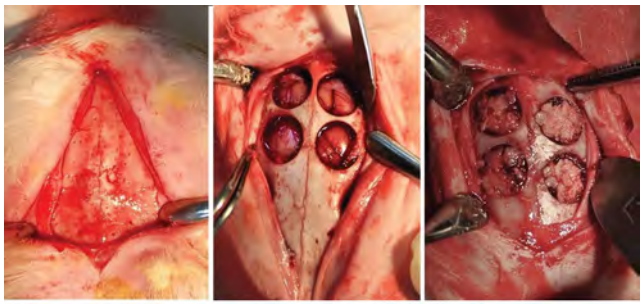

Fig.1: Photographic images of the critical-sized bone defects (8 mm in diameter) in rabbit's calvaria left to right: Flap elevation, defects preparation with trephine bur, defect filling with materials.

Laser irradiation

In the third and fourth defects of each rabbit, Aluminum Gallium Arsenide (GaAlAs) laser (Konf™-Konftec Corporation, Taiwan), wavelength 808nm, power 250 mW, density 0.4 Watt/cm^2, and spot size 0.5 cm^2 with frequency 5 J/cm^2 for 20 seconds were applied. Laser irradiation was done every other day for two-week post-surgery. The center of each defect was marked by a non-absorbable suture on the skin and laser irradiation was done in the center of this marking to avoid any mistakes.

Histological assessment

On 30- and 60-days post-surgery, animals were euthanized with xylazine (Alafason, Woeden, Holland), and the harvested tissue (defect area of calvarial bone) was fixed in the 10% neutral buffered formalin (NBF, pH=7.26) for 48 hours. The samples were decalcified in 10% EDTA, processed, and embedded in paraffin. Then, 5 µm thick sections were prepared and stained with hematoxylin and eosin (H & E), and Masson trichrome (MT). The histological slides were independently assessed by two pathologists using light microscopy (Olympus BX51, Olympus, Tokyo, Japan). The percentage of the new bone formation was assessed in the total area of the defect section. To differentiate the autogenous bone graft (ABG) in defects area from the new bone formation, the area with live osteocyte lacuna was identified as a new bone formation. In addition, to perform histomorphometric analysis, the number of fibroblast and osteoblast was assessed and pictured utilizing Image-Pro Plus® V.6 (Media Cybernetics, Inc., Silver Spring, USA).

Statistical analysis

The sample size was determined based on the effect size of the relevant studies, considering a significance level of 0.05 and 80% study power. Descriptive statistics were reported with mean, frequency, standard deviation (SD), and percentage of parameters in each group. Considering testing normal assumptions for all parameters, one-way ANOVA and Kruskal Walis test were used to calculate differences between groups. Hence, the Bonferroni test and Dunn Post-Hoc test were conducted to test for differences in all possible pairs. Man-Witney test was used to compare means of parameters between the samples one month and two-month post-surgery. A $P<0.05$ was considered a significant value. All statistical analyses were performed using statistical package for the social sciences for windows, version 25 (SPSS, Inc., Armonk, NY, IBM Corp).

Ethics statement

The protocol of the present research was reviewed and approved (IR.SHAHED.REC.1397.054) by the Shahed University of Medical Sciences Ethics Committee. All experiments followed the guidelines of the Iran Animal Care Committee.

Results

Micrographs of the normal calvarial and histological findings after one- and two months post-surgery can be seen in Figures 2 to 4. In the control group, the defect area was repleted with fibrous connective tissue (FCT) and ABG at one-month post-surgery. After two months, the new bone formation (NB) was negligible and the autogenous bone graft was also removed from the defect area via multi-nucleated giant cells, and the defect area was filled by FCT. In the treatment groups, less fibrous tissue and larger areas of NB were observed compared to the control group. Histomorphometric analysis of four calvarial defects after one-month post-surgery depicted a small area consisting of new bone formation around the ABG in the LLLT group (Fig.3).

At one-month post-surgery, the results showed that fibroblast level was significantly different among the four experimental groups (Table 1, Fig.3). Based on the result, a higher degree of fibroblast appeared in the control group, while the lowest was in the LP group. Moreover, the percentage of the new bone formation was higher in LP, followed by the PRF, but the number of osteoblasts was higher in the LP group in the first month after surgery. There was a statistically significant difference in the amount of bone neoformation among all groups ($P=0.001$). Results from pairwise comparisons showed that there were significant differences between LP and other groups except for the PRF group. The highest percentage of new bone formation was seen in the LP group compared to the control group (19.0 ± 3.8 vs.

2.0 ± 1.2). Similarly, the number of osteoblasts was statistically different between LP and the other groups (P<0.05), but no significant difference was observed between LP and PRF (19.0 ± 3.8 first then 13.2 ± 2.8).

Table 1: Comparison of the mean scores and standard deviations of histological variables between treatment groups after one-month post-operation

Group	Between groups	Fibroblast	Osteoblast	Bone formation
C		118.6 ± 6.9	1.1 ± 0.4	2.0 ± 1.2
	C-LLLT (p)	0.1	0.18	0.26
	C-PRF (p)	0.045*	0.041*	0.052
	C-LP (p)	0.000*	0.000*	0.001*
LLLT		87.2 ± 5.9	7.8 ± 3.3	4.2 ± 0.84
	LLLT-PRF (p)	0.18	0.17	0.8
	LLLT-LP (p)	0.045*	0.04*	0.038*
PRF		63.0 ± 6.4	18.4 ± 1.4	13.2 ± 2.8
	PRF-LP (p)	0.18	0.2	0.22
LP		24.0 ± 3.2	31.8 ± 2.6	19.0 ± 3.8

Data are presented as mean ± SD. C; Control, LLLT; Low-level laser therapy, PRF; Leukocyte-platelet rich fibrin, LP; PRF+LLLT, (p); P value, and *; Significant difference between groups (significant level=0.05).

Likewise, after two months, the results showed that fibroblast level, number of osteoblasts, and percentage of bone neoformation were statistically different among all groups (Table 2, Fig.4). The LP group had a significantly higher percentage of bone formation and osteoblast compared to the other groups. In contrast, the degree of fibroblast proliferation was higher in the control than in the LP (186.1 ± 8.6 vs. 13.8 ± 16.9). The results revealed that the amount of bone neoformation was higher in the LP group compared with the control group (63.8 ± 28.1 vs. 5.8 ± 1.6). Meanwhile, there was no significant difference between PRF and LP groups, while significant differences were seen between LP and other groups.

The findings suggested significant differences in the level of fibroblast, the percentage of new bone formation, and osteoblast level between two one-and-two months after surgery (Figs. 3, 4). Additionally, the combined effect of LLLT and PRF on bone formation, osteoblast, and fibroblast was significant as there was a statistically significant difference between the LP and the control group in both samples (Tables 1, 2).

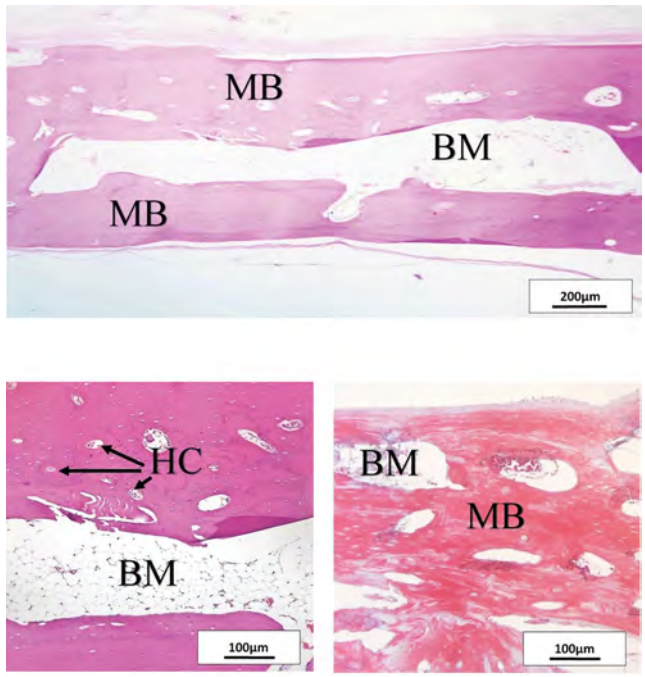

Fig.2: Histopathological evaluation of the normal calvarium. MB; Mature bone, BM; Bone marrow, HC; Haversian canal, H & E; Hematoxylin and eosin, and MT; Masson trichrome.

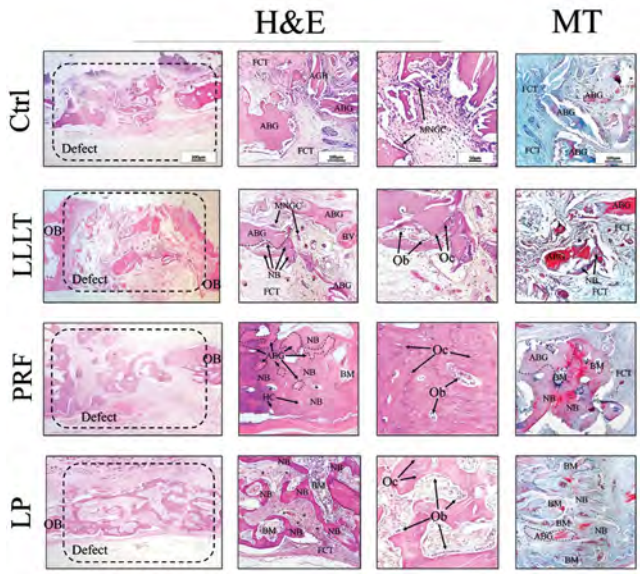

Fig.3: Histological findings for the effect low-level laser therapy and leukocyte and- platelet rich fibrin on fibrous tissue formation on calvarium bone regeneration in rabbit, 1-month post-surgery. OB; Old bone, ABG; Autogenous bone graft, MNGC; Multi nucleated giant cell, FCT; Fibrous connective tissue, BV; Blood vessels, Ob; Osteoblasts, Oc; Osteocytes, *; Newly formed blood vessels, NB; New bone formation, HC; Haversian canal, BM; bone marrow, H & E; Hematoxylin and eosin, MT; Masson trichrome, Ctrl; Control, LLLT; Low-level laser therapy, PRF; Leukocyte-platelet rich fibrin, and LP; PRF+LLLT.

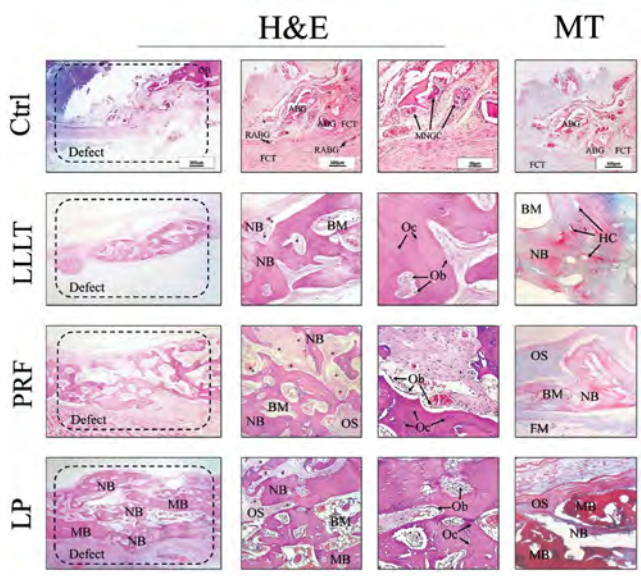

Fig.4: Histological findings for the effect of low-level laser therapy and leukocyte and- platelet rich fibrin on fibrous tissue formation on calvarium bone regeneration in rabbit, 2-month post-surgery. FCT; Fibrous connective tissue, ABG; Autogenous bone graft, RABG; Residue of autogenous bone graft, Ob; Osteoblasts, Oc; Osteocytes, *; Newly formed blood vessels, NB; New bone formation, HC; Haversian canal, BM; Bone marrow, OS; Osteoid, MB; Mature bone, H & E; Hematoxylin and eosin, MT; Masson trichrome, Ctrl; Control, LLLT; Low-level laser therapy, PRF; Leukocyte-platelet rich fibrin, and LP; PRF+LLLT.

Table 2: Comparison of the mean scores and standard deviations of histological variables between paired treatment groups after two-month post-operation

Group	Between groups	Fibroblast	Osteoblast	Bone formation
C		186.1 ± 8.6	3.2 ± 0.5	5.8 ± 1.6
	C-LLLT (p)	0.65	0.44	0.65
	C-PRF (p)	0.028*	0.035*	0.02*
	C-LP (p)	0.002*	0.003*	0.003*
LLLT		40.8 ± 6.2	47.2 ± 5.6	41.8 ± 2.8
	LLLT-PRF (p)	0.22	0.47	0.18
	LLLT-LP (p)	0.28	0.55	0.36
PRF		29.8 ± 5.3	54.2 ± 3.3	52.0 ± 2.8
	PRF-LP (p)	0.45	0.47	0.59
LP		13.8 ± 16.9	74.4 ± 31.7	63.8 ± 28.1

Data are presented as mean ± SD. C; Control, LLLT; Low-level laser therapy, PRF; Leukocyte-platelet rich fibrin, LP; PRF+LLLT, (p); P value, and *; Significant difference between groups (significant level=0.05).

Discussion

Bone structure is capable of regeneration and repair itself, but this process can be hampered due to certain diseases and the size of the bone lesion (15). To date, numerous methods have been proposed to speed up the process of bone healing. While our lit review revealed that drug therapy and surgery are the most recognized methods, others including laser therapy and using bioactive material have been also suggested (19). The present study aimed to evaluate the effect of the LLLT in combination with PRF on calvarium bone regeneration in rabbits.

As suggested by Kramer et al. (22), we created four circled defects of 8mm in diameter on the parietal bones of rabbit's calvaria. Using standardized defects of 8mm allows a remarkable increment in their interaction with bone graft materials without affecting the other defects (23).

The histological assessment showed that bone neoformation and the number of osteoblasts and fibroblasts were not different between PRF and LP groups, while a pairwise comparison of PRF with the control group indicated a significant difference. As results showed, the effect of PRF was observed in creating osteoblast and new bone formation within the defect area.

Chang and Zhao (24) reported that PRF increases phosphorylated extracellular signal-regulated protein kinase, osteoprotegerin, and alkaline phosphatase activity which provide benefits for periodontal regeneration in human osteoblast cell and pulp cells and suppress osteolytic activity. Additionally, Leucocytes secrete a considerable amount of vascular endothelial growth factor (VEGF) and platelets that contain angiogenesis stimulators including VEGF and basic fibroblast growth factors (25). A study on the effect of PRF on the rabbit's cranial lesions showed that the degree of immunostaining for VEGF was higher compared to the control group. As suggested, PRF can increase the number of bone marrow cells in calvarial defects (26). Another experimental study on rabbits found that there was more new bone formed around the defect area in the PRF group than in the control group after one-month post-surgery, but no significant difference was seen between the PRF group and the other treatment groups including biphasic calcium phosphate and Bio-Oss (27). On the other hand, an *in vivo* study on the effect of PRF and leukocytes on bone regeneration including hemispheres implanted in rabbit calvaria reported no additional effect on bone regeneration at 1 week, 5 weeks and 12 weeks after surgery. As suggested by Knapen et al. (21), further investigations are required using critical size defect model.

In the low-level laser therapy group, a small area of new bone formation around the autogenous bone graft was observed one-month post-surgery, but there was no significant difference between this group and the PRF group. After two months, the percentage of bone formation increased, although osteointegration and mineralization of the bone matrix were inadequate and immature. Recently, Atasoy et al. (28) reported that GaAlAs 940 nm laser with different energy intensities (5,

10 and 20 J/cm^2) have no significant impact on the course of bone healing in both stages of bone formation. The bio modulatory effects of laser are dose-dependent and highly influenced by the method of use. There is no standard energy density for the stimulation of bone healing. Some reports suggested energy densities of 1-5 J/cm2 while others referred to a total energy density of 16 J/cm2 seems to be more efficient for bone metabolism (29). One systematic review on the effect of the low-level laser therapy on the maxillofacial bone defects supported that the improvement in bone density can be obtained when using LLLT after maxillofacial bone defects surgery. It has been reported that LLLT has anti-inflammatory and analgesic potential and accelerates the healing process. However, the authors suggested that protocols for using LLLT should be standardized before drawing any concrete conclusions (15). Another review found that low-level laser treatment reduces the duration of the bone healing process, although there are no standardized protocols for the surgical procedure (19).

In this study, a significant increment in formation of new bone was seen in the LP group compared to the control group, whereas no significant difference was found between LLLT and the control group. On contrary, several studies supported that the isolated effect of LLLT was significant on bone regeneration, but the synergistic effect of combined LLLT could not improve bone regeneration significantly. For example, a study on the synergistic effect of LLLT (GaAlAs, 810 nm) and mesenchymal stem cells on bone regeneration in rabbit's calvarial defects reported that although LLLT significantly enhanced bone regeneration, there was no significant synergistic effect of combined LLLT and mesenchymal stem cells (30). In addition, a histological study revealed that the isolated effect of low-level laser therapy and low-intensity pulsed ultrasound boosted bone formation in the rabbit calvarium, but combined therapy failed to produce an additive effect on the reconstruction of defects (31). The mechanism of how LLLT enhances tissue healing is not completely understood, but it seems that absorbed laser light by tissue increases mitochondrial activity, local blood circulation, ATP synthesis, collagen synthesis, and the release of VEGF (32). Another study addressing the effect of LLLT and platelet concentration on bone repair in rats found that LLLT reduced inflammation and increased bone formation. However, platelet concentrate therapy with autogenous failed to increase bone repair alone or in combination with LLLT. The ineffectiveness of LLLT in the combined group is questionable, but in the platelet concentrate group, the result is predictable due to the use of sodium citrate as an anticoagulant in platelet concentrate. To support our result, the ineffectiveness of LLLT could be due to not having a single documented protocol for using low-level laser therapy which could be regarded as shortcoming of the present study. We suggest further investigations on this topic with more sample size as well as a longer-term evaluation.

Conclusion

In the present study, Leukocyte- and PRF improved bone regeneration by increasing the formation of new bone and reducing fibrosis. The best treatment results were in the Leukocyte- and PRF group with low-level laser therapy, but low-level laser treatment alone did not significantly improve the bone regeneration process.

Acknowledgments

There is no financial support and conflict of interest in this study.

Authors' Contributions

F.T., F.Sh., M.T.; Contributed to conception and design. A.Kh., M.H.T., M.T., F.Sh.; Contributed to all experimental work, data and statistical analysis, and interpretation of data. F.T., F.Sh.; Were responsible for overall supervision. F.Sh., M.H.T.; Drafted the manuscript, which was revised by A.Kh., F.T. All authors read and approved the final manuscript.

References

1. Penteado LA, Colombo CE, Penteado RA, Assis AO, Gurgel BC. Evaluation of bioactive glass and platelet-rich plasma for bone healing in rabbit calvarial defects. J Oral Sci. 2013; 55(3): 225-232.
2. Hämmerle CH, Giannobile WV. Biology of soft tissue wound healing and regeneration--consensus report of group 1 of the 10th european workshop on periodontology. J Clin Periodontol. 2014; 41 Suppl 15: S1-5.
3. Lioubavina-Hack N, Carmagnola D, Lynch SE, Karring T. Effect of Bio-Oss with or without platelet-derived growth factor on bone formation by "guided tissue regeneration": a pilot study in rats. J Clin Periodontol. 2005; 32(12): 1254-1260.
4. Zhang Y, Yang S, Zhou W, Fu H, Qian L, Miron RJ. Addition of a synthetically fabricated osteoinductive biphasic calcium phosphate bone graft to BMP2 improves new bone formation. Clin Implant Dent Relat Res. 2016; 18(6): 1238-1247.
5. Wang Z, Weng Y, Lu S, Zong C, Qiu J, Liu Y, et al. Osteoblastic mesenchymal stem cell sheet combined with Choukroun platelet-rich fibrin induces bone formation at an ectopic site. J Biomed Mater Res B Appl Biomater. 2015; 103(6): 1204-1216.
6. Dohan Ehrenfest DM, Rasmusson L, Albrektsson T. Classification of platelet concentrates: from pure platelet-rich plasma (P-PRP) to leucocyte- and platelet-rich fibrin (L-PRF). Trends Biotechnol. 2009; 27(3): 158-167.
7. Khorshidi H, Raoofi S, Bagheri R, Banihashemi H. Comparison of the mechanical properties of early leukocyte- and platelet-rich fibrin versus PRGF/endoret membranes. Int J Dent. 2016; 2016: 1849207.
8. Mowla AE, Sherif H, Bashir D. Evaluation of the effect of platelet rich fibrin (PRF) on bone regeneration in the tibia of diabetic rats (histological and immunohistochemical studies). Egypt J Histol. 2020; 43(3): 777-790.
9. Dohan Ehrenfest DM, Del Corso M, Diss A, Mouhyi J, Charrier JB. Three-dimensional architecture and cell composition of a choukroun's platelet-rich fibrin clot and membrane. J Periodontol. 2010; 81(4): 546-555.
10. do Lago ES, Ferreira S, Garcia IR Jr, Okamoto R, Mariano RC. Improvement of bone repair with l-PRF and bovine bone in calvaria of rats. histometric and immunohistochemical study. Clin Oral Investig. 2020; 24(5): 1637-1650.
11. Simonpieri A, Del Corso M, Vervelle A, Jimbo R, Inchingolo F, Sammartino G, et al. Current knowledge and perspectives for the use of platelet-rich plasma (PRP) and platelet-rich fibrin (PRF) in oral and maxillofacial surgery part 2: Bone graft, implant and reconstructive surgery. Curr Pharm Biotechnol. 2012; 13(7): 1231-1256.
12. Miron RJ, Zucchelli G, Pikos MA, Salama M, Lee S, Guillemette V, et al. Use of platelet-rich fibrin in regenerative dentistry: a systematic review. Clin Oral Investig. 2017; 21(6): 1913-1927.

13. Jonasson TH, Zancan R, de Oliveira Azevedo L, Fonseca AC, Silva MCD, Giovanini AF, et al. Effects of low-level laser therapy and platelet concentrate on bone repair: Histological, histomorphometric, immunohistochemical, and radiographic study. J Craniomaxillofac Surg. 2017; 45(11): 1846-1853.
14. Khadra M, Lyngstadaas SP, Haanaes HR, Mustafa K. Effect of laser therapy on attachment, proliferation and differentiation of human osteoblast-like cells cultured on titanium implant material. Biomaterials. 2005; 26(17): 3503-3509.
15. Santinoni CD, Oliveira HF, Batista VE, Lemos CA, Verri FR. Influence of low-level laser therapy on the healing of human bone maxillofacial defects: a systematic review. J Photochem Photobiol B. 2017; 169: 83-89.
16. Coombe AR, Ho CT, Darendeliler MA, Hunter N, Philips JR, Chapple CC, et al. The effects of low level laser irradiation on osteoblastic cells. Clin Orthod Res. 2001; 4(1): 3-14.
17. Stein A, Benayahu D, Maltz L, Oron U. Low-level laser irradiation promotes proliferation and differentiation of human osteoblasts in vitro. Photomed Laser Surg. 2005; 23(2): 161-166.
18. García-Morales JM, Tortamano-Neto P, Todescan FF, de Andrade JC Jr, Marotti J, Zezell DM. Stability of dental implants after irradiation with an 830-nm low-level laser: a double-blind randomized clinical study. Lasers Med Sci. 2012; 27(4):703-711.
19. Noba C, Mello-Moura ACV, Gimenez T, Tedesco TK, Moura-Netto C. Laser for bone healing after oral surgery: systematic review. Lasers Med Sci. 2018; 33(3): 667-674.
20. Chung I, Choung P, Jo Y. Bioengineering of the tooth and jaw. J Tissue Eng Regen Med. 2005; 2(2): 86.
21. Knapen M, Gheldof D, Drion P, Layrolle P, Rompen E, Lambert F. Effect of leukocyte- and platelet-rich fibrin (L-PRF) on bone regeneration: a study in rabbits. Clin Implant Dent Relat Res. 2015; 17 Suppl 1: e143-152.
22. Kramer IR, Killey HC, Wright HC. A histological and radiological comparison of the healing of defects in the rabbit calvarium with and without implanted heterogeneous anorganic bone. Arch Oral Biol. 1968; 13(9): 1095-1106.
23. Takauti CA, Futema F, Brito Junior RB, Abrahão AC, Costa C, Queiroz CS. Assessment of bone healing in rabbit calvaria grafted with three different biomaterials. Braz Dent J. 2014; 25(5): 379-384.
24. Chang YC, Zhao JH. Effects of platelet-rich fibrin on human periodontal ligament fibroblasts and application for periodontal infrabony defects. Aust Dent J. 2011; (4): 365-371.
25. Yamada Y, Ueda M, Hibi H, Baba S. A novel approach to periodontal tissue regeneration with mesenchymal stem cells and platelet-rich plasma using tissue engineering technology: a clinical case report. Int J Periodontics Restorative Dent. 2006; 26(4): 363-369.
26. Yoon JS, Lee SH, Yoon HJ. The influence of platelet-rich fibrin on angiogenesis in guided bone regeneration using xenogenic bone substitutes: a study of rabbit cranial defects. J Craniomaxillofac Surg. 2014; 42(7): 1071-1077.
27. Ozdemir H, Ezirganli S, Isa Kara M, Mihmanli A, Baris E. Effects of platelet rich fibrin alone used with rigid titanium barrier. Arch Oral Biol. 2013; 58(5): 537-544.
28. Atasoy KT, Korkmaz YT, Odaci E, Hanci H. The efficacy of low-level 940 nm laser therapy with different energy intensities on bone healing. Braz Oral Res. 2017; 31: e7.
29. Bossini PS, Rennó AC, Ribeiro DA, Fangel R, Ribeiro AC, Lahoz Mde A, et al. Low level laser therapy (830nm) improves bone repair in osteoporotic rats: similar outcomes at two different dosages. Exp Gerontol. 2012; 47(2): 136-142.
30. Fekrazad R, Sadeghi Ghuchani M, Eslaminejad MB, Taghiyar L, Kalhori KA, Pedram MS,et al. The effects of combined low level laser therapy and mesenchymal stem cells on bone regeneration in rabbit calvarial defects. J Photochem Photobiol B. 2015; 151: 180-185.
31. Acar AH, Yolcu Ü, Altındiş S, Gül M, Alan H, Malkoç S. Bone regeneration by low-level laser therapy and low-intensity pulsed ultrasound therapy in the rabbit calvarium. Arch Oral Biol. 2016; 61: 60-65.
32. Kazancioglu HO, Ezirganli S, Aydin MS. Effects of laser and ozone therapies on bone healing in the calvarial defects. J Craniofac Surg. 2013; 24(6): 2141-2146.